

EFFECTS OF ENVIRONMENTAL FACTORS ON THE AQUEOUS CORROSION OF HIGH-LEVEL RADIOACTIVE WASTE CONTAINERS—EXPERIMENTAL RESULTS AND MODELS

Prepared for

Nuclear Regulatory Commission
Contract NRC-02-97-009

Prepared by

Center for Nuclear Waste Regulatory Analyses
San Antonio, Texas

September 1999



**EFFECTS OF ENVIRONMENTAL FACTORS ON THE AQUEOUS
CORROSION OF HIGH-LEVEL RADIOACTIVE WASTE
CONTAINERS—EXPERIMENTAL RESULTS AND MODELS**

Prepared for

**Nuclear Regulatory Commission
Contract NRC-02-97-009**

Prepared by

**Darrell S. Dunn
Yi-Ming Pan
Gustavo A. Cragolino**

**Center for Nuclear Waste Regulatory Analyses
San Antonio, Texas**

September 1999

PREVIOUS REPORTS IN SERIES

<u>Number</u>	<u>Name</u>	<u>Date Issued</u>
CNWRA 91-004	A Review of Localized Corrosion of High-Level Nuclear Waste Container Materials—I	April 1991
CNWRA 91-008	Hydrogen Embrittlement of Candidate Container Materials	June 1991
CNWRA 92-021	A Review of Stress Corrosion Cracking of High-Level Nuclear Waste Container Materials—I	August 1992
CNWRA 93-003	Long-Term Stability of High-Level Nuclear Waste Container Materials: I—Thermal Stability of Alloy 825	February 1993
CNWRA 93-004	Experimental Investigations of Localized Corrosion of High-Level Nuclear Waste Container Materials	February 1993
CNWRA 93-014	A Review of the Potential for Microbially Influenced Corrosion of High-Level Nuclear Waste Containers	June 1993
CNWRA 94-010	A Review of Degradation Modes of Alternate Container Designs and Materials	April 1994
CNWRA 94-028	Environmental Effects on Stress Corrosion Cracking of Type 316L Stainless Steel and Alloy 825 as High-Level Nuclear Waste Container Materials	October 1994
CNWRA 95-010	Experimental Investigations of Failure Processes of High-Level Radioactive Waste Container Materials	May 1995
CNWRA 96-004	Thermal Stability and Mechanical Properties of High-Level Radioactive Waste Container Materials: Assessment of Carbon and Low-Alloy Steels	May 1996
CNWRA 97-010	An Analysis of Galvanic Coupling Effects on the Performance of High-Level Nuclear Waste Container Materials	August 1997
CNWRA 98-004	Effect of Galvanic Coupling Between Overpack Materials of High-Level Nuclear Waste Containers—Experimental and Modeling Results	March 1998
CNWRA 98-008	Effects of Environmental Factors on Container Life	July 1998

PREVIOUS REPORTS IN SERIES (cont'd)

Number	Name	Date Issued
CNWRA 99-003	Assessment of Performance Issues Related to Alternate Engineered Barrier System Materials and Design Options	September 1999

ABSTRACT

Uniform passive corrosion, localized crevice corrosion, and stress corrosion cracking (SCC) of Alloy 22 were investigated in a range of simulated near-field repository environments, including solutions containing high chloride concentrations near or above that corresponding to the aqueous solubility of NaCl. Passive current densities were measured potentiostatically on as-received, heat treated, and welded specimens as a function of potential, chloride concentration, pH, and temperature and used to calculate uniform corrosion rates using Faraday laws. Relationships between the repassivation potential for crevice corrosion and the chloride concentration were obtained for as-received and welded specimens of Alloy 22 at temperatures below and above the boiling point of water. Repassivation potentials for Alloy 22 were compared as a function of chloride concentration with those of type 316L stainless steel (SS) and other Ni-Cr-Mo alloys such as Alloys 825 and 625. Wedge-loaded double cantilever beam specimens of Alloy 22 and type 316L SS were used to study the SCC susceptibility in a deaerated, acidified (pH 2.7) NaCl solution at 90 °C. No crack propagation was observed in tests lasting more than 8 mo. Whereas crack propagation in concentrated MgCl₂ solutions at 110 °C was detected in a few days in type 316L SS specimens, no crack growth was observed in the Alloy 22 specimens after an 8-mo test period. The results of these laboratory investigations are discussed in the context of improving the ability of the performance assessment codes, such as Total-system Performance Assessment Version 3.2 code, to estimate both the time for the onset of different corrosion modes affecting the container life and the corresponding corrosion penetration rates.

CONTENTS

Section	Page
FIGURES	ix
TABLES	xi
ACKNOWLEDGMENTS	xiii
EXECUTIVE SUMMARY	xv
1 INTRODUCTION	1-1
1.1 WASTE PACKAGE DESIGN AND MATERIALS	1-1
1.2 CONTAINER DEGRADATION MODES	1-3
1.3 MODELING AND RESULTS IN THE U.S. DEPARTMENT OF ENERGY PERFORMANCE ASSESSMENT	1-4
1.4 CORROSION MODELING OF Ni-Cr-Mo ALLOYS IN NUCLEAR REGULATORY COMMISSION/CENTER FOR NUCLEAR WASTE REGULATORY ANALYSES PERFORMANCE ASSESSMENT CODES	1-6
2 EXPERIMENTAL METHODS	2-1
2.1 SPECIMENS	2-1
2.2 TEST METHODS	2-3
2.2.1 Passive Corrosion Rate Tests	2-3
2.2.2 Repassivation Potential Tests	2-4
2.2.3 Stress Corrosion Cracking Tests	2-4
3 RESULTS	3-1
3.1 PASSIVE CORROSION OF ALLOY 22	3-1
3.2 LOCALIZED CORROSION	3-6
3.3 STRESS CORROSION CRACKING	3-12
3.3.1 Control Tests	3-12
3.3.2 Stress Corrosion Cracking Tests	3-14
4 DISCUSSION	4-1
4.1 PASSIVE CORROSION	4-1
4.2 LOCALIZED CORROSION	4-2
4.3 STRESS CORROSION CRACKING	4-4
4.4 MODELING OF CONTAINER CORROSION IN TOTAL PERFORMANCE ASSESSMENT VERSION 3.2 CODE	4-8
5 SUMMARY AND FUTURE WORK	5-1
6 REFERENCES	6-1

FIGURES

Figure	Page
2-1	Schematic and dimensions of (a) cylindrical specimens (b) crevice corrosion specimens 2-2
2-2	Dimensions of the double cantilever beam specimen according to NACE TM0177-90 (NACE International, 1990) 2-3
2-3	Bending stress versus crack length (and crack length/width ratio) curves for various loads for double cantilever beam specimen 2-6
2-4	Initial stress intensity versus crack length (and crack length/width ratio) curves for various loads for double cantilever beam specimen 2-6
2-5	Initial stress intensity versus bending stress relations for various loads for double cantilever beam specimen 2-7
3-1	Cyclic polarization of Alloy 22 in deaerated 0.028 M chloride showing the corrosion potential, passive, and transpassive regions 3-1
3-2	Anodic current transients measured for Alloy 22 specimens under potentiostatic conditions in deaerated 4 M chloride, pH 8.0, at 95 °C 3-2
3-3	Anodic current density measured for Alloy 22 under potentiostatic conditions. 3-3
3-4	Anodic current transients measured for Alloy 22 specimens thermally aged 4 h at 870 °C under potentiostatic conditions in deaerated 4 M chloride, pH 8.0, at 95 °C 3-4
3-5	Anodic current transients measured for welded Alloy 22 specimens under potentiostatic conditions in deaerated 4 M chloride, pH 8.0, at 95 °C 3-5
3-6	Crevice corrosion repassivation potentials for Alloy 625 as a function of chloride concentration and temperature 3-6
3-7	Crevice corrosion repassivation potentials for Alloys 316L SS, 825, 625, and 22 as a function of chloride concentration 3-7
3-8	Transpassive dissolution potential of Alloy 22 as a function of pH in 0.28 M chloride solution 3-8
3-9	Repassivation potential for Alloy 22 measured in autoclave system at temperatures up to 175 °C 3-9
3-10	Crevice corrosion penetration depth measured on Alloy 22 specimens following cyclic potentiodynamic polarization scans conducted in the autoclave system at temperatures ranging from 95 to 175 °C 3-10
3-11	Repassivation potential as a function of chloride concentration for Alloy 22 measured in autoclave system at temperatures up to 150 °C 3-10
3-12	Repassivation potential as a function of chloride concentration for mill annealed and welded Alloy 22 measured in autoclave system at temperatures of 95 and 125 °C 3-11
3-13	Photograph of Alloy 22 specimens (a) mill annealed tested in 4 M chloride at 125 °C, (b) welded Alloy 22 tested in 4 M chloride at 125 °C, (c) untested as-welded specimen 3-12
3-14	Fractograph showing three distinct regions on the fracture surface of the Alloy 22 specimen mechanically overloaded to failure for control test 3-13
3-15	Fractograph showing fatigue striations in the enlarged precracked region on the fracture surface of the Alloy 22 control specimen 3-13

FIGURES (cont'd)

Figure	Page
3-16	Fractograph showing microvoids in the ductile failure region on the fracture surface of the Alloy 22 control specimen 3-14
3-17	Fractograph showing a mixed feature of microvoid and ductile tearing in the transition region on the fracture surface of the Alloy 22 control specimen 3-15
3-18	Scanning electron micrograph showing the initial precrack tip morphology of the long transverse-longitudinal direction (T-L) Alloy 22 specimen 3-16
3-19	Scanning electron micrograph showing the precrack tip morphology of the long transverse-longitudinal direction (T-L) Alloy 22 specimen after 32-wk exposure 3-17
3-20	Scanning electron micrograph showing grain boundary attack of the long transverse-longitudinal direction (T-L) Alloy 22 specimen after 22-wk exposure 3-17
3-21	Scanning electron micrograph showing minor secondary cracks of the long transverse-longitudinal direction (T-L) Alloy 22 specimen after 10-wk exposure 3-18
3-22	Scanning electron micrograph showing transverse crack branches of the type 316L stainless steel specimen after 3-wk exposure to 40 percent MgCl ₂ solution at 110 °C 3-18
3-23	Fractograph showing transgranular stress corrosion cracking on the fracture surface of the type 316L stainless steel specimen after 3.8-d exposure to 30 percent MgCl ₂ solution at 110 °C 3-19
3-24	Crack growth rate as a function of potential for double cantilever beam specimens of type 316L stainless steel in 30 percent MgCl ₂ solution at 110 °C 3-20
4-1	Effect of stress intensity on the crack growth rate of solution annealed type 304L stainless steel exposed to 42 percent MgCl ₂ solution at 130 °C and to 22 percent NaCl solution at 105 °C (Speidel, 1981). 4-5
4-2	Effect of Ni content on the crack growth rate of various Ni-Cr-Mo-Fe alloys in 22 percent NaCl solution at 105 °C (Speidel, 1981), 5 percent NaCl solution at 90 °C (Roy et al., 1998; McCright, 1998), and type 316L stainless steel in 30 percent MgCl ₂ solution at 110 °C 4-6
4-3	Effect of Ni content on the threshold stress intensity of various Ni-Cr-Mo-Fe alloys in 22 percent NaCl solution at 105 °C (Speidel, 1981), 5 percent NaCl solution at 90 °C (Roy et al., 1998; McCright, 1998), and type 316L stainless steel in 30 percent MgCl ₂ solution at 110 °C 4-7
4-4	Localized corrosion penetration rate measured using type 316L stainless steel and Alloy 625. Data from Dunn et al. (1996b), Cramer et al. (1984), and TPA code Version 3.2. 4-11
4-5	Waste package failure distribution for various container materials using TPA code Version 3.2 calculations 4-11

TABLES

Table		Page
2-1	Chemical compositions of the materials used in this study (in weight percent)	2-1
3-1	Passive corrosion rates for Alloy 22 calculated from passive current density measured under potentiostatic conditions	3-4
3-2	Results of stress corrosion cracking (SCC) tests of type 316L stainless steel and Alloy 22 in chloride solutions	3-15

ACKNOWLEDGMENTS

This report was prepared to document work performed by the Center for Nuclear Waste Regulatory Analyses (CNWRA) for the Nuclear Regulatory Commission (NRC) under Contract No. NRC-02-97-009. The activities reported here were performed on behalf of the NRC Office of Nuclear Material Safety and Safeguards, Division of Waste Management. The report is an independent product of the CNWRA and does not necessarily reflect the views or regulatory position of the NRC.

The authors gratefully acknowledge useful discussions with N. Sridhar, as well as his technical review, the programmatic review of B. Sagar, and the editorial reviews of A. Woods and B. Long. Appreciation is due to J. Gonzalez for assistance in preparation of this report. The authors also acknowledge the laboratory work performed by K. Gruss, W. Machowski, and J. Sievert.

QUALITY OF DATA, ANALYSES, AND CODE DEVELOPMENT

DATA: Sources of data are referenced in each chapter. CNWRA-generated laboratory data contained in this report meet quality assurance (QA) requirements described in the CNWRA QA Manual. Data from other sources, however, are freely used. The respective sources of non-CNWRA data should be consulted for determining levels of QA.

ANALYSES AND CODES: SigmaPlot Version 4.0.1 and Grapher Version 2.0 computer codes were used for analyses contained in this report. These are commercial computer codes and are not controlled under the CNWRA Technical Operating Procedure-018 (Development and Control of Scientific and Engineering Software).

EXECUTIVE SUMMARY

The U.S. Department of Energy (DOE) strategy for radioactive waste disposal at the proposed repository at Yucca Mountain (YM) is to contain the radionuclides within the waste packages (WPs) for thousands of years and to ensure that annual doses to a person living near the site will be acceptably low throughout the compliance period. The proposed repository is located in an arid site with a low annual precipitation rate and a low flow of groundwater into the repository horizon to minimize degradation of the containers by corrosion. A double metallic barrier concept was incorporated into the WP design for the viability assessment (VA) of the repository in an attempt to prolong the time during which the radioactive waste can be contained.

Following the presentation to Congress of the VA and the completion of the License Application Design Selection process, two alloys were selected as container materials for the Enhanced Design Alternative II (EDA II). The WP, to be emplaced horizontally in drifts, will be composed of an outer container made of Alloy 22 (Ni-22Cr-13Mo-3W) surrounding a shrink-fitted inner container fabricated of type 316L or 316NG (Fe-18Cr-12Ni-2.5Mo) stainless steel (SS). The inner container is designed to provide sufficient structural strength during the lifetime of the WP to avoid mechanical failure as a result of rock fall, but no performance allocation in terms of corrosion resistance is assigned to this container. A self-supported drip shield made of Ti-grade 7 (Ti-0.2 Pd) will be extended over the length of the emplacement drifts to impede dripping of water onto the WPs. Alloy 22 was selected in EDA II as outer container material for the WPs by assuming that uniform passive corrosion will lead to WP lifetimes well beyond 10,000 yr for a container with a 2-cm wall thickness. It was assumed that Alloy 22 will be immune to localized (crevice) corrosion because a relative humidity greater than 80 percent will be attained only at WP surface temperatures lower than 80°C due to a combination of low thermal loading and high rates of ventilation during preclosure. It is expected by the DOE that under such thermal and environmental conditions a passive oxide film will form on the Alloy 22 surface and uniform dissolution of metal through this protective film, called passive corrosion, will occur at a low rate.

In support of the Nuclear Regulatory Commission High-Level Nuclear Waste Program, the Center for Nuclear Waste Regulatory Analyses is developing a performance assessment capability for the purpose of evaluating the overall performance of the proposed repository at YM. As part of the activities conducted initially in the Container Life and Source Term and later in the Total System Performance Assessment and Integration Key Technical Issues, the Engineered Barrier System Performance Assessment Code (EBSPAC) Version 1.1 was developed as a deterministic code to provide a means for evaluating the WP lifetime and radionuclide release rates. The part of EBSPAC dealing with WP degradation was adapted and incorporated as the EBSFAIL module to the probabilistic Total-system Performance Assessment (TPA) code Version 3.2 used to evaluate the DOE VA design. The EBSFAIL module can accommodate, with relatively minor changes, different WP designs and has sufficient flexibility for evaluating different container materials by changing only certain input parameters. The WP lifetimes are calculated by determining the predominant corrosion mode and the corresponding corrosion rate. At corrosion potentials below the repassivation potential for localized corrosion, degradation of the container occurs at a slow rate governed by the passive current density. Localized corrosion is assumed to occur without an induction time when the corrosion potential exceeds the repassivation potential. The aim of the laboratory investigations reported here is to provide input to the EBSFAIL module to improve the ability of the code to estimate both the time for the onset of different corrosion modes and the corrosion penetration rates.

Because sensitivity analyses, performed with TPA code Version 3.2, have shown that in the absence of localized corrosion the passive corrosion rate determines the lifetime of the Alloy 22 container, the passive corrosion rates of the base alloy and weldments are needed to accurately calculate container lifetimes. In addition, some considerable uncertainty exists with regard to the SCC susceptibility of Alloy 22. Numerous investigations, showing that Ni-Cr-Mo alloys with more than 45 percent Ni are immune to SCC in chloride solutions at temperatures up to 150 °C, have been contradicted by recent data reported by Lawrence Livermore National Laboratory (LLNL) indicating SCC of Alloy 22 in 5 percent chloride at 95 °C. Because this possible degradation mode could lead to early, unexpected failures of the WP, it is necessary to resolve the uncertainty surrounding the susceptibility of Alloy 22 to SCC.

The objective of this report is to present the results of experimental investigations on passive dissolution, localized crevice corrosion, and SCC of Alloy 22 in chloride solutions under a range of environmental conditions including temperature, chloride concentrations, and potential relevant to the container performance in the repository. This report is essentially focused on Alloy 22 as a result of the importance attributed to the performance of this alloy in the new DOE WP design, but also includes useful information on type 316L SS. The experimental data are discussed taking into consideration the relative importance of those failure modes in the performance assessment codes used in the VA by the DOE and in TPA code Version 3.2.

Laboratory investigations were conducted using potentiostatic measurements to determine the effects of potential ranging from -200 to 800 mV versus saturated calomel electrode (SCE), chloride concentration (0.028 to 4.0 M), temperature (20 and 95 °C), and pH (2.7 and 8.0) on the passive current density of Alloy 22. It was found that, with the possible exception of temperature, the effect of these variables on the passive current density is minor. However, at potentials above 400 mV_{SCE}, potentials that are difficult to reach under naturally corroding conditions, significant increases in current were observed as a result of the transpassive dissolution of Cr in the alloy. Nevertheless, pitting corrosion was not observed under such conditions. Uniform passive corrosion rates, calculated from these measurements using Faraday's law, suggest that Alloy 22 containers may have lifetimes well beyond 10,000 yr. These lifetimes can be shortened, however, by heat treatments (a few hours at 870 °C) that promote accelerated corrosion at potentials lower than 400 mV_{SCE}. Measurements on welded specimens did not reveal a detrimental effect of welding on the passive corrosion rate.

Because inducing localized corrosion in Alloy 22 at temperatures up to 95 °C in saturated chloride solutions was difficult, repassivation potential measurements for Alloy 22 were conducted in an autoclave system at temperatures ranging from 95 to 175 °C in solutions containing 0.5 to 4 M NaCl. Although the presence of liquid water above the boiling point is not anticipated in the proposed repository at YM, testing at above boiling temperatures will help define the region of susceptibility of Alloy 22. A strong effect of temperature on the repassivation potential was noted, particularly between 95 and 125 °C. The repassivation potential decreased with both increasing temperature and chloride concentration, exhibiting the typical linear dependence on the logarithm of the chloride concentration with a slope that is temperature dependent. The repassivation potential for welded specimens of Alloy 22 at 95 °C is more than 100 mV lower than that of non welded specimens over the whole range of chloride concentrations studied; but at 125 °C, no difference was observed. Results of similar repassivation potential measurements for Alloy 22 obtained in glass cells at 95 °C when plotted as a function of the chloride concentration and compared to those obtained for type 316L SS and other Ni-Cr-Mo alloys, such as Alloys 825 and 625, reveal the significant improvement in resistance to crevice corrosion attainable with Alloy 22. Only at high chloride concentrations (>4 M), did the repassivation potential decrease to the low potential values attainable under open circuit conditions in naturally aerated systems. However, the significant decrease in the repassivation potential within a narrow

range of chloride concentrations at temperatures close to the boiling point of water suggests that similar to the results obtained in the autoclave system, minor metallurgical and environmental variations may induce localized corrosion in a corrosion resistant material such as Alloy 22 that otherwise would exhibit a stable passive behavior.

The susceptibility of Alloy 22 to SCC in deaerated, acidified (pH 2.7) chloride solutions at 90 °C was studied using wedge-loaded double cantilever beam (DCB) specimens to confirm the occurrence of SCC as reported by investigators at the LLNL. However, no cracking was observed in tests lasting more than 8 mo, even in a far more concentrated MgCl₂ solution at a higher temperature (110 °C) than that studied by LLNL. Limited grain boundary attack and minor secondary cracks were detected in 40 percent MgCl₂, but no signs of crack propagation was observed at an initial stress intensity of 32.7 MPa·m^{1/2}. On the contrary, crack propagation was observed in DCB specimens of type 316L SS at applied potentials above the repassivation potential, including the open-circuit potential, in less concentrated MgCl₂ solutions and at a lower stress intensity. Type 316L SS was used for comparison, given its known susceptibility to SCC in hot, concentrated chloride solutions. Nevertheless, DCB specimens of type 316L SS did not exhibit crack propagation after 8 mo in the deaerated, acidified (pH 2.7) chloride solution at 90 °C originally used in the LLNL tests. Ductile tearing was observed on the fracture surface of a control test, performed by fatigue precracking an Alloy 22 DCB specimen and mechanically breaking the specimen without any exposure to a chloride containing solution. The appearance of this ductile tearing region, which occurred during mechanical overloading, is somewhat similar to that of an SCC fracture surface. The results of the control test and the lack of SCC of both Alloy 22 and type 316L SS in 5 percent NaCl observed in this study suggest that the apparent SCC observed in the tests conducted at LLNL were artifacts induced by the mechanical fracture of the specimens after the completion of the tests.

The results of these investigations are discussed to highlight the importance of the repassivation potential concept in the performance assessment of container materials. The use of the repassivation potential expressions for various materials to define regimes of localized corrosion or SCC affords flexibility in the TPA code to evaluate different container materials and to accommodate possible changes in WP design through minor modifications in the code.

1 INTRODUCTION

In the U.S. Department of Energy (DOE) strategy for waste containment and isolation for the proposed high-level radioactive waste (HLW) repository at Yucca Mountain, Nevada (U.S. Department of Energy, 1998a) there are four key attributes of the repository system important to meeting the postclosure performance objectives of near-complete containment of radionuclides within the waste packages (WPs) for thousands of years and an acceptably low annual dose to a member of the receptor group living near the site. These four attributes are

- Limited water contacting the WPs
- Long WP lifetime
- Low rate of release of radionuclides from breached WPs
- Radionuclide concentration reduction during transport from WPs

The WP is the primary engineered barrier to the release of radionuclides to the biosphere. The performance of WPs for the initial several thousand years after radioactive waste emplacement is extremely important to protecting public health and safety. As identified by the U.S. Department of Energy (1998a), four hypotheses should be satisfied to assure containment of the radionuclides for a prolonged period:

- Heat reduces the relative humidity (RH) at the WP surface
- Corrosion of WP materials is slow
- The inner WP barrier will be protected by the outer barrier
- Engineered enhancements can extend the containment time

The relative importance of these hypotheses has varied with the changes in WP and engineered barrier subsystem (EBS) designs for the proposed site recommendation. Nevertheless, two of these hypotheses, slow corrosion of WP materials and engineered enhancements to extend WP lifetime, are becoming even more important after the sensitivity studies conducted for the Total System Performance Assessment (TSPA) viability assessment (VA) (U.S. Department of Energy, 1998b).

1.1 WASTE PACKAGE DESIGN AND MATERIALS

After many design modifications to improve the performance of the EBS, the DOE proposed as a reference design in the VA (U.S. Department of Energy, 1998c) a WP composed of two concentric containers of different metallic materials emplaced in a horizontal drift with a concrete liner as ground support. The outer container, with a wall thickness of 100 mm, was proposed to be made of a corrosion allowance material, American Society for Testing and Materials (ASTM) A516 carbon steel. Alloy 22, a corrosion resistant material of the class of austenitic Ni-Cr-Mo alloys, was selected for the inner container, with a wall thickness of 20 mm. According to the performance assessment (PA) studies conducted for the VA (U.S. Department of Energy, 1998b), the major factors affecting postclosure performance for the VA reference design are the chemistry of the water contacting the WP and the integrity of both the outer and inner WP.

Following the completion and submittal to Congress of the VA, the DOE initiated the License Application Design Selection process to evaluate design alternatives and design features for the repository (Harrington, 1999). Design alternatives are defined as different conceptual designs for the repository and design features as elements or attributes that could be added to any design alternative to enhance its

performance. Among the design alternatives, tailored WP spatial distribution, low thermal loading, continuous postclosure ventilation, and the VA design with options were considered. Among many other design features, drip shields, backfill, ceramic coatings, aging and blending of spent nuclear fuel (SNF) and vitrified HLW, fuel rod consolidation, drift spacing and diameter, WP spacing, WP radiation self-shielding, WP additives and fillers, and WP corrosion-resistant materials were evaluated. Alloy 22 was selected as outer container material in four of the five Enhanced Design Alternatives (EDAs) (Harrington, 1999). In these four designs, carbon steel (the outer container material selected for the VA) was replaced by type 316L or 316 Nuclear Grade (NG) stainless steel (SS), which is proposed, however, as the inner container material. All the EDAs exhibit as common features the selection of drip shields, carbon steel ground support, steel invert with granular (sand or gravel) ballast, and preclosure ventilation.

A detailed comparison of the VA design with the EDA II was presented in Cragolino et al. (1999). About a 30 percent decrease in the areal mass loading (thermal loading) was attained by an almost three times increase in drift spacing combined with a lower peak WP power as a result of SNF blending. The main objective of the reduced thermal loading is to maintain the center of the pillars between drifts below the boiling point of water at the repository horizon (96 °C) to reduce uncertainties associated with altered flow paths and water chemistry changes as a result of excessive rock heating. In addition, line loading and SNF blending are proposed in EDA II to attenuate temperature variations along the drift, whereas a significant increase in the preclosure ventilation rate is introduced as means to reduce peak temperatures.

The main difference between the VA and EDA II WP materials and design is the elimination of ASTM A516 carbon steel as container material. A combination of factors prompted this decision (Pasupathi, 1998). There were concerns regarding the possible wedging action of iron corrosion products (i.e., oxides and oxihydroxides) in the gap between the steel outer container and the Alloy 22 inner container as a result of the localized corrosion penetration of the outer container. Another detrimental factor considered was the possible generation of FeCl_3 at the localized corrosion sites that may lead to accelerated corrosion and, eventually, crevice corrosion of Alloy 22. An additional factor may be the predictable loss of structural strength that can be expected as a consequence of wall thinning due to uniform corrosion of carbon steel. A reverse VA design, with Alloy 22 as outer container material was also considered (Pasupathi, 1998). However, in addition to fabrication and eventual handling problems, the concerns regarding the wedging action of iron corrosion products and the deleterious effect of FeCl_3 following localized penetration of Alloy 22 remained.

Alloy 22 is selected in EDA II as the outer container material for the WPs by assuming that uniform passive corrosion will lead to WP lifetimes well beyond 10,000 yr for a container with a 2-cm wall thickness. The WP is planned to be fabricated by shrink fitting the outer container to a 5-cm thick inner container fabricated of types 316 NG or 316L SS. The dimensions of the WP are about 5.34 or 5.30 m in length and 1.65 to 1.97 m in outer diameter, depending on the internal content (SNF or codisposal of DOE-owned SNF and HLW). The inner container is designed to provide sufficient structural strength during the lifetime of the WP to avoid mechanical failure as a result of rock fall, but no performance allocation in terms of corrosion resistance is assigned to this container. It is assumed that Alloy 22 will be immune to localized (crevice) corrosion because a RH greater than 80 percent will be attained only at WP surface temperatures lower than 80 °C due to a combination of low thermal loading and high rates of ventilation during preclosure (Blink, 1999). It is expected that under such thermal and environmental conditions only uniform passive corrosion of Alloy 22 will occur.

Additionally, a self-supported, mailbox-shaped drip shield with overlapping sections will be extended over the length of the emplacement drifts to enclose the top and sides of the WPs. The purpose of the drip shield is to avoid water seepage or dripping during the thermal pulse period (where environmental conditions leading to localized corrosion of Alloy 22 can be attained) and presumably to attenuate the direct impact of rock fall on the WPs. The material of choice for the drip shield is Ti-grade 7 plate or sheet having a thickness of about 2 cm.

Another material change with respect to the VA design is the elimination of the concrete liner to avoid the generation of alkaline conditions by reaction with the altered groundwater. The concrete liner is planned to be replaced by steel sets and lagging or rock bolts and mesh depending on ground conditions. Concrete is also removed from the design of the invert structure and replaced by steel beams with sand or gravel ballast. Backfill may be used to cover the drip shield, even though a design without backfill is still being considered (Blink, 1999). The final configuration and the material for the pedestal used to support the WPs have not yet been selected.

1.2 CONTAINER DEGRADATION MODES

For the reasons discussed previously, it is clear that container life is extremely dependent on the performance of Alloy 22. Under anticipated repository conditions, corrosion is expected to be the dominant failure mode limiting container life (Cragolino and Sridhar, 1991, 1992; Sridhar et al., 1995). In recent PA studies (Wilson et al., 1994; TRW Environmental Safety Systems, Inc., 1995; Nuclear Regulatory Commission, 1995; Kessler and McGuire, 1996; U.S. Department of Energy, 1998b), container life is determined mainly by the failure time resulting from the penetration of the outer and inner containers caused by corrosion. Leaving aside disruptive events and mechanical failure, it is assumed in these studies that radionuclide release cannot take place until the container is breached by through-wall penetration as a result of corrosion.

Environmental variables such as temperature, pH, chloride ion concentration, and concentration of oxidizing and inhibiting species in the aqueous media contacting the container, as well as the physical metallurgical conditions of the construction materials, are critical factors determining the mode of container corrosion. As a result of its chemical composition, Alloy 22 will exhibit passive dissolution as the predominant form of uniform corrosion under the expected repository environmental conditions due to the formation of a protective, chromium-rich oxide film, as previously discussed (Cragolino et al., 1999).

If localized corrosion occurs under a specific combination of elevated temperatures, high chloride ion concentration, and strongly oxidizing conditions, it presumably would be in the form of crevice corrosion rather than pitting corrosion due to the high potentials required to nucleate pit on an openly exposed surface in Ni-Cr-Mo alloys with high Cr and Mo (plus W) contents (Cragolino et al., 1999). Nevertheless, thermal and residual stress effects associated with welding operations during closure of the WP, followed by prolonged exposures to elevated temperatures in the emplacement drifts, may affect the phase stability of corrosion-resistant Alloy 22. In this case, as discussed in detail in Cragolino et al. (1999), generation of short- and long-range ordered structures or formation of brittle intermetallic phases [i.e., topologically closed packed (TCP) phases] may accelerate uniform and localized corrosion processes and even affect mechanical properties.

In addition, other degradation processes such as stress corrosion cracking (SCC) and hydrogen embrittlement (HE), which depend on the presence of tensile stresses either applied or residual, of sufficient magnitude, may become even more possible under such thermally induced material modifications. As recently reviewed (Cragolino et al., 1999), Ni-Cr-Mo alloys with Ni content above 40 percent are resistant to SCC in concentrated chloride solutions at temperatures around 100 °C. However, the experimental data available were obtained in relatively short-term tests compared to the expected container life in the repository. As discussed, prolonged tests and more sensitive techniques for measuring crack growth rate may be required to determine a “true” threshold stress intensity for SCC. It appears that Alloy 22 in the annealed condition is not susceptible to HE, but ordered microstructures may be susceptible under certain conditions (Cragolino et al., 1999). Nevertheless, this failure mode is not considered to be as important as SCC under the oxidizing conditions expected in the unsaturated repository system proposed at Yucca Mountain.

As briefly discussed in Cragolino et al. (1999), Alloy 22 appears resistant to microbially influenced corrosion (MIC) under the environmental conditions expected to prevail in the emplacement drift after the initial thermal period when sufficient water and nutrients will become available for bacterial growth. For these reasons, no experimental work has been conducted on MIC of these Ni-Cr-Mo alloys.

The objective of this report is to present the results of experimental investigations on passive dissolution, crevice corrosion, and SCC of Alloy 22 in chloride solutions under a range of environmental conditions including temperature, chloride concentrations, and potential that could be relevant to the performance in the repository. As presented in more detail in the following sections, the experimental data are discussed in this report taking into consideration two purposes. The first purpose is to evaluate the approach adopted in the PA codes used in the VA (U.S. Department of Energy, 1998b) to consider these container degradation modes. The second purpose is to describe the approach adopted in development of the EBSFAIL module of the Total-system Performance Assessment (TPA) code Version 3.2 and to illustrate the use of experimental data as input parameters.

1.3 MODELING AND RESULTS IN THE U.S. DEPARTMENT OF ENERGY PERFORMANCE ASSESSMENT

DOE evaluated container life in TSPA-VA (U.S. Department of Energy, 1998b) using an updated version, with several enhancements for the consideration of corrosion processes, of the stochastic WASTE Package DEGRADATION (WAPDEG) Version 1.0 code (Atkins and Lee, 1996). WAPDEG is a probabilistic code designed to run stochastic simulations in which random values are sampled to represent parameters in the corrosion models for determining the WP failure time. Although DOE considered the VA design with carbon steel as an outer overpack, this discussion is focused only on the approach adopted to evaluate the corrosion behavior of the Alloy 22 inner overpack (TRW Environmental Safety Systems, Inc., 1998a).

In the absence of water dripping (only water condensation from humid air exposure), it is assumed in the TSPA-VA that Alloy 22 experiences general (or uniform) passive corrosion with rates derived from expert elicitation estimates ranging from 2×10^{-8} to 2×10^{-4} mm/yr, with a median value of 3.4×10^{-6} mm/yr, at 100 °C. Under water dripping conditions, general (or uniform) corrosion rates of Alloy 22 were also based on expert elicitation estimates. Three environmental conditions were considered: (i) a moderately oxidizing [340 mV versus standard hydrogen electrode (SHE)] environment with a pH of 3 to 10 and a probability of occurrence of 84 percent, (ii) a moderately oxidizing environment (340 mV_{SHE}) with a pH of 2.5 and a probability of occurrence of 13 percent, and (iii) a highly oxidizing environment (640 mV_{SHE}) at a pH of 2.5

with a probability of occurrence of 3 percent. These environments were assumed to form under localized corrosion sites of the outer container in the form of patches ($\sim 310 \text{ cm}^2$) even though the corrosion itself was considered to be uniform. At $100 \text{ }^\circ\text{C}$, the composite cumulative distribution of corrosion rates ranged from 1×10^{-7} to $2 \times 10^{-2} \text{ mm/yr}$, with a median value of $4 \times 10^{-5} \text{ mm/yr}$, as a result of the expert elicitation estimates. These estimated corrosion rates exhibited such a broad range of values under both dripping and no dripping conditions that they are difficult to justify in terms of experimental observations.

Pitting corrosion of Alloy 22 was also modeled on the bases of the input provided by the expert elicitation process. It was assumed that pitting corrosion of the Alloy 22 inner container did not occur below $80 \text{ }^\circ\text{C}$ as a critical pitting temperature and the probability of occurrence was uniformly distributed ranging from 0 at $80 \text{ }^\circ\text{C}$ to 1.0 at $100 \text{ }^\circ\text{C}$. The pit growth rate was assumed controlled by a diffusional process with a time dependence factor equal to $(\text{time})^{-0.5}$. The penetration (P) due to localized corrosion was then computed on the bases of data obtained at the Lawrence Livermore National Laboratory (LLNL) from long-term tests in simulated groundwaters and potentiodynamic polarization measurements in NaCl and FeCl_3 solutions and data reported by Haynes International for exposures to 10 percent FeCl_3 , using the following expression: $P \text{ (mm)} = \exp [C + Q/T + \varepsilon] t^{0.5}$. In this expression, C is a term derived from the data, which is dependent on pH, and NaCl and FeCl_3 concentrations and equal to 11.274, T is the absolute temperature, Q multiplied by the gas constant is equivalent to an activation energy of 46.13 kJ/mol, ε is a normally distributed term with a mean of zero representing uncertainties not accounted for in the correlation, and t is given in yr. The expression predicts that the localized corrosion rate will decay with time and the mean value at $100 \text{ }^\circ\text{C}$ after 1,000 yr exposure will be about $4 \times 10^{-7} \text{ mm/yr}$, whereas the highest value for the three standard deviation will be $7 \times 10^{-4} \text{ mm/yr}$. In this case, the range of corrosion rate values is extremely wide and above all, neither the mean value nor even the highest value for the three standard deviation can be considered characteristic of a localized corrosion process. On the contrary, these are values typical of dissolution under passive conditions.

On the bases of these abstracted models, the basecase results for TSPA-VA (U.S. Department of Energy, 1998b), in which dripping and no dripping conditions are included and the 50th percentile is used for the Alloy 22 corrosion rate, indicate that the first WP failure due to pit penetration occurred at about 3,000 yr and all the WPs failed in 1,000,000 yr. The mean lifetime is about 180,000 yr. However, if only dripping conditions with the 95th percentile of the corrosion rate are assumed, all WPs failed in 200,000 yr and the mean lifetime is reduced to approximately 20,000 yr. Nevertheless, one of the most important factors affecting the evaluation of the WP lifetime is the uncertainty in the corrosion rate, as recognized in the DOE sensitivity analyses. If the 95th percentile for the corrosion rate is used instead of the 50th (basecase) the mean lifetime is also reduced to approximately 20,000 yr and all the WPs failed in 200,000 yr.

Recent computations for the EDA II design, in which a Ti-grade 7 drip shield is included, exhibited a significant delay in the occurrence of the first WP failure, which occurred at about 100,000 yr (Howard, 1999). In addition, the mean WP lifetime increased to almost 400,000 yr and 90 percent of the WPs failed after 1,000,000 yr. However, similar to the calculations of the TSPA-VA (U.S. Department of Energy, 1998b), these extremely long WP lifetimes are based on limited data on corrosion rates of Alloy 22 determined using gravimetric methods under experimental conditions in which no distinction can be established between uniform or localized corrosion process.

1.4 CORROSION MODELING OF Ni-Cr-Mo ALLOYS IN NUCLEAR REGULATORY COMMISSION/CENTER FOR NUCLEAR WASTE REGULATORY ANALYSES PERFORMANCE ASSESSMENT CODES

The EBSFAIL module in TPA code Version 3.2 (Mohanty and McCartin, 1998) is used to calculate the failure times of the WPs from various corrosion processes. Above a certain critical value of RH, aqueous corrosion is assumed to occur. The aqueous environments considered in EBSFAIL are those derived, adopting several simplifications, from coupled thermal-hydrological-chemical calculations. The aqueous corrosion processes for both the outer and inner overpacks are governed by the corrosion potential and the critical potential required to initiate localized corrosion. This approach uses well-established electrochemical kinetics equations for calculating the corrosion potential, which depends on environmental variables, such as temperature, oxygen partial pressure, and pH, as well as experimentally measured values of the critical potentials.

The repassivation potential (E_p), which depends on alloy composition, temperature and chloride concentration, is the critical potential used to define the occurrence of localized corrosion. Once the corrosion potential exceeds the E_p , the initiation time for pitting corrosion is assumed to be negligible, but pit growth rates are calculated by using experimentally determined expressions and parameters. Failure of the WP is defined as penetration of both overpacks by a single pit or by general dissolution. The beneficial effect of galvanic coupling on the inner overpack is assessed through an equation that computes the couple corrosion potential using experimental values from the literature and an efficiency coefficient as an input parameter. Different container materials can be assessed by changing values of several input parameters. The coefficients of the E_p expressions, rates of uniform and localized corrosion, and threshold chloride concentration for localized corrosion can be listed, among others, as the corrosion-related input parameters for the container materials.

2 EXPERIMENTAL METHODS

2.1 SPECIMENS

The chemical compositions of Alloys 316L, 825, 625, and 22 are shown in table 2-1. Geometry and dimensions of the various specimens used in this study are shown in figure 2-1. Cylindrical rod specimens (figure 2-1a) were used in cyclic potentiodynamic polarization (CPP), passive dissolution, and potentiostatic polarization tests. They were machined to 6.3 mm (0.25 in) in diameter and 48.6 mm (1.9 in) in length. Specimens used for the crevice corrosion studies were fabricated to the dimensions shown in figure 2-1b and had an exposed surface area of approximately 20 cm².

Tests with mill annealed Alloy 22 were conducted using specimens machined from hot-rolled and annealed, 12.7-mm thick plate (heat 2277-8-3175). Tests were also conducted with Alloy 22 crevice specimens machined from two 12.7-mm thick sections (heat 2277-8-3235) that were welded across the crevice area using an Alloy 622 filler rod (heat XX1045BG11). In addition, tests were also conducted with cylindrical and creviced Alloy 22 specimens (heat 2277-8-3175), thermally aged at temperatures of 870°C for times ranging from 1 to 240 h. Prior to the start of a test, all specimens were polished to a 600 grit finish, cleaned ultrasonically in detergent, rinsed in deionized (DI) water, ultrasonically cleaned in acetone, and

Table 2-1. Chemical compositions of the materials used in this study (in weight percent)

Material (Heat Number)	Fe	Ni	Cr	Mo	W	Co	Mn	Si	S	C	Others
316L SS (P80746)	Bal.	10.04	16.35	2.07	—	—	1.58	0.49	0.018	0.014	Cu:0.27 N:0.06
825 (HH4371FG)	30.41	41.06	22.09	3.21	—	—	0.35	0.19	0.023	0.016	Cu:1.79 Ti:0.82
625 (NX9936AG)	3.96	Bal.	21.72	9.01	—	0.15	0.08	0.16	0.001	0.020	Nb:3.48 Ti:0.24
22 (2277-8-3175)	3.80	Bal.	21.40	13.60	3.00	0.09	0.12	0.030	0.002	0.004	P:0.008 V:0.15
22 (2277-8-3235)	3.94	Bal.	21.40	13.47	2.87	1.31	0.24	0.023	0.001	0.003	P:0.008 V:0.17
622 (XX1045BG11)	3.05	Bal.	20.73	14.13	3.15	0.09	0.24	0.06	0.001	0.006	Cu: 0.09 P: 0.007 V: 0.01
22 (2277-6-3193)	4.01	Bal.	21.79	13.42	2.97	1.62	0.20	0.024	0.001	0.003	P:0.008 V:0.13
22 (2277-7-3101)	5.17	Bal.	21.57	13.39	2.90	0.37	0.26	0.023	0.002	0.003	P:0.011 V:0.16

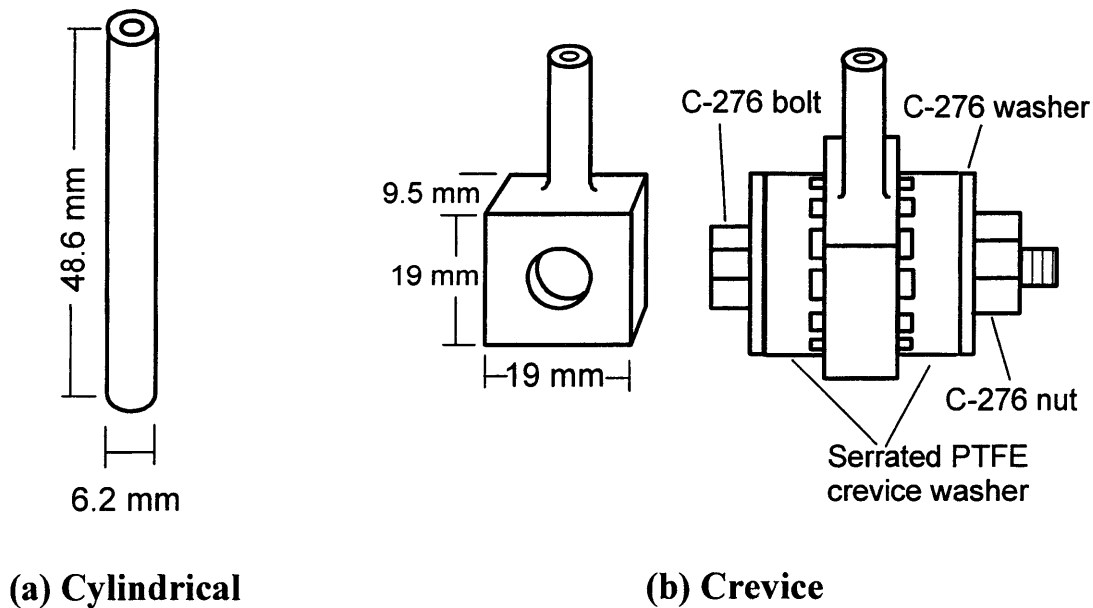


Figure 2-1. Schematic and dimensions of (a) cylindrical specimens (b) crevice corrosion specimens

dried. Crevice corrosion specimens were fitted with two polytetrafluoroethylene (PTFE) crevice forming washers held with insulated Alloy C-276 hardware. At the completion of each test, the specimens were rinsed in DI water and dried. Most specimens were cleaned ultrasonically in an inhibited hydrochloric acid (HCl) solution that contained 4 mL of 2-butyne-1,4-diol (35 percent aqueous solution) and 3 mL of concentrated HCl. A post-test visual examination was performed with an optical microscope and a scanning electron microscope (SEM).

SCC tests were conducted using wedge-loaded double cantilever beam (DCB) specimens. Alloy 22 specimens were machined from hot-rolled and annealed plates, 12.7 mm (heat 2277-6-3193) and 25.4 mm (heat 2277-7-3101) in thickness. The 12.7-mm plate was used for specimens with long transverse-longitudinal direction (T-L) orientation where the crack plane is perpendicular to the width direction (T direction) and the crack propagation is in the longitudinal rolling direction (L direction). The 25.4-mm plate was used for the S-L orientation specimens where the fracture plane is perpendicular to the short transverse direction (S direction) and the crack propagation is also in the L direction (American Society for Testing and Materials, 1999a). Type 316L (heat P80746) DCB specimens with a T-L orientation were machined from a 12.7-mm thick plate. Specimen dimensions, according to NACE International TM0177-90 (NACE International, 1990), are shown in figure 2-2.

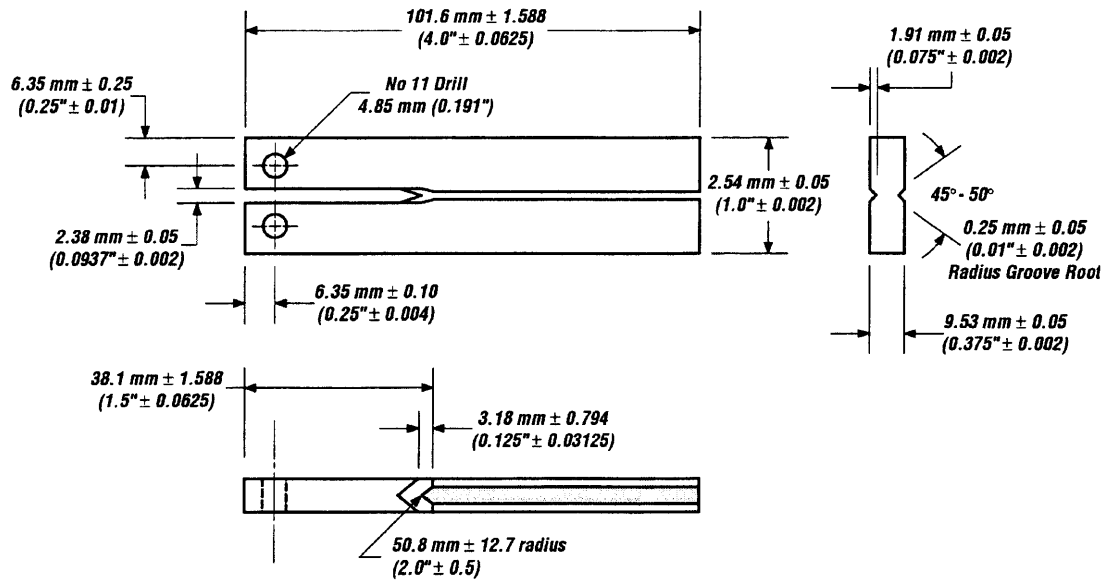


Figure 2-2. Dimensions of the double cantilever beam specimen according to NACE TM0177-90 (NACE International, 1990)

2.2 TEST METHODS

2.2.1 Passive Corrosion Rate Tests

Passive dissolution rates of Alloy 22 specimens were measured in solutions containing 0.028 to 4.0 M chloride under potentiostatic polarization. Tests were conducted in a 2-L glass cell with a PTFE lid. The cells were fitted with a water-cooled Allihn-type condenser and a water trap to minimize solution loss at elevated temperatures and air intrusion. A saturated calomel electrode (SCE) was used as a reference electrode in all experiments. The SCE was connected to the solution through a water-cooled Luggin probe with a porous silica tip so that the reference electrode was maintained at room temperature. A platinum flag was used as a counter electrode. All solutions were deaerated with high-purity nitrogen (99.999 percent) for a period of at least 24 h prior to the start of the tests in order to obtain accurate anodic current density measurements at potentials ranging from -200 to 800 mV_{SCE}. Specimens were held potentiostatically for a period of 2 d while the anodic current density was recorded. An EG&G Princeton Applied Research (PAR) VersaStat potentiostat controlled by a personal computer running the PAR Model 352 Corrosion Software was used to perform the anodic current density measurements. The resolution of the system was determined to be 1.25×10^{-10} A/cm². At the conclusion of the test, the specimens were reweighed and examined microscopically for signs of corrosion.

2.2.2 Repassivation Potential Tests

Repassivation potentials were determined on specimens with artificially formed crevices using CPP tests (Dunn et al., 1999). The CPP test procedure is similar to that given in ASTM Standard G61 (American Society for Testing and Materials, 1999b), which involves scanning the potential applied to the specimen and monitoring the current response. CPP testing was performed using potentiostats controlled by a personal computer. The CPP scans were conducted in deaerated solutions using a scan rate of 0.167 mV/s. The scans were reversed at a current density of 5 mA/cm². Standard test cells were used for tests conducted at 60 and 95 °C. The test cells were equipped with a platinum counter electrode and a SCE used as a reference and maintained at room temperature. Solutions contained 1.6 × 10⁻⁴ to 4 M NaCl, 85 ppm HCO₃⁻, 20 ppm SO₄²⁻, 10 ppm NO₃⁻, and 2 ppm F⁻, added as sodium salts. Additional tests were conducted in 9 and 11 M LiCl.

High-temperature CPP tests of Alloy 22 specimens equipped with PTFE crevice washers were conducted at temperatures ranging from 95 to 175 °C in a 316L SS autoclave with a PTFE liner. The autoclave was equipped with a platinum counter electrode and an internal Ag/AgCl (0.1 M KCl) reference electrode. For comparison, all potential values were converted to the SCE scale at 25 °C. At the conclusion of each CPP test, the Ag/AgCl reference electrode was checked versus an SCE in order to monitor the reference electrode performance. Tests were conducted in deaerated solutions containing 0.5, 1, and 4 M NaCl along with minor additions of NaHCO₃, Na₂SO₄, NaNO₃, and NaF as previously described.

2.2.3 Stress Corrosion Cracking Tests

The SCC tests were conducted according to NACE Standard DCB Test TM0177-90 (NACE International, 1990) using a crack-arrest type fracture mechanics method for measuring the susceptibility of metals to SCC. Stress calculations were performed assuming that the DCB specimen was a straight beam subjected to pure bending. The bending stress of the DCB specimen arm at the crack tip can be calculated according to Eq. (2-1) (Crandall et al., 1978):

$$\sigma = \frac{My}{I} \quad (2-1)$$

where M is the bending moment, y is the half specimen height, and I is the moment of inertia. For the DCB specimen geometry

$$M = P \cdot a \quad (2-2)$$

$$y = \frac{h}{2} \quad (2-3)$$

and

$$I = \frac{1}{12}bh^3 \quad (2-4)$$

where P is the wedge load, a is crack length, h is specimen height, and b is specimen thickness. Substituting Eqs. (2-2), (2-3), and (2-4) into Eq. 2-1 yields

$$\sigma = \frac{6Pa}{bh^2} \times 10^{-6} \quad (2-5)$$

where σ is in MPa, P is in Newtons, and a, b, and h are in meters.

The initial stress intensity, K_I , for the side grooved DCB specimen can be expressed as follows (Heady, 1977; NACE International, 1990):

$$K_I = \frac{Pa(2\sqrt{3} + 2.38h/a)(b/b_n)^{1/\sqrt{3}}}{bh^{3/2}} \quad (2-6)$$

where b_n is the net thickness of the specimen at the side grooves.

The DCB specimens, shown in figure 2-2, were used in an attempt to strictly duplicate the test conditions reported by Roy et al. (1998) and McCright (1998). However, the following discrepancies were noted between the work at LLNL and the recommended test procedures (ASTM E399-90) for fracture mechanics type specimens.

- The initial crack length used by Roy et al. (1998) was 29.6 mm. This appears to be too short and would not extend past the chevron notch of the fracture surface. Generally the crack length to specimen length (a/w) ratio of 0.45 to 0.55 is specified as the starting condition. In contrast, the initial crack length used by Roy et al. (1998) gives an a/w ratio of 0.31.
- Roy et al. (1998) reported K_I values of 35.3 to 42.2 MPa·m^{1/2} for Alloy 22 DCB specimens. Initial calculations based on Eqs. (2-1) to (2-6) indicate that with an a/w ratio of 0.31, plastic deformation of the DCB specimen arms would occur at approximately 40 MPa·m^{1/2}.

In this investigation, tests were conducted using DCB specimens with the same dimensions as those used by Roy et al. (1998); however, as a result of the apparent discrepancy between the LLNL procedure and ASTM E399-90, the initial conditions used in this investigation were not identical to those used at LLNL. The DCB specimens were fatigue-precracked under load control at 20 Hz, with a load ratio of 0.10 and a maximum stress intensity of 19.6 MPa·m^{1/2} for Alloy 22 and 17.6 MPa·m^{1/2} for type 316L SS. Compliance curves were measured during precracking and prior to wedge loading. The initial crack length for all specimens was approximately 32.8 mm. Double-tapered wedges made of the same material as the specimens were used to load the specimens to the selected stress intensities. An initial stress intensity of 25.0 MPa·m^{1/2} was selected for type 316L SS specimens. Alloy 22 specimens were tested using a stress intensity of 32.7 MPa·m^{1/2}. The selection of these initial conditions was based on calculations of K_I and the DCB arm bending stress using Eqs. (2-1) to (2-6). The calculated bending stress at crack tip versus crack length for different loads is shown in figure 2-3, and K_I versus crack length for different loads is shown in figure 2-4. The relationship between K_I and bending stress is shown in figure 2-5. The yield strength of Alloy 22 is 344 MPa. For a crack length of 32.8 mm, an initial loading of 2,482 N is required to achieve a K_I value of 34.8 MPa·m^{1/2} (figure 2-4). Under these loading conditions, the bending stress at the crack tip is 317 MPa (see

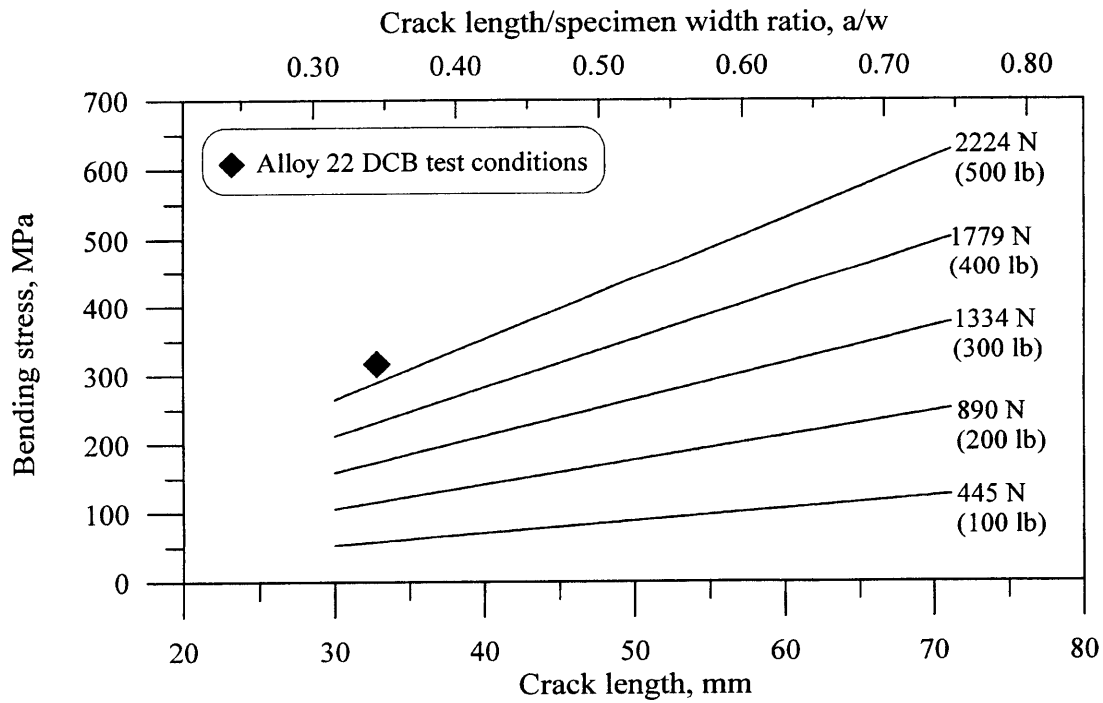


Figure 2-3. Bending stress versus crack length (and crack length/width ratio) curves for various loads for double cantilever beam specimen

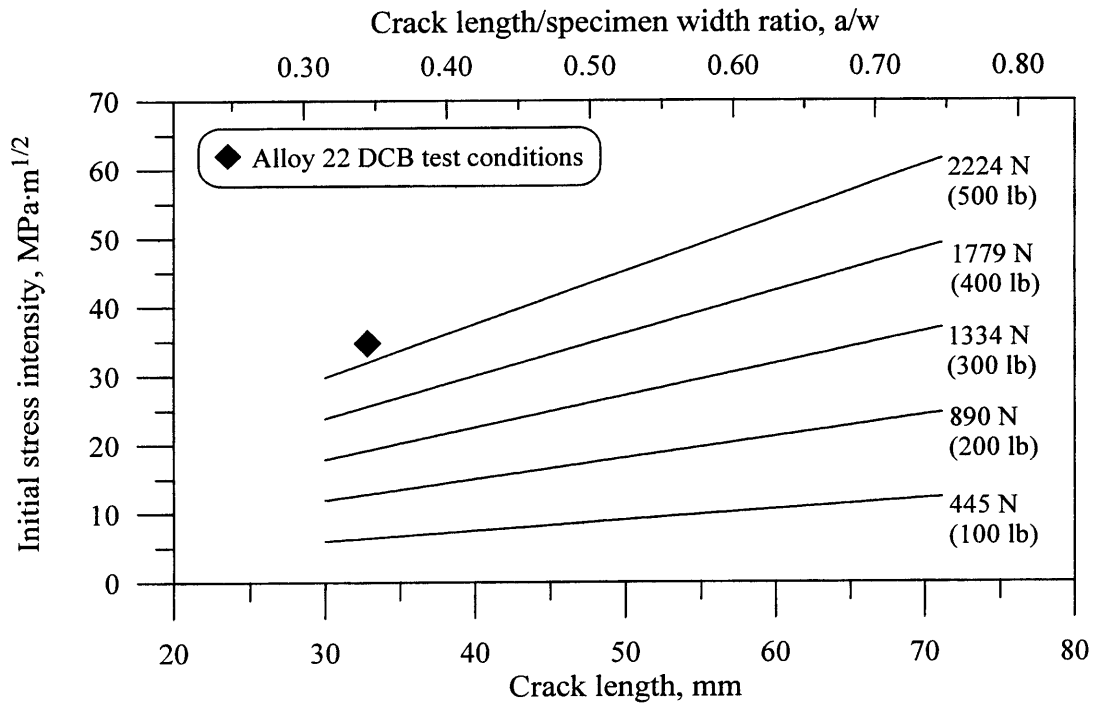


Figure 2-4. Initial stress intensity versus crack length (and crack length/width ratio) curves for various loads for double cantilever beam specimen

figures 2-3 and 2-5), which is close to the yield strength of Alloy 22. In order to avoid plastic deformation, it is apparent from the calculations shown in figures 2-3 through 2-5 that, with a crack length of 32.8 mm, the maximum initial stress intensity for the Alloy 22 DCB specimens is $38 \text{ MPa}\cdot\text{m}^{1/2}$.

All SCC tests were conducted in 2-L test cells equipped with a fritted gas bubbler, platinum counter electrode, temperature probe, and a water cooled Luggin probe with a SCE used as a reference maintained at room temperature. Specimens were connected to a computer controlled multichannel potentiostat. The SCC susceptibility of both type 316L SS and Alloy 22 was evaluated in 5 weight percent NaCl solutions (0.9 M chloride) at 90°C and in 30 and 40 weight percent MgCl_2 solutions (9.1 and 14.0 M chloride) at 110°C under open-circuit conditions. The tests in 5 percent NaCl solutions, acidified to pH 2.7 by the addition of HCl, were purged with high-purity N_2 gas to remove the dissolved oxygen and duplicate the test conditions reported by Roy et al. (1998). In addition, a series of SCC propagation tests on type 316L SS were conducted in 30 weight percent MgCl_2 solutions at 110°C under potentiostatic conditions to measure crack growth rates as a function of potential.

The specimens were periodically removed from the test cells and inspected with an optical microscope at low magnification. A 2-wk inspection interval was used initially for the Alloy 22 specimens and for the type 316L SS exposed to acidified NaCl solution, but it was later extended to approximately 1 mo. SEM photographs were used to document the starting condition of the specimens and changes in surface features and/or signs of cracking. Comparisons of the crack tip morphology prior to exposure and after each exposure interval were used to assess SCC propagation. At the end of each test, the wedge was removed by loading the specimen in a servo-hydraulic load frame. A clip gage, installed to measure crack opening

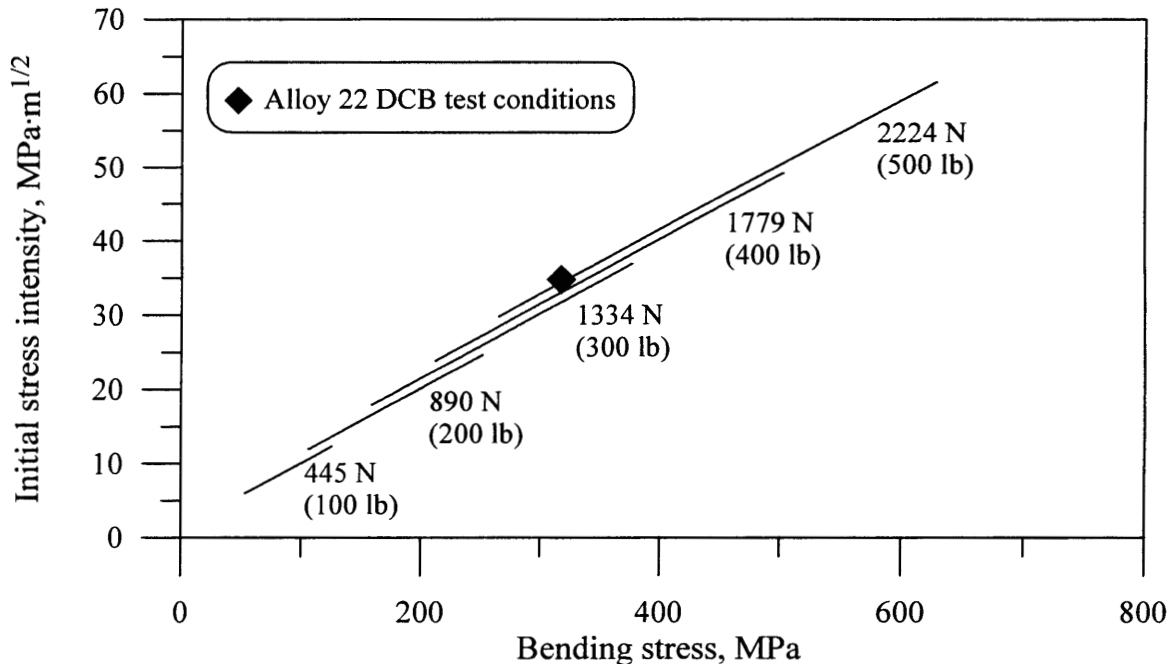


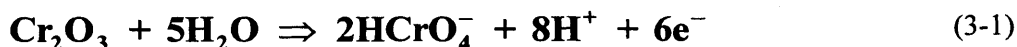
Figure 2-5. Initial stress intensity versus bending stress relations for various loads for double cantilever beam specimen

displacement, was used for the final compliance measurement. The final wedge load was also determined. The stress at which the crack is arrested, expressed in terms of a threshold stress intensity, K_{ISCC} , can then be calculated. Specimens were then heat-treated at 371 °C for 2.5 h in an air atmosphere furnace and broken open to reveal the fracture surfaces. Examination of the fracture surfaces with the SEM was used to determine the final crack length.

3 RESULTS

3.1 PASSIVE CORROSION OF ALLOY 22

A CPP curve for as-received Alloy 22 in 1,000 ppm chloride solution at pH 8 and 95 °C is shown in figure 3-1. The CPP was obtained by slowly increasing the potential in the anodic direction and measuring the current response. The direction of the scan was reversed when the current density reached 5 mA/cm². The corrosion potential (E_{corr}), passive, and transpassive regions are identified. The passive range corresponds to very slow dissolution of the alloy through production of metal cations and the formation of a chromium-rich oxide film (Cr_2O_3). Passive corrosion occurs at potentials lower than those corresponding to the initiation of transpassive dissolution. The transpassive region is related to the dissolution of the Cr_2O_3 in the film according to the following equation.



Transpassive dissolution may coexist with or precede the evolution of oxygen produced by the electrolytic oxidation of water. A hysteresis loop in the CPP scan, such as that shown in figure 3-1, is often an indication that localized corrosion was initiated on the specimen. For the CPP scan in figure 3-1, the hysteresis does not indicate localized corrosion, but transpassive dissolution given by Eq. (3-1).

The passive corrosion current density in this scan varied from 10^{-8} to 4×10^{-6} A/cm². However, it must be noted that the passive corrosion rates in CPP scans are measured while the potential is slowly increasing. As a result of the non steady-state measurement conditions, CPP scans can greatly overestimate the passive corrosion rates.

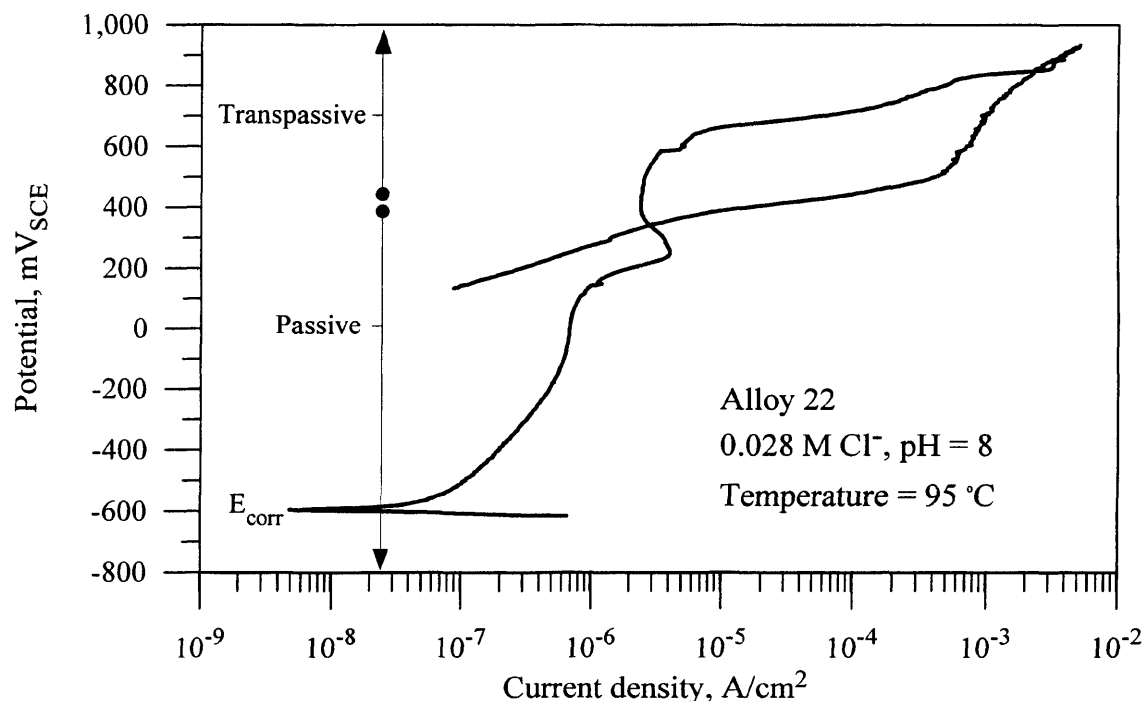


Figure 3-1. Cyclic polarization of Alloy 22 in deaerated 0.028 M chloride showing the corrosion potential, passive, and transpassive regions

Potentiostatic current transients obtained from as-received Alloy 22 specimens at various anodic potentials in 4 M chloride solutions are shown in figure 3-2. After the initial potentiostatic step, the anodic current density decreased with time at both 400 and 600 mV_{SCE}, exhibiting passive behavior. The steady-state current density after 40 h of polarization at 400 mV_{SCE} was approximately 3×10^{-8} A/cm². At the conclusion of the test the specimen was removed and examined. No evidence of localized corrosion was observed; however, the specimen was covered with a tightly adherent gold colored film. The steady-state current density increased to 7×10^{-8} A/cm² at 600 mV_{SCE}. Again, no localized corrosion was observed and a dark gold colored film covered the surface. The small anodic current spikes observed at 400 and 600 mV_{SCE} are likely to be rapid localized corrosion initiation and repassivation events. Since inspection of the specimen following the potentiostatic test did not reveal any pitting corrosion, it is apparent that the oxide film breakdown events did not propagate. The shape of the transient and the high anodic current density observed at 800 mV_{SCE} was a result of transpassive dissolution. Post test examination revealed that the specimen was covered with loosely adherent black and green corrosion products and some etching of the grain boundaries was observed. Steady-state anodic current densities for the dissolution of Alloy 22 are shown in figure 3-3 as a function of potential, chloride concentration, and pH. Passive corrosion was observed for all test conditions when the applied potential was not greater than 400 mV_{SCE}. The higher anodic current density observed at 600 mV_{SCE} in 4 M chloride at pH 2.7 may be related to the formation and repassivation of incipient pits. At pH 8, significant transpassive dissolution was observed in 0.028 or 4 M chloride at potentials of 800 mV_{SCE}.

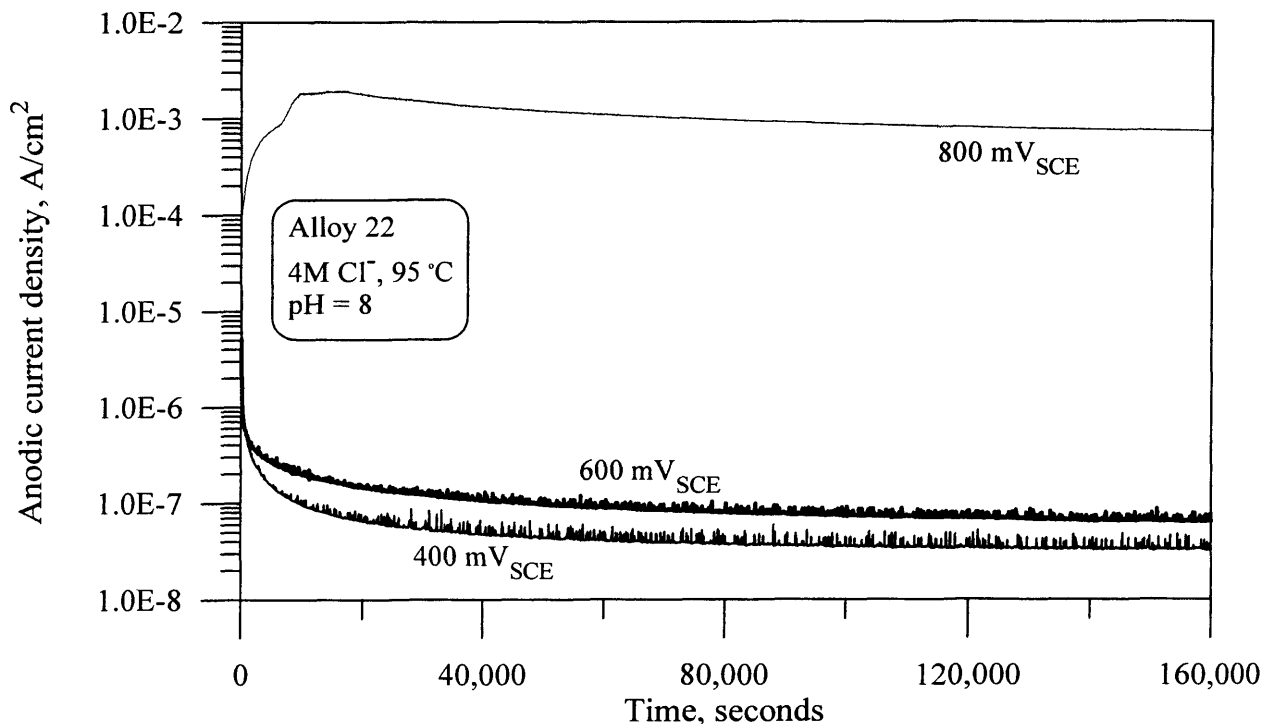


Figure 3-2. Anodic current transients measured for Alloy 22 specimens under potentiostatic conditions in deaerated 4 M chloride, pH 8.0, at 95 °C

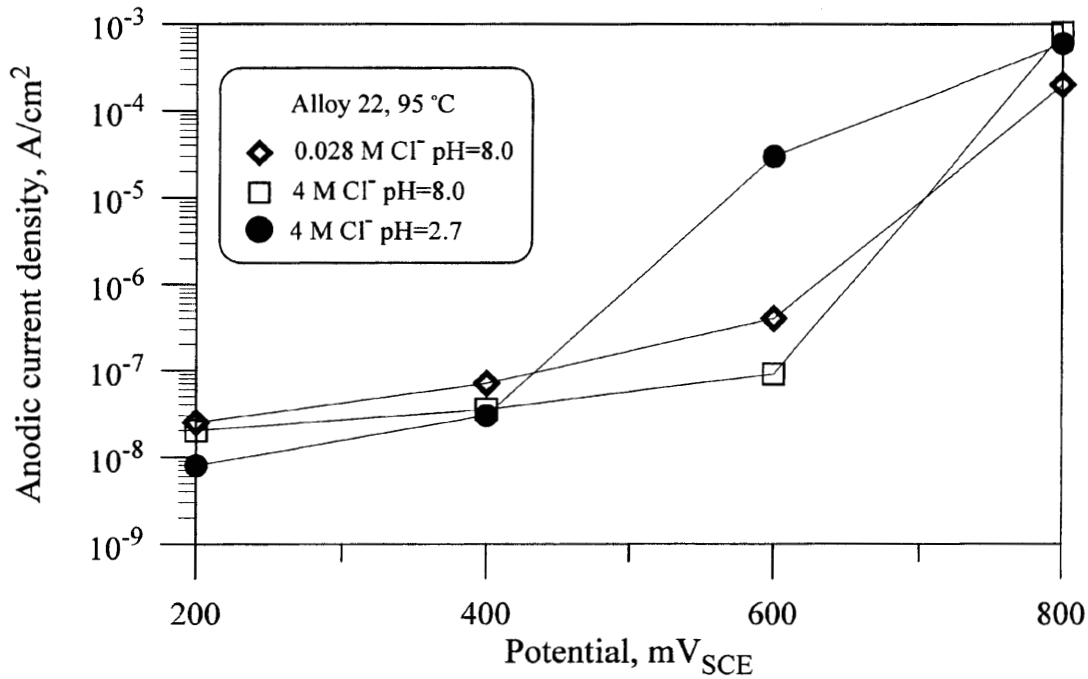


Figure 3-3. Anodic current density measured for Alloy 22 under potentiostatic conditions

Corrosion rates, shown in table 3-1, were calculated using Eq. (3-2)

$$CR \text{ (mm / yr)} = \frac{K i_{\text{corr}} EW}{\rho} \quad (3-2)$$

where i_{corr} is the passive corrosion current density in A/cm^2 , EW is the equivalent weight, K is a conversion factor ($3,270 \text{ mm} \cdot \text{g} \cdot \text{A}^{-1} \cdot \text{cm}^{-1} \cdot \text{yr}^{-1}$) and ρ is the density in g/cm^3 . For Alloy 22, ρ is 8.69 g/cm^3 . Assuming congruent dissolution of the major alloying elements as Ni^{2+} , Cr^{3+} , Mo^{3+} , Fe^{2+} , and W^{4+} , the EW for Alloy 22 is $26.04 \text{ g/equivalent}$ (American Society for Testing and Materials, 1999c). At 200 and 400 mV_{SCE} , the passive current was in the range of 1×10^{-8} to $3 \times 10^{-8} \text{ A/cm}^2$ and was relatively independent of the chloride concentration and solution pH. The increase in the anodic current density observed at pH 0.7 at an applied potential of 400 mV_{SCE} may be a result of oxide film dissolution in the acidic solution. Temperature, on the other hand, had a significant effect on the passive corrosion rate in dilute chloride solutions. The passive corrosion rate increased by a factor of 10 when the temperature of the 0.028 M chloride solution (pH 8.0) was increased from 20 to 95 °C. However, practically no temperature effect was noted in the 4 M chloride at pH 8.0.

Potentiostatic anodic current transients for Alloy 22 specimens thermally aged 4 h at 870 °C are shown in figure 3-4. The temperature of 870 °C was selected because the formation of secondary phases in Alloy 22 occurs most rapidly in the range of 800 to 900 °C (Heubner et al., 1989). At -200 mV_{SCE} , the anodic dissolution current is close to $8 \times 10^{-8} \text{ A/cm}^2$ at the start of the test and decreases below the resolution limit of the instrument after 20 h. Several large anodic current spikes were also observed suggesting a periodic

Table 3-1. Passive corrosion rates for Alloy 22 calculated from passive current density measured under potentiostatic conditions

Chloride Concentration (M)	pH	Solution Temperature (°C)	Potential (mV _{SCE})	Anodic Current Density (A/cm ²)	Corrosion Rate (mm/yr)
0.028	8.0	20	200	1.2×10^{-9} to 2.8×10^{-9}	1.2×10^{-5} to 2.7×10^{-5}
0.028	8.0	95	200	2.0×10^{-8} to 4.0×10^{-8}	1.9×10^{-4} to 3.9×10^{-4}
0.028	0.7	95	200	6.0×10^{-8} to 9.0×10^{-8}	5.9×10^{-4} to 8.8×10^{-4}
0.028	0.7	95	400	1.1×10^{-7} to 1.3×10^{-7}	1.0×10^{-3} to 1.2×10^{-3}
1.0	8.0	95	200	9.0×10^{-9} to 2.4×10^{-8}	8.8×10^{-5} to 2.3×10^{-4}
4.0	2.7	95	200	5.0×10^{-9} to 7.0×10^{-9}	4.9×10^{-5} to 6.9×10^{-5}
4.0	2.7	95	400	2.6×10^{-8} to 4.0×10^{-8}	2.5×10^{-4} to 3.9×10^{-4}
4.0	8.0	20	200	1.1×10^{-8} to 2.0×10^{-8}	1.1×10^{-4} to 1.9×10^{-4}
4.0	8.0	95	0	9.0×10^{-9} to 2.0×10^{-8}	8.8×10^{-5} to 1.9×10^{-4}
4.0	8.0	95	200	1.2×10^{-8} to 4.0×10^{-8}	1.2×10^{-4} to 3.9×10^{-4}
4.0	8.0	95	400	3.2×10^{-8} to 5.4×10^{-8}	3.1×10^{-4} to 5.3×10^{-4}
Low Dissolution Rate in TPA code Version 3.2				6.0×10^{-8}	5.9×10^{-4}
High Dissolution Rate in TPA code Version 3.2				2.0×10^{-7}	1.9×10^{-3}

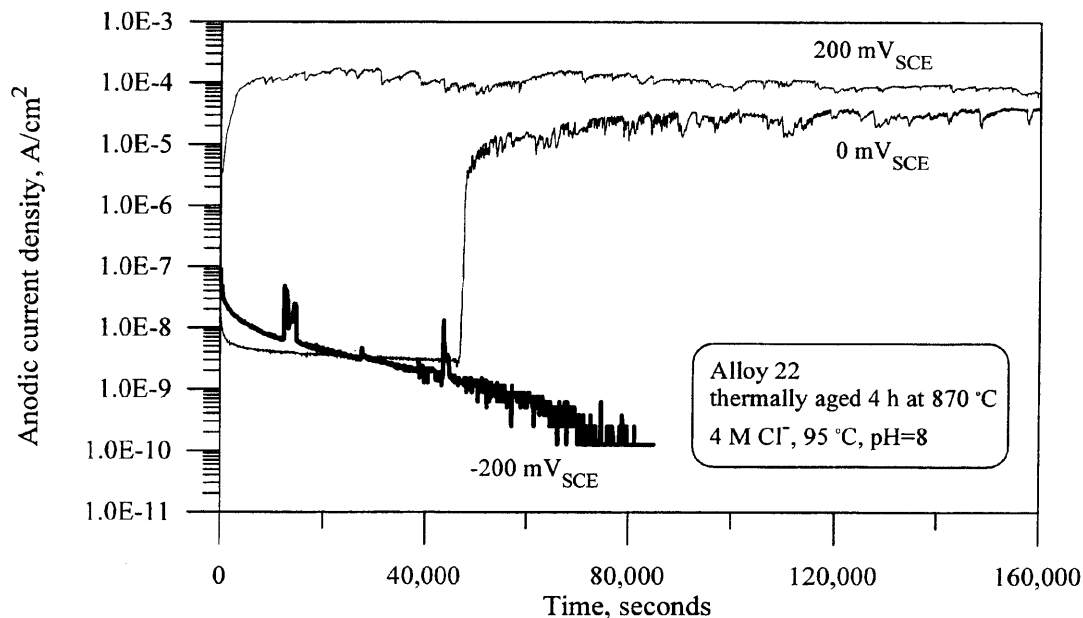


Figure 3-4. Anodic current transients measured for Alloy 22 specimens thermally aged 4 h at 870 °C under potentiostatic conditions in deaerated 4 M chloride, pH 8.0, at 95 °C

increase in the dissolution rate for the aged specimens. A slightly lower initial anodic dissolution current density was measured when the specimen was polarized to 0 mV_{SCE}. However, after 12 h, the anodic current density sharply increased to over 10⁻⁵ A/cm². Significant intergranular corrosion was observed at the specimen/PTFE gasket. Similar results were obtained at 200 mV_{SCE} with the exception that the initiation time for intergranular corrosion was much shorter. Intergranular corrosion was only observed on a small surface area of the specimen. Note that in figure 3-4 the dissolution current is normalized to the entire exposed surface area. As a result, the anodic current density in the areas where intergranular corrosion occurred is actually greater than that depicted in figure 3-4. Similar results were obtained for specimens thermally aged for longer times. The initiation of intergranular corrosion at potentials lower than 200 mV_{SCE} was inconsistent and significant variations were observed in the measured anodic dissolution current densities among different specimens. When no intergranular corrosion was initiated, the anodic current density was similar to that measured for mill annealed specimens. Increasing the potential and the thermal aging time resulted in the appearance of numerous anodic current spikes indicating highly variable corrosion rates. Grain boundary etching and incipient intergranular corrosion were noted on these specimens whereas severe intergranular attack was observed on all specimens where the anodic current density was greater than 10⁻⁵ A/cm².

Potentiostatic anodic current transients were also measured on welded Alloy 22 specimens. These specimens have a significantly larger surface area compared to the cylindrical specimen used for the majority of the passive corrosion tests. Approximately one-fourth of the total exposed specimen surface area (20 cm²) was weldment. All of the corners and edges were rounded prior to testing in order to prevent preferential attack in these areas. The results of anodic dissolution rate measurements of the welded specimen are shown in figure 3-5. An anodic passive dissolution current density of 3 × 10⁻⁸ A/cm² was measured at 200 mV_{SCE} which was similar to the passive current density measured for the base alloy. This increased to 5 × 10⁻⁸ A/cm² at 400 mV_{SCE} and 7 × 10⁻⁸ A/cm² at 600 mV_{SCE}. Many small anodic spikes were also observed in the anodic current transient at 600 mV_{SCE}. Examination of the specimens following the exposures revealed no localized

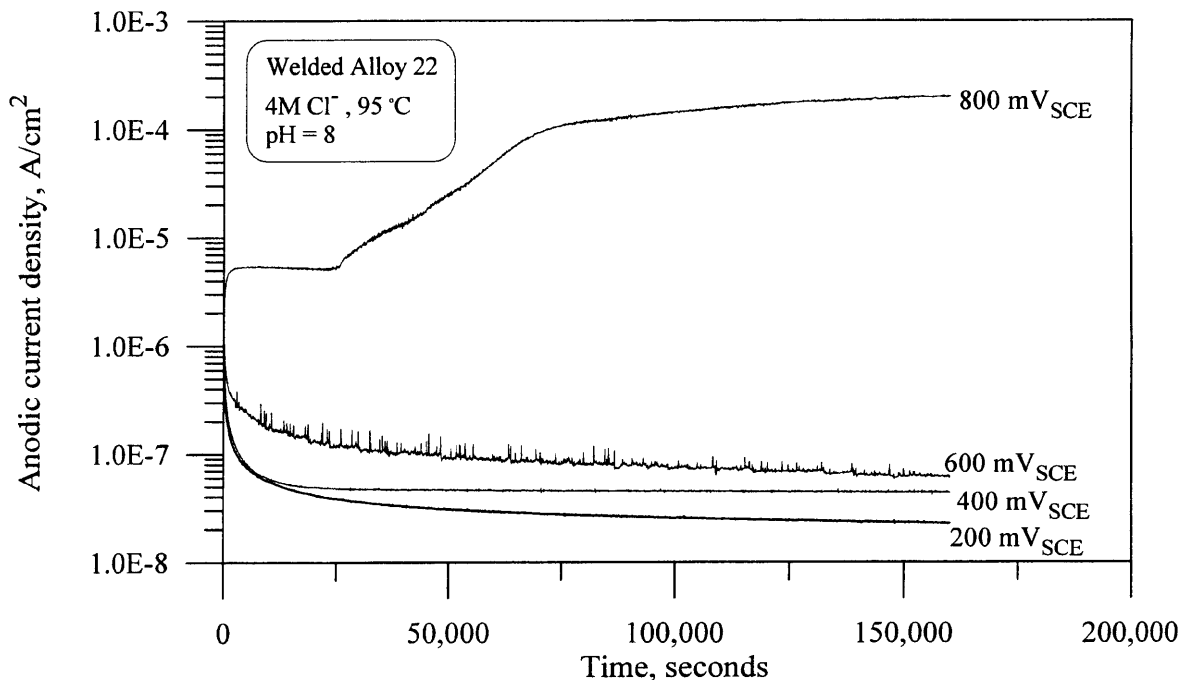


Figure 3-5. Anodic current transients measured for welded Alloy 22 specimens under potentiostatic conditions in deaerated 4 M chloride, pH 8.0, at 95 °C

attack or grain boundary etching on either the base metal or the weldments. At 800 mV_{SCE}, the anodic current density was initially 5×10^{-6} A/cm². After 7 h, the current density rapidly increased to over 10^{-4} A/cm². Post test examination of the specimen revealed preferential attack in the weld region that exposed the weld microstructure; however, no intergranular corrosion was observed.

3.2 LOCALIZED CORROSION

The effect of anions, other than chloride, as well as Mg²⁺ cations on the localized corrosion of candidate container materials has been reviewed by Sridhar et al. (1995). Slight inhibition of localized corrosion was observed in the sequence of decreasing inhibition $\text{NO}_3^- > \text{SO}_4^{2-} > \text{HCO}_3^-$ for type 316L SS in 1,000 ppm chloride at 95 °C. The inhibitive effects of these anions were similar for Alloy 825 although this alloy, more than type 316L SS, is resistant to localized corrosion in 1,000 ppm chloride. In addition, the inhibition of short-term pit initiation was observed but none of the anions were observed to increase the repassivation potential for localized corrosion. While the effects of these anions on localized corrosion of Alloy 22 were not examined specifically, based on previous results on Alloy 825, they are considered to be of secondary importance. These anions are not expected to accelerate localized corrosion of Alloy 22. On the other hand, the chloride concentration and temperature were found to have a significant effect on the localized corrosion susceptibility of several candidate container materials. Laboratory investigations have focused on evaluating the localized corrosion susceptibility of Ni-Cr-Mo alloys by measuring the repassivation potential for pitting, E_{rp} , and crevice corrosion, E_{rcrev} , as a function of chloride concentration and temperature. In some cases, chloride concentrations greater than those corresponding to the solubility of NaCl were used (e.g., LiCl solutions) in order to establish correlations and improve the mechanistic understanding of localized corrosion and repassivation.

Since crevice corrosion was previously found to be preferentially initiated on Ni-Cr-Mo-Fe alloys (Sridhar et al., 1995), tests were conducted to measure the E_{rcrev} on Alloys 625 and 22. The E_{rcrev} is the potential at which crevice corrosion ceases and a protective passive film is formed over the previously actively corroding areas on the alloy surface. At potentials below the E_{rcrev} , passive corrosion of the alloy occurs at a slow rate. The E_{rcrev} values for Alloy 625 are shown in figure 3-6. The E_{rcrev} was greater than 500 mV_{SCE} in 4 M NaCl solutions at 60 °C. Crevice corrosion was observed on 5 to 8 of 24 possible locations. The depth of attack in these locations was shallow, ranging between 10 and 30 μm. For higher chloride concentrations, the E_{rcrev} decreased by more than 700 mV to values of -255 mV_{SCE} in 9 M LiCl and -275 mV_{SCE} in 11 M LiCl. At 95 °C, a large decrease in E_{rcrev} was observed when the chloride concentration was greater than 0.028 M and large variations in the value of E_{rcrev} were measured when the chloride concentrations were less than 4 M. Examination of the specimens revealed that the severity of crevice corrosion increased with chloride concentration. The four specimens tested in 4 M NaCl all had severe crevice corrosion attack with penetration depths exceeding 100 μm. There was no effect of pH which was either 2.5 or 8.0. In the concentrated LiCl solutions (pH 5.6), crevice corrosion was initiated and spread over a large fraction of the specimen surface. As a result, the localized attack was shallow.

Values of E_{rcrev} measured for Alloy 22 as a function of chloride concentration at 95 °C are shown in figure 3-7. Specimens exhibiting crevice corrosion are clearly indicated by filled symbols whereas open symbols represent specimens that did not show localized corrosion. For comparison, figure 3-7 shows the E_{rcrev} as a function of chloride concentration for other Ni-Cr-Mo-Fe alloys (Sridhar et al., 1995; Dunn et al., 1999). At chloride concentrations less than 10^{-4} M, no localized attack was initiated on the test specimens and the measured E_{rcrev} values were highly variable. When the chloride concentration was

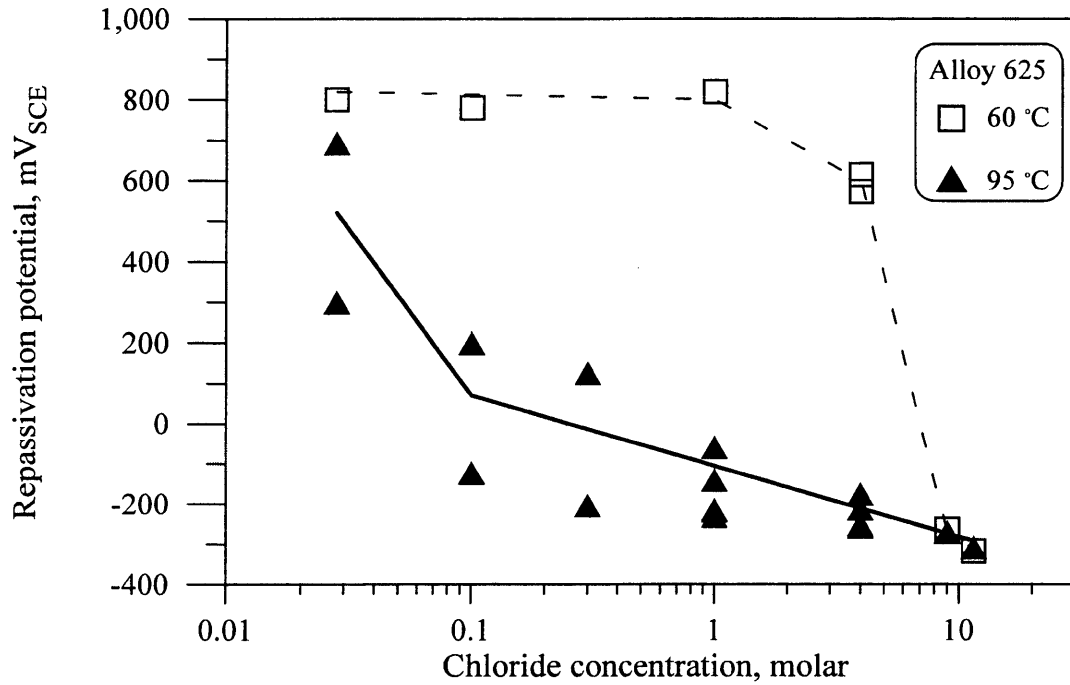


Figure 3-6. Crevice corrosion repassivation potentials for Alloy 625 as a function of chloride concentration and temperature

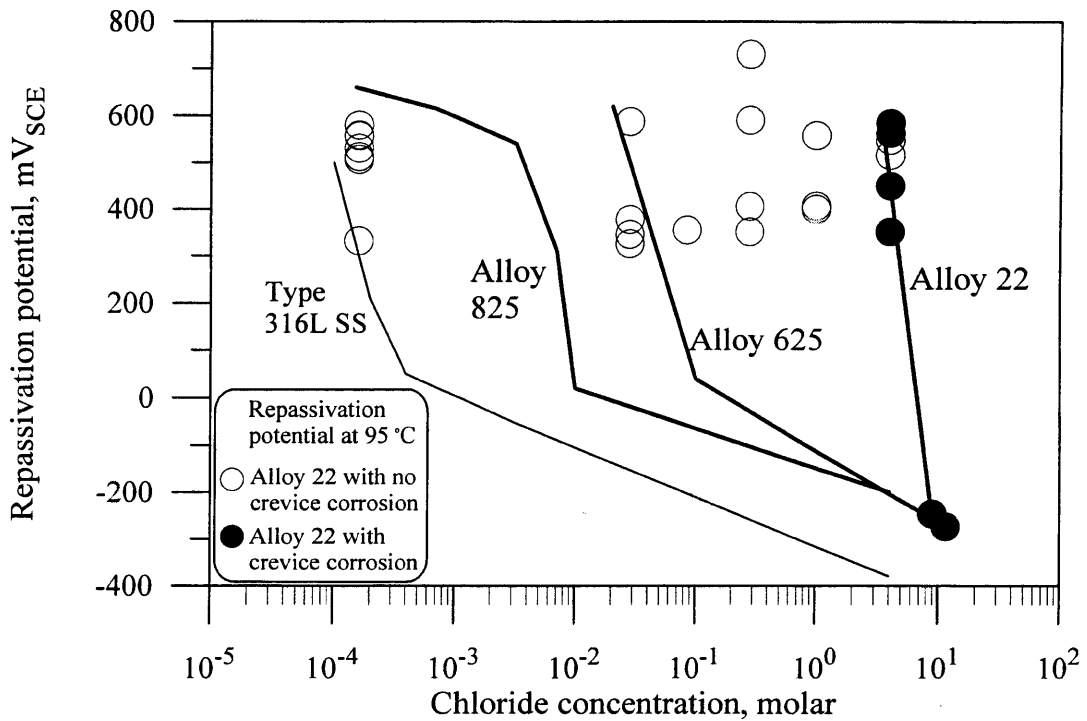


Figure 3-7. Crevice corrosion repassivation potentials for Alloys 316L SS, 825, 625, and 22 as a function of chloride concentration

increased above 10^{-4} M, localized corrosion of type 316L SS was observed and the measured E_{rcrev} values for this alloy were found to be a strong function of chloride concentration. At even higher chloride concentrations, E_{rcrev} exhibits the typical linear dependence on the logarithm of chloride concentration reported many times for pitting initiation (Szklańska-Smiałowska, 1986). Similar behavior was observed for the other alloys at higher chloride concentrations. For each alloy, there was a critical chloride concentration below which the alloy was very resistant to localized corrosion, as indicated by high E_{rcrev} values and the inconsistent initiation of localized corrosion, and above which severe localized corrosion was observed. The major difference in the performance of the alloys was that no localized corrosion was observed on Alloy 22 specimens at chloride concentrations less than 4 M, which is close to the solubility of NaCl at 95 °C. As shown in figure 3-7, the E_{rcrev} of Alloy 22 decreased by more than 500 mV and was virtually the same as the Alloy 625 only in LiCl solutions (9 and 11 M chloride).

The pH of the solution did not affect the E_{rcrev} measured for Alloy 22 when localized corrosion was initiated. In the absence of localized corrosion, the intersection of the forward and reverse scans during CPP tests indicates the transpassive dissolution potential, E_{tpd} , and are shown in figure 3-7 as open circles. A wide range of apparent E_{tpd} values are shown in figure 3-7 for 0.28 M chloride solution that are replotted in figure 3-8 as a function of solution pH. It is evident that there is a linear relationship between E_{tpd} and pH especially when the solution pH is less than 5.0. This result suggests that, when no localized corrosion is initiated, the potential at which transpassive dissolution occurs is dependent on pH. The regression line in figure 3-8 has a slope of -94 mV/pH which is close to the theoretical value of -87 mV/pH calculated by Lee (1981) at 100 °C for the transpassive dissolution of Cr_2O_3 , according to Eq. (3-1).

Measurements of the E_{rcrev} for Alloy 22 conducted in autoclaves at temperatures from 95 to 175 °C, are shown in figure 3-9. The E_{rcrev} was found to be a strong function of temperature. In 0.5 M NaCl, the E_{rcrev} is 250 mV_{SCE} at 95 °C and decreased to -100 mV_{SCE} when the temperature was increased to 125 °C. Further

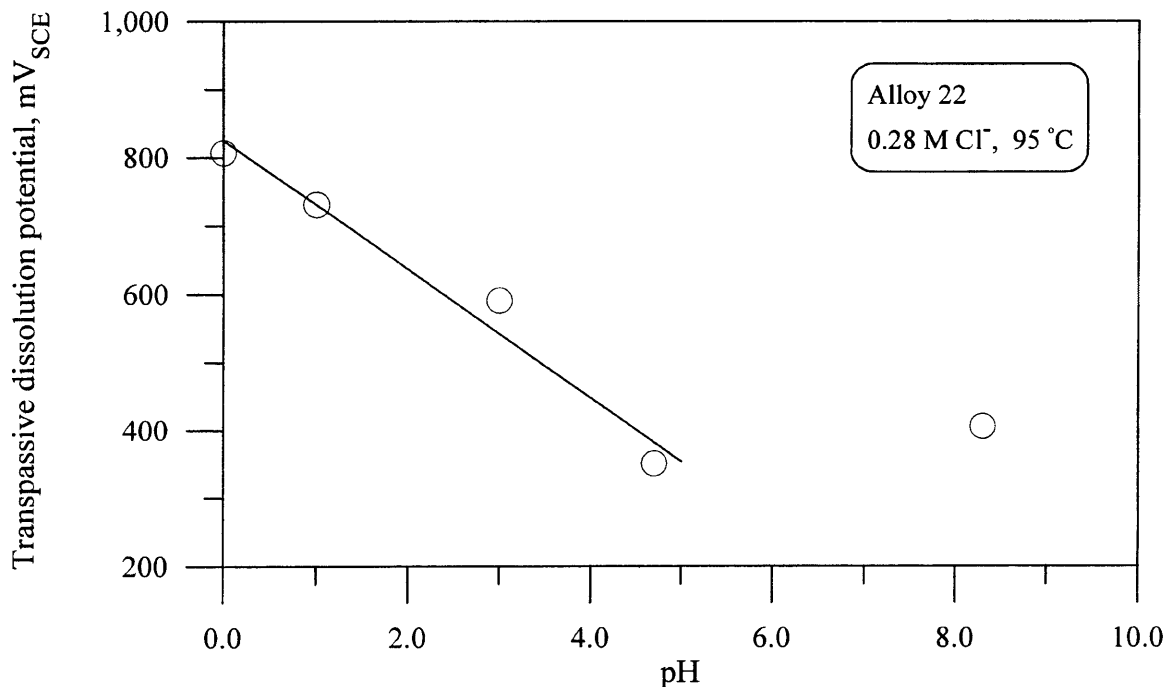


Figure 3-8. Transpassive dissolution potential of Alloy 22 as a function of pH in 0.28 M chloride solution

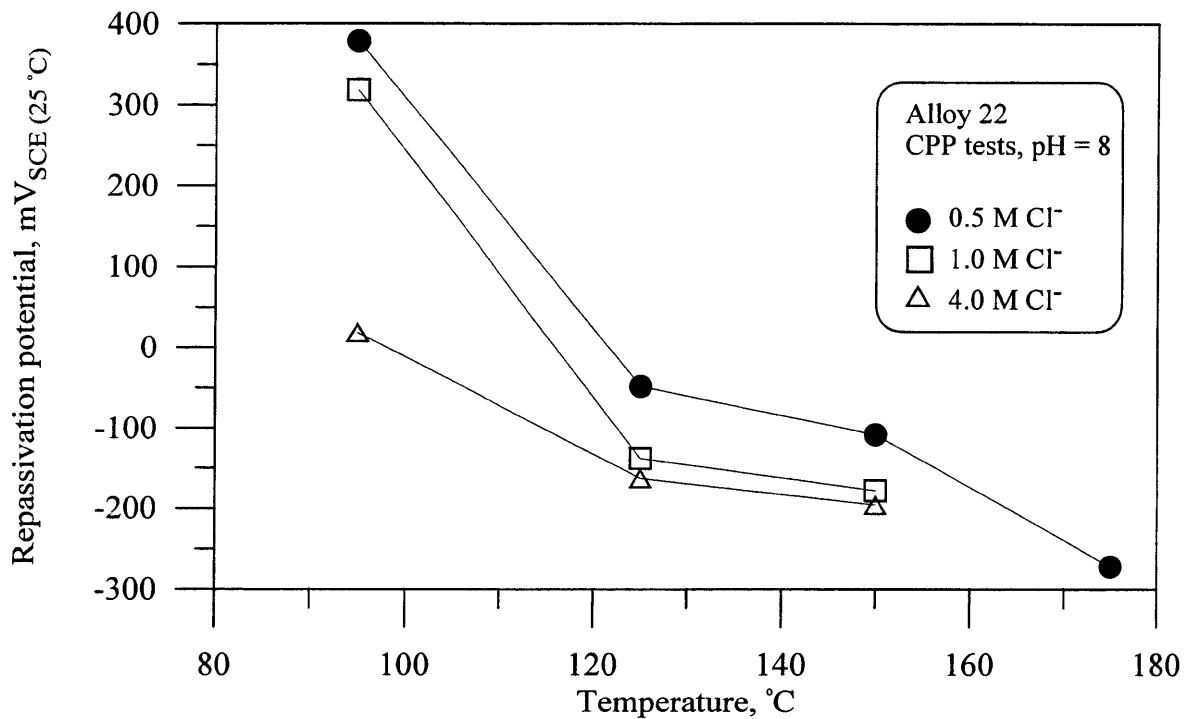


Figure 3-9. Repassivation potential for Alloy 22 measured in autoclave system at temperatures up to 175 °C

increases in temperature result in less pronounced reductions in the E_{rcrev} . At temperatures above 95 °C, the E_{rcrev} values measured in 4 M NaCl are only slightly lower than the E_{rcrev} values measured at lower concentrations.

Post test examination of the specimens revealed crevice corrosion at the interface between the PTFE crevice forming washer and the mating specimen surfaces. In contrast with the results shown in figure 3-7, localized attack was observed at 95 °C in solutions with 0.5 and 1.0 M chloride concentrations; however, crevice corrosion was not observed on all of the 24 crevice areas. Average crevice corrosion penetration depth, measured with an optical microscope, is shown in figure 3-10 for all of the specimens tested. Error bars indicate the standard deviation in the crevice corrosion penetration depth measurements on each specimen, using a minimum of four sites where crevice corrosion was initiated. It is apparent from figure 3-10 that the penetration depth was more strongly dependent on temperature than on chloride concentration. The data shown in figure 3-10 do not provide a means to predict penetration rates since the localized corrosion was produced under applied potential conditions and the penetration rate was not limited by the reduction of oxygen as under natural corroding solutions.

The E_{rcrev} measurements from the autoclave tests are also shown in figure 3-11, where the E_{rcrev} values are plotted as a function of chloride concentration for temperatures ranging from 95 to 150 °C. A regression through the data can be expressed as Eq. (3-3)

$$E_{\text{rcrev}} = E_{\text{rcrev}}^0(T) + B(T)\text{Log}[\text{Cl}^-] \quad (3-3)$$

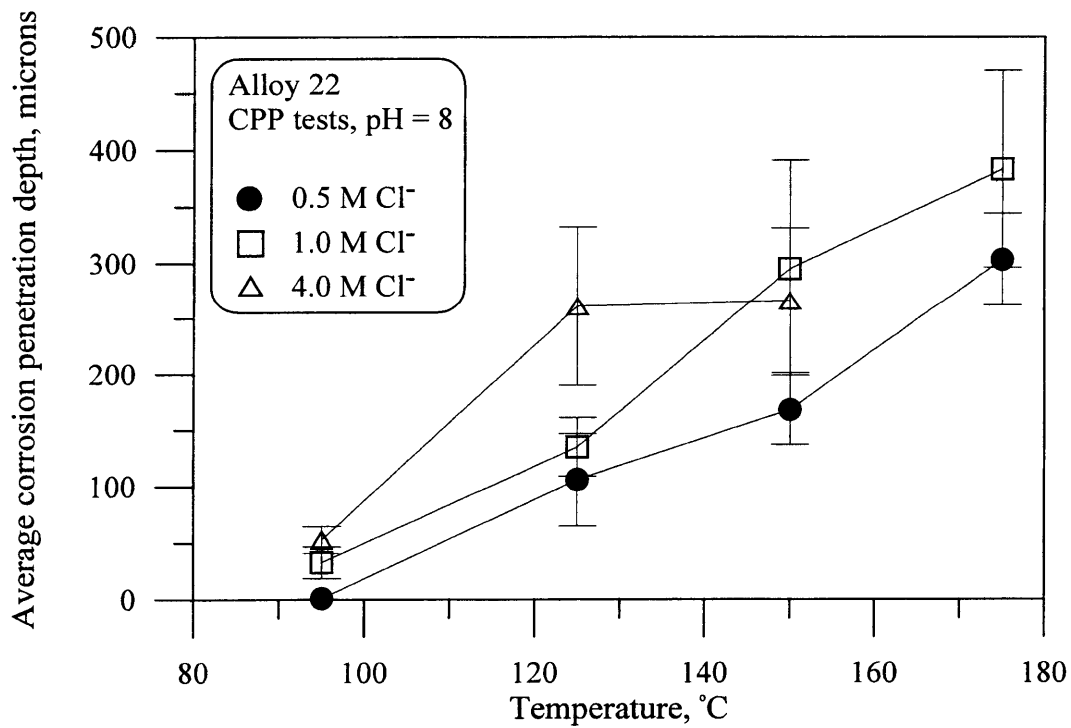


Figure 3-10. Crevice corrosion penetration depth measured on Alloy 22 specimens following cyclic potentiodynamic polarization scans conducted in the autoclave system at temperatures ranging from 95 to 175 °C

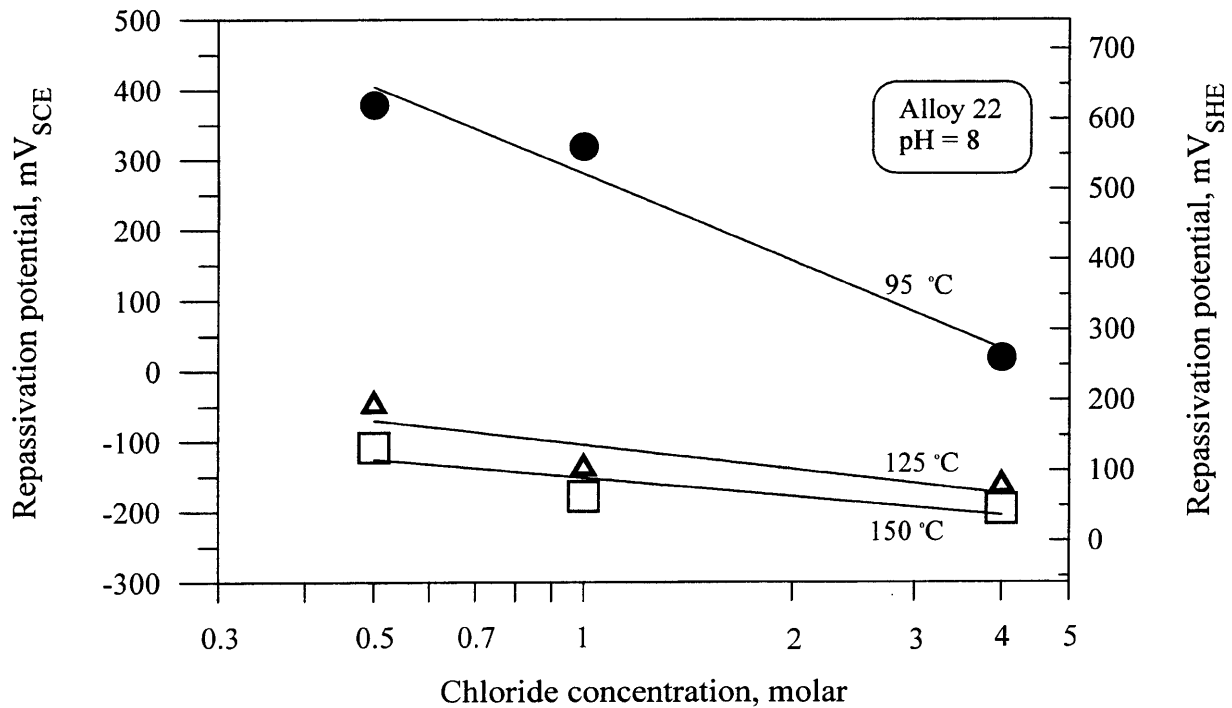


Figure 3-11. Repassivation potential as a function of chloride concentration for Alloy 22 measured in autoclave system at temperatures up to 150 °C

Using data only for 95 and 125 °C, an approximate temperature dependence can be determined as given by

$$E_{\text{rcrev}}^0 = (T) = 2,006 - 15.2(T); B(T) = -590.7 + 4.3(T) \quad (3-4)$$

where T is temperature in °C and E_{rcrev} is in mV_{SHE}. Note that Eq. (3-4) does not include data for temperatures higher than 125 °C. If these are considered, the temperature dependence becomes nonlinear. Since these temperatures are not of interest to TPA, a linear expression over a more limited temperature regime was chosen. It is apparent from Eq. (3-4) that E_{rcrev} is strongly dependent on temperature. In addition, the positive temperature coefficient for B(T) indicates that the slope of the E_{rcrev} expression Eq. (3-4) is less dependent on chloride concentration as the temperature increases.

A limited number of tests were conducted with welded specimens in the autoclave system. Comparisons of the E_{rcrev} values for welded versus the mill annealed Alloy 22 are shown in figure 3-12. For the welded material, the E_{rcrev} measured at 95 °C was approximately 100 mV lower than that for the mill annealed material. At 125 °C, no significant difference in the E_{rcrev} values was observed. Preferential localized attack was observed in the welded region. Figure 3-13 shows the crevice corrosion attack for both the as-received material and the welded specimen. An untested, as-welded specimen is also shown for comparison. Examination of the crevice corrosion areas of the welded specimens revealed deep penetrations and a substantial degree of intergranular corrosion that was not observed on the surface of the as-received specimens.

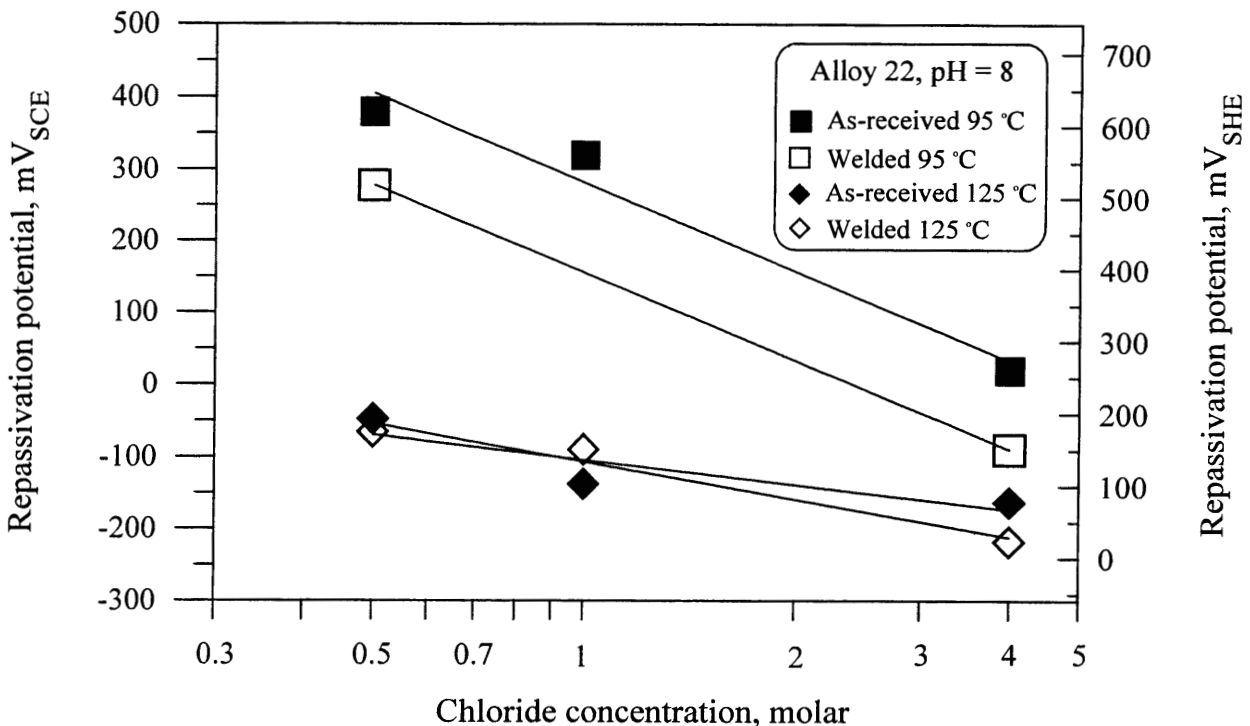


Figure 3-12. Repassivation potential as a function of chloride concentration for mill annealed and welded Alloy 22 measured in autoclave system at temperatures of 95 and 125 °C

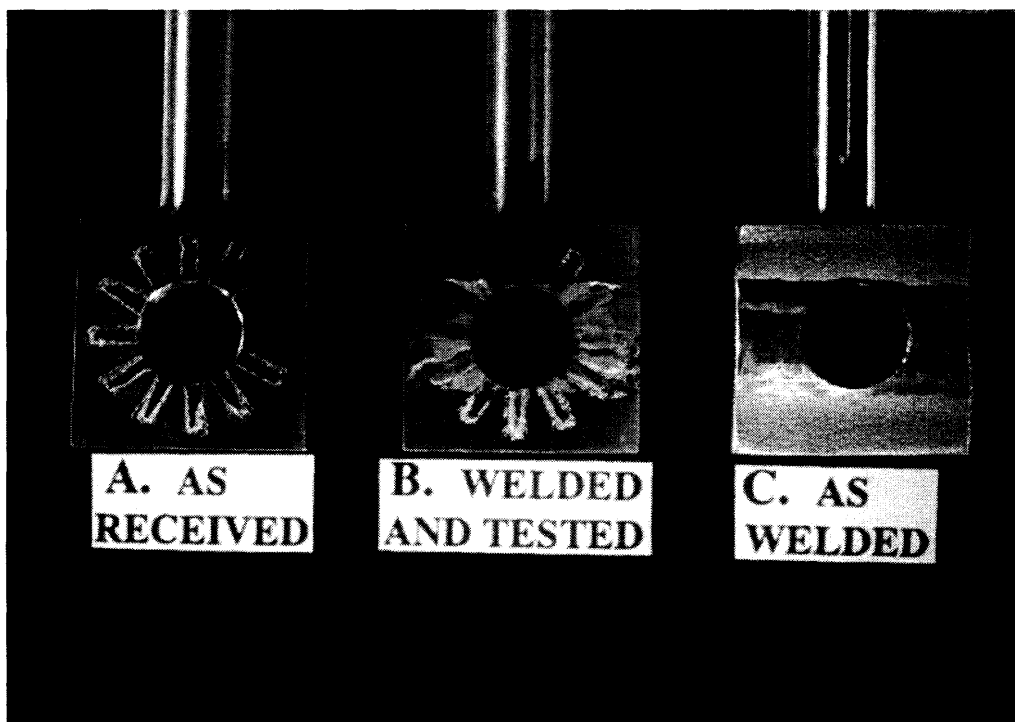


Figure 3-13. Photograph of Alloy 22 specimens (a) mill annealed tested in 4 M chloride at 125 °C, (b) welded Alloy 22 tested in 4 M chloride at 125 °C, (c) untested as-welded specimen

3.3 STRESS CORROSION CRACKING

3.3.1 Control Tests

Control tests were performed on both type 316L SS and Alloy 22 DCB specimens. In these tests, a precrack was grown to various lengths by cyclic loading in air and compliance curves at specific crack lengths were measured. After the last compliance curve was recorded, the specimen was heat-tinted and then mechanically overloaded to failure so that fatigue precrack could be examined at high magnifications. The exposed surfaces of the specimen, including the fatigue precrack, are covered with a dark gold colored oxide layer after heat-tinting. It is important to note that heat-tinting (2.5 h at 371 °C) does not alter either the microstructure or the mechanical properties of the alloy. After mechanical failure of the DCB specimen, the fatigue precrack and any crack advance occurring as a result of compliance measurements will be easily distinguishable by the gold colored oxide film, whereas any feature of the fracture surface that is not covered with the gold colored oxide occurred during the mechanical failure of the specimen. A SEM micrograph of the fracture surface of Alloy 22 clearly displayed three distinct fracture regions is shown in figure 3-14. The fatigue cracked region (region A), exhibiting clearly visible fatigue striations as can be seen in an enlarged area in figure 3-15, was tinted from the thermal exposure prior to mechanical failure. In addition to the fatigue precracked region, two other clearly defined regions (regions B and C) were visible. Both of these regions were not heat-tinted and are therefore a result of the final mechanical failure rather than a result of either the fatigue precracking or crack advance during compliance measurements. It is evident that region C in figure 3-14 was the result of ductile failure, as revealed by significant microvoid coalescence (see figure 3-16).

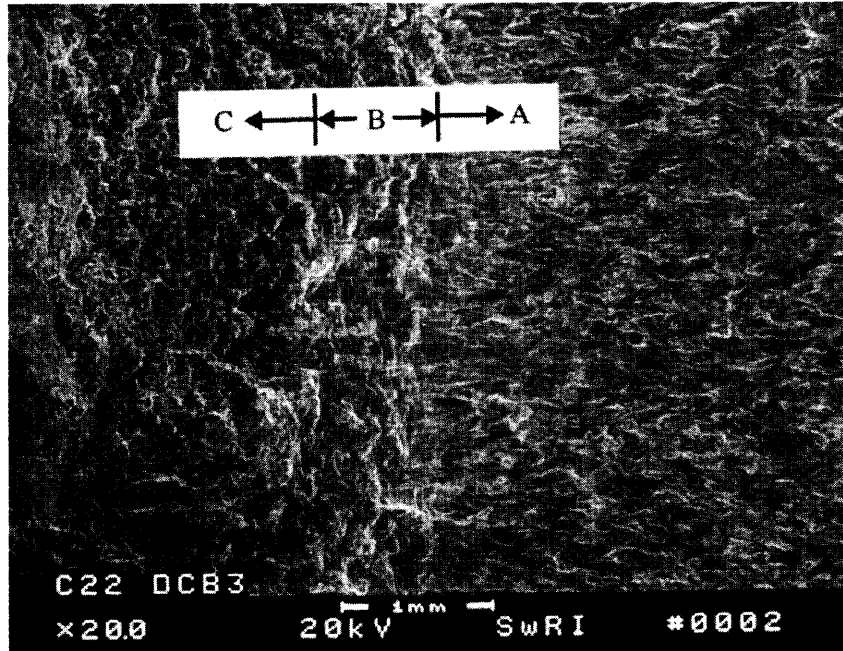


Figure 3-14. Fractograph showing three distinct regions on the fracture surface of the Alloy 22 specimen mechanically overloaded to failure for control test (A-precracked region, B-transition region, C-ductile failure region)

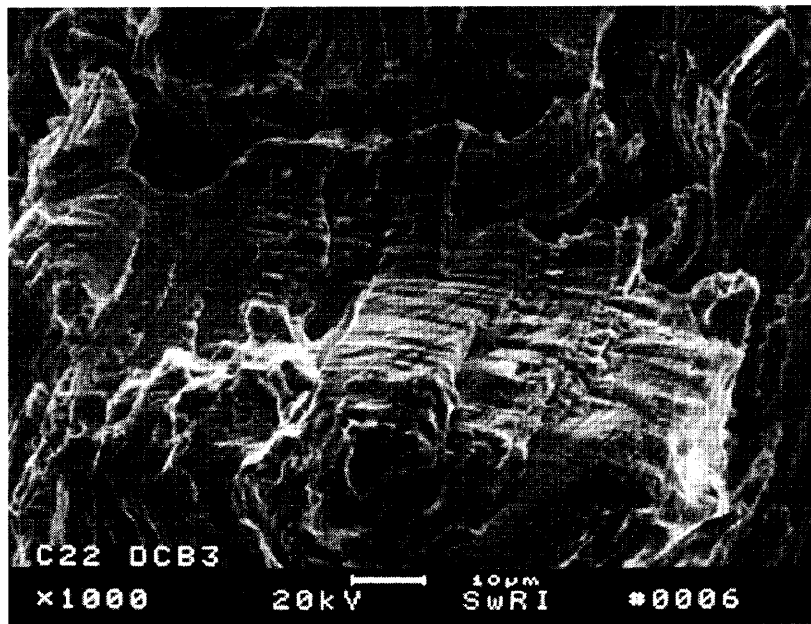


Figure 3-15. Fractograph showing fatigue striations in the enlarged precracked region on the fracture surface of the Alloy 22 control specimen

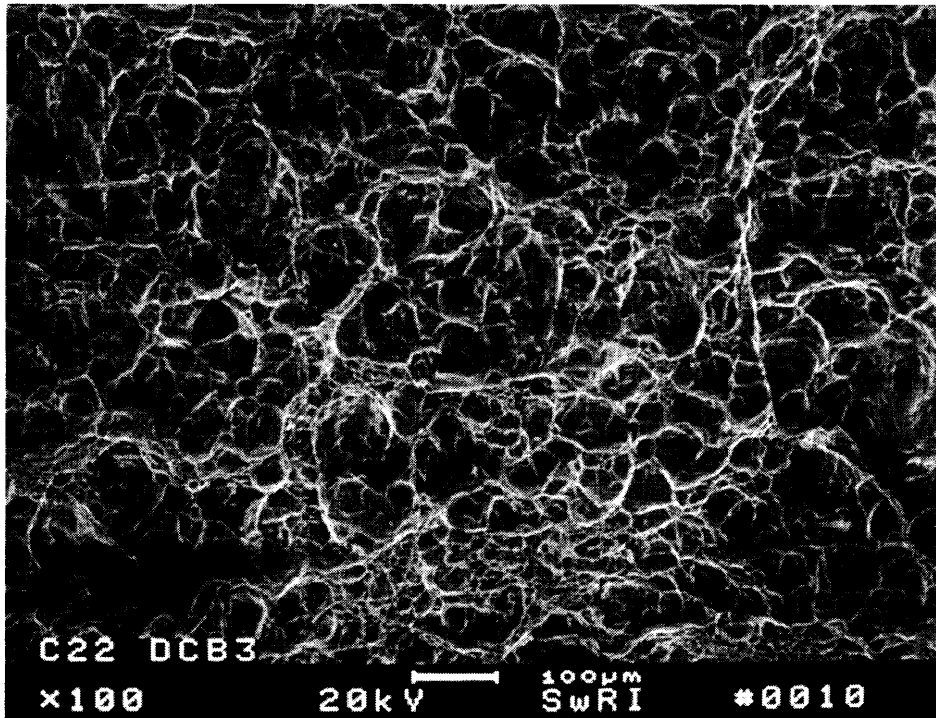


Figure 3-16. Fractograph showing microvoids in the ductile failure region on the fracture surface of the Alloy 22 control specimen

Region B in figure 3-14 is the intermediate region in which microvoid coalescence did not predominate and resulted from ductile tearing during final failure (see figure 3-17). The length of this ductile tearing region was determined to be approximately 0.9 mm. The size and appearance of this ductile tearing region may be influenced by the value of the mechanical parameters (e.g. strain rate) used to break open the specimen in order to examine the fracture surface. This ductile tearing artifact, in some cases, may appear to be transgranular SCC. In contrast, only two distinct regions, the fatigue cracked region and the ductile region, were observed on the fracture surface of the type 316L SS control specimen.

3.3.2 Stress Corrosion Cracking Tests

The SCC susceptibility of both type 316L SS and Alloy 22 was investigated in chloride solutions using the test conditions shown in table 3-2. No evidence of stress corrosion crack propagation was observed for either type 316L SS or Alloy 22 in deaerated, acidified (pH 2.7) 5 percent NaCl solution at 90 °C for a cumulative test time of 36 wk. It is apparent that the test conditions, including chloride concentration, temperature, and initial stress intensity, were not sufficiently severe for SCC to occur. These tentative conclusions are based on the examination of the crack morphology in the side grooves rather than on fractographs of the actual fracture surfaces. A final evaluation of the SCC resistance of the materials will be performed after the specimens are heat-tinted and mechanically fractured to expose the fracture surfaces.

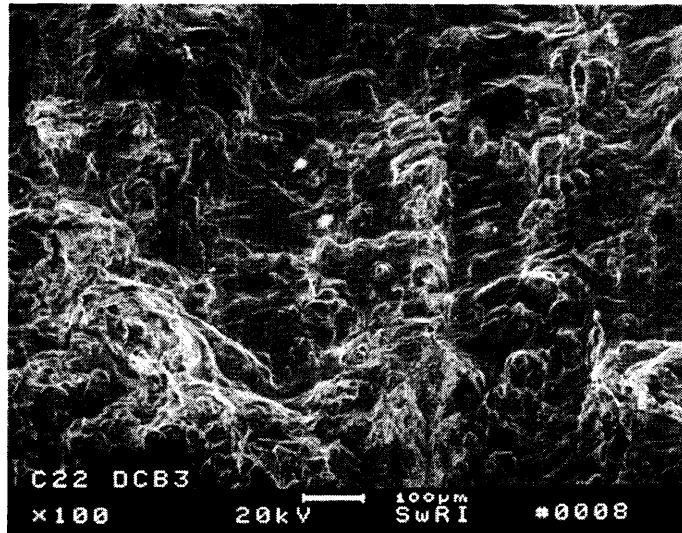


Figure 3-17. Fractograph showing a mixed feature of microvoid and ductile tearing in the transition region on the fracture surface of the Alloy 22 control specimen

Table 3-2. Results of stress corrosion cracking (SCC) tests of type 316L stainless steel and Alloy 22 in chloride solutions

Specimen ID (Orientation)	Initial K_I (MPa·m ^{1/2})	Test Solution	Potential (mV _{SCE})	Test Duration	Result (Crack Growth Rate)
316L-1(T-L)	25.0	5% NaCl, pH 2.7 90 °C, N ₂ deaerated	-340 to -320 (O.C.)*	252 d (6,048 h)	No SCC
316L-2(T-L)	25.0	40% MgCl ₂ , 110 °C	-320 to -300 (O.C.)	20.5 d (492 h)	SCC—Extensive Transverse Cracks
316L-6(T-L)	21.8	30% MgCl ₂ , 110 °C	-330 to -320 (O.C.)	3.8 d (92 h)	SCC (1.0 × 10 ⁻⁸ m/s)
316L-5(T-L)	21.8	30% MgCl ₂ , 110 °C	-340	40.4 d (970 h)	SCC (2.5 × 10 ⁻⁹ m/s)
316L-7(T-L)	21.8	30% MgCl ₂ , 110 °C	-360	17.6 d (423 h)	SCC (2.0 × 10 ⁻⁹ m/s)
316L-8(T-L)	21.8	30% MgCl ₂ , 110 °C	-380	17.8 d (427 h)	SCC (7.3 × 10 ⁻¹⁰ m/s)
22-1(T-L)	32.7	5% NaCl, pH 2.7 90 °C, N ₂ deaerated	-330 to -310 (O.C.)	252 d (6,048 h)	No SCC
22-2(T-L)	32.7	40% MgCl ₂ , 110 °C	-280 to -260 (O.C.)	252 d (6,048 h)	No SCC—Grain Boundary Attack
22-7(S-L)	32.7	40% MgCl ₂ , 110 °C	-270 to -250 (O.C.)	178 d (4,272 h)	No SCC—Minor Secondary Cracks

*O.C.—Open-Circuit

For Alloy 22, no substantial crack growth was observed after a total exposure period of 36 wk for a T-L specimen and 25 wk for an S-L specimen tested in 40 percent MgCl_2 solutions at 110°C under open-circuit conditions. The corrosion potential of the specimens ranged from -280 to -250 mV_{SCE} which is close to the E_{crev} for Alloy 22 in concentrated chloride solutions. The SEM photographs of side groove areas in figures 3-18 and 3-19 document both the initial precrack tip morphology and that after exposure to the solution for 32-wk from the T-L specimen. Periodic examination of the specimen surfaces using the SEM revealed that grain boundary attack (figure 3-20) occurred in the T-L specimen after testing for 21 wk. A minor secondary cracking (figure 3-21) near the main precrack, perhaps indicative of SCC initiation, was observed in the S-L specimen tested for 10 wk. After continued exposure, these secondary cracks observed near the tip of the fatigue precrack did not propagate. It is generally known that grain boundary attack can be attributed to the lower corrosion resistance along the grain boundaries and the formation of the secondary cracks observed here may be related to near-surface defects in the test specimen. Regardless of the presence of these minor cracks, Alloy 22 appears to be extremely resistant to SCC in concentrated MgCl_2 solutions.

Significant crack growth was observed in a type 316L SS specimen after a 5.6-d exposure under open-circuit conditions in 40 percent MgCl_2 solutions at 110°C . After 3 wk, many transverse cracks almost perpendicular to the direction of the fatigue precrack were observed on the arms of the DCB specimen (figure 3-22). To reduce this, a lower initial stress intensity ($21.8 \text{ MPa}\cdot\text{m}^{1/2}$) and a less concentrated solution (30 weight percent MgCl_2) were selected for the following tests. In spite of the lower stress intensity and reduced chloride concentration, transverse cracks were again observed on the arms of the DCB specimen when tested under open-circuit conditions where the E_{corr} varied from -330 to -320 mV_{SCE} . However, the effect of transverse cracks on the final equilibrium wedge load was evaluated to be negligible by comparing compliance measurements performed before and after exposure. From the final wedge load measurement of 890 N, a K_{ISCC} of $13.1 \text{ MPa}\cdot\text{m}^{1/2}$ was calculated for type 316L SS in 30 percent MgCl_2 at 110°C using Eq. (2-6). A SEM photograph of the fracture surface is shown in figure 3-23. Although SCC was clearly

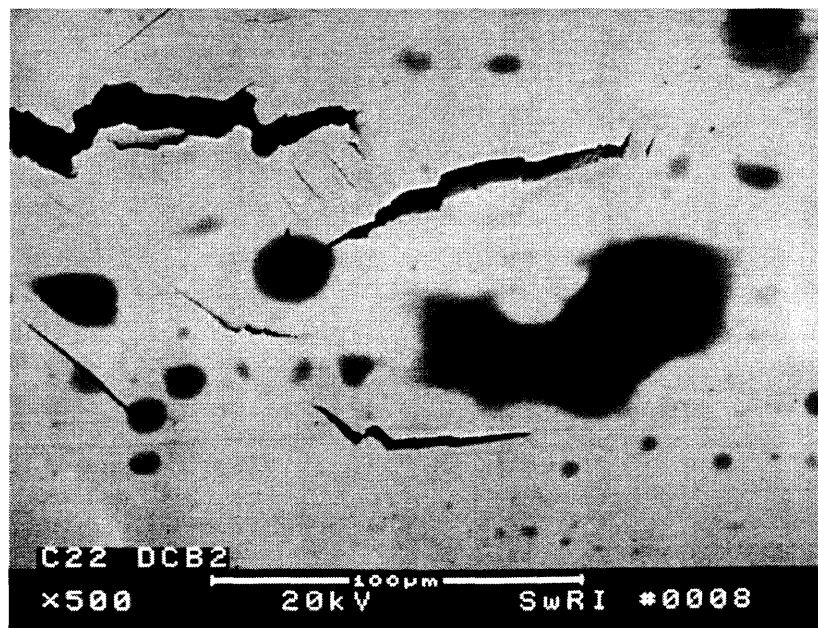


Figure 3-18. Scanning electron micrograph showing the initial precrack tip morphology of the long transverse-longitudinal direction (T-L) Alloy 22 specimen before stress corrosion cracking test

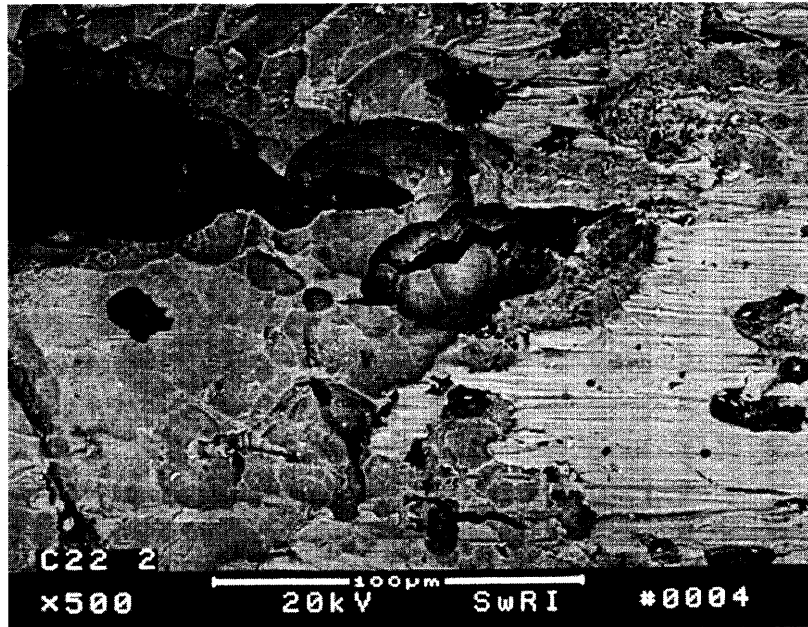


Figure 3-19. Scanning electron micrograph showing the precrack tip morphology of the long transverse-longitudinal direction (T-L) Alloy 22 specimen after 32-wk exposure to 40 percent MgCl₂ solution at 110 °C

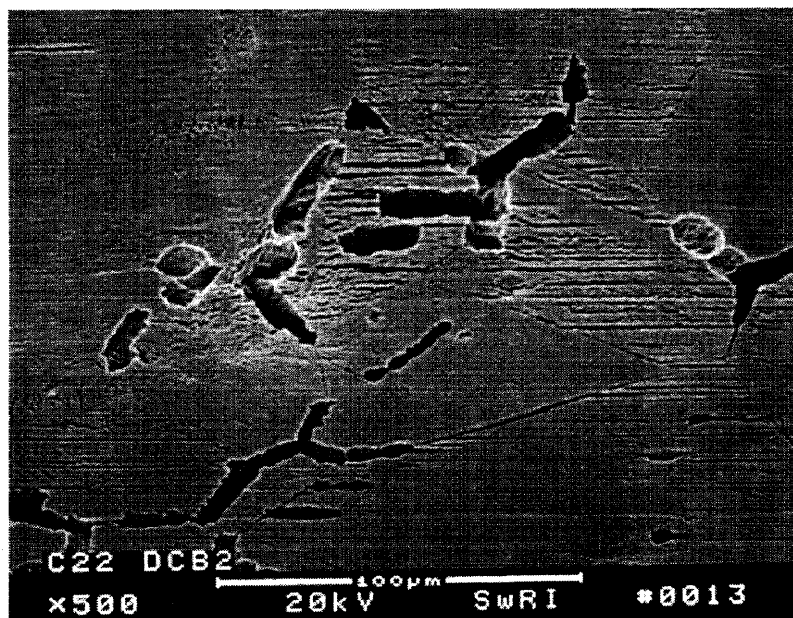


Figure 3-20. Scanning electron micrograph showing grain boundary attack of the long transverse-longitudinal direction (T-L) Alloy 22 specimen after 22-wk exposure to 40 percent MgCl₂ solution at 110 °C

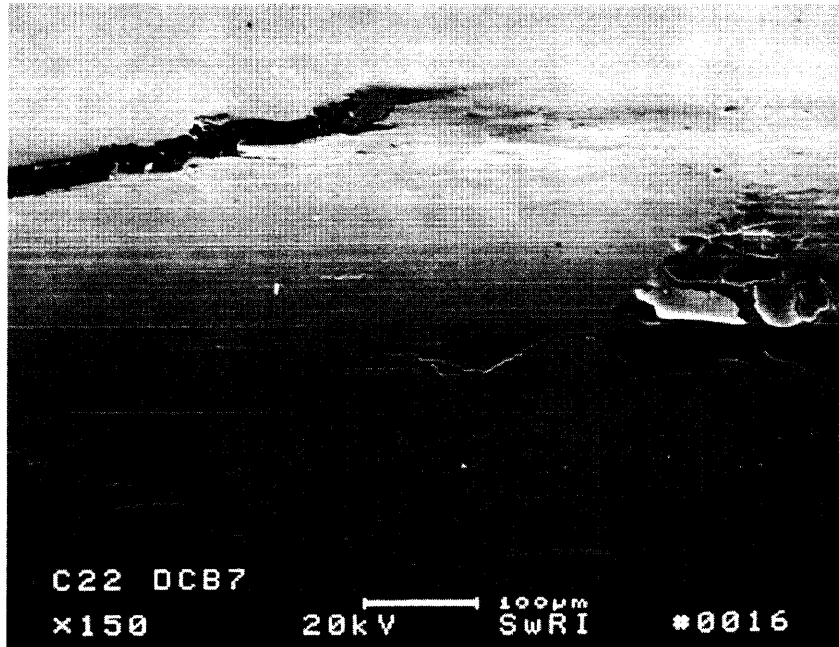


Figure 3-21. Scanning electron micrograph showing minor secondary cracks of the long transverse-longitudinal direction (T-L) Alloy 22 specimen after 10-wk exposure to 40 percent $MgCl_2$ solution at 110 °C

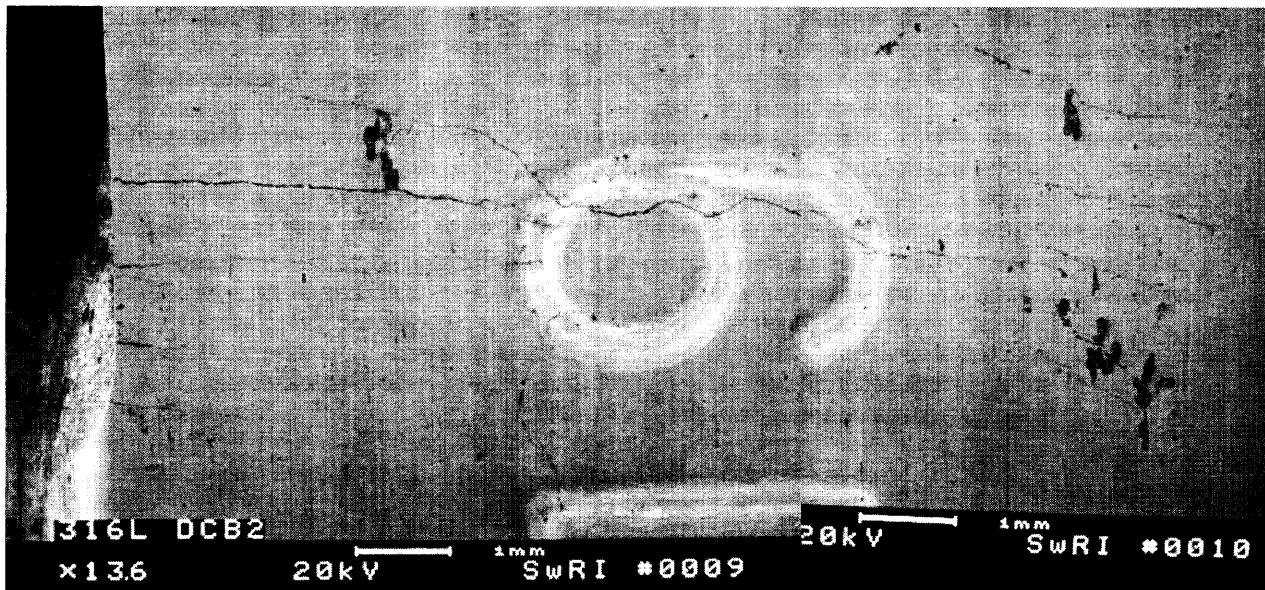


Figure 3-22. Scanning electron micrograph showing transverse crack branches of the type 316L stainless steel specimen after 3-wk exposure to 40 percent $MgCl_2$ at 110 °C

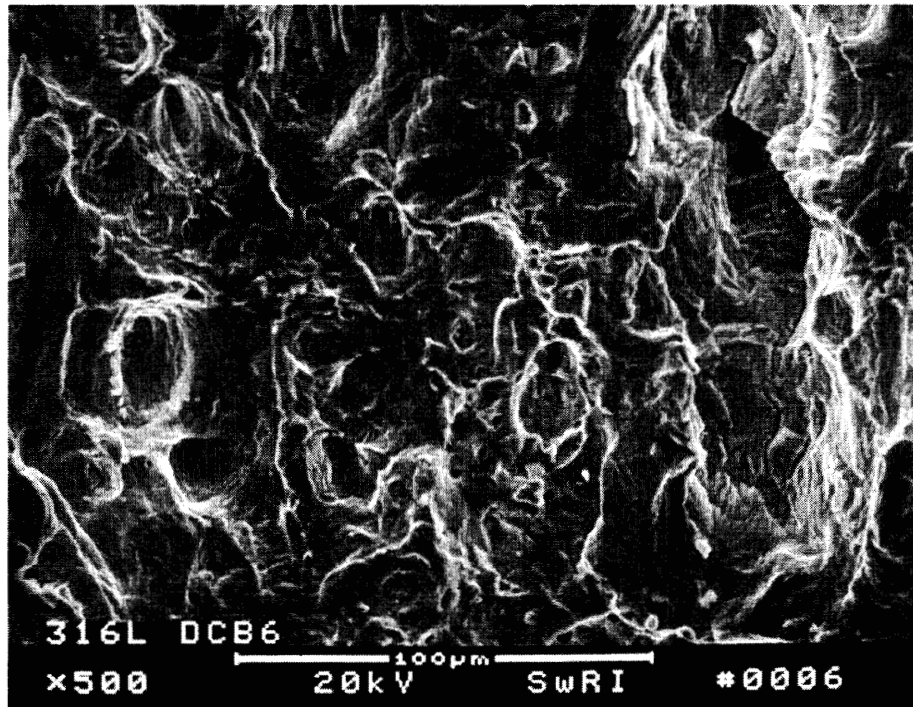


Figure 3-23. Fractograph showing transgranular stress corrosion cracking on the fracture surface of the type 316L stainless steel specimen after 3.8-d exposure to 30 percent MgCl_2 at $110\text{ }^\circ\text{C}$

identified, the fracture surface does not exhibit the quasi-cleavage features typical of transgranular SCC of austenitic SS in hot concentrated chloride solutions. An average crack growth rate of 1.0×10^{-8} m/s was calculated by dividing the final crack length by the total test time. Table 3-2 provides initial stress intensity values because the stress intensity decreases with time as a result of load relaxation due to crack growth.

One of the main objectives of the SCC tests conducted with DCB specimens was to determine the effect of potential on the SCC propagation rate. Initial results, obtained with smooth tensile specimens using a slow strain rate technique, suggest that the repassivation potential for localized corrosion may also define the minimum potential for SCC propagation on type 316L SS exposed to hot chloride solutions (Cragolino et al., 1994; Sridhar et al., 1995). The effect of applied potential on the SCC propagation of type 316L SS is summarized in table 3-2. From the crack growth rate versus potential curve shown in figure 3-24, it is apparent that the SCC propagation decreased as the potential was decreased. It appears that no SCC propagation would occur below the repassivation potential which is approximately $-390\text{ mV}_{\text{SCE}}$ for type 316L SS in 30 percent MgCl_2 (Sridhar et al., 1995; Cragolino et al., 1994). While a trend of decreasing crack propagation rates was observed as the applied potential of the specimen approached the repassivation potential, additional tests are necessary to completely evaluate the relationship between crack growth rate and potential. With the current techniques, the lowest crack propagation rate that can be detected is approximately 1×10^{-11} m/s.

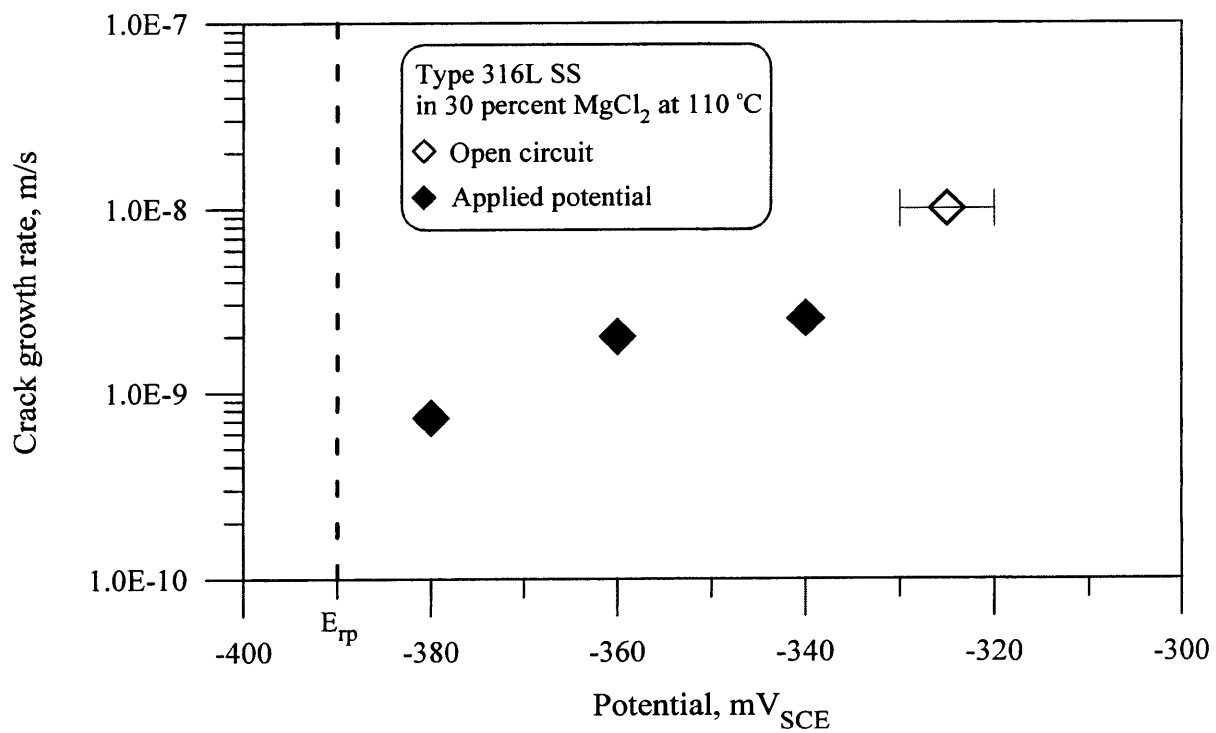


Figure 3-24. Crack growth rate as a function of potential for double cantilever beam specimen of type 316L stainless steel in 30 percent MgCl₂ at 110 °C and an initial stress intensity of 21.8 MPa·m^{1/2}

4 DISCUSSION

The performance of corrosion resistant candidate container materials with more than 12 percent Cr is dependent on the presence of a Cr rich passive film. Under conditions where passivity is maintained, the corrosion rate is limited by the low solubility of the oxide film and slow transport of metal cations across the oxide layer. Breakdown of the passive film in the presence of an aggressive species such as chloride anion can result in the initiation of localized corrosion and the rapid penetration of localized attack. Assessment of the candidate material performance requires knowledge of the passive dissolution rate, localized corrosion and SCC susceptibility, localized corrosion penetration rate, and the SCC propagation rate. In addition to the assessment of the base material, the effects of WP fabrication and welding must be considered.

4.1 PASSIVE CORROSION

Passive dissolution rate of Ni-Cr-Mo-Fe alloys can be determined by several methods. It is conceptually possible to measure the passive dissolution rate by monitoring the weight loss of a specimen exposed to a representative environment. Practically, such measurements are difficult and subject to large measurement error in relatively short-term tests. Growth of the oxide film may result in a net weight gain that could falsely indicate low corrosion rates or even negative values. The deposition of dissolved species can also cause artificially low corrosion rates. Measurement of metal ion concentrations in the electrolyte solutions after exposure can be used to calculate the passive corrosion rates (Kirchheim et al., 1989). This technique can also be used to determine deviations from congruent dissolution. The main disadvantages of this technique are the complexity of the instrumentation and test procedures and a resolution of about 2×10^{-8} A/cm² (Kirchheim et al., 1989). Passive dissolution rates can also be obtained using electrochemical methods with a greater resolution of 1.25×10^{-10} A/cm². Potentiodynamic polarization with a slow scan rate typically overestimates the passive dissolution rate because these measurements are not performed under steady-state conditions. Potentiostatic polarization can yield steady-state corrosion rates but requires instrumentation with adequate resolution. There are also several disadvantages to the technique including the need to thoroughly deaerate the system to avoid interference with the oxygen reduction reaction that may reduce the measured anodic current to values lower than the true dissolution current under passive conditions. The application of a potential may also alter the composition and thickness of the oxide layer.

In this investigation, potentiostatic polarization methods were used to obtain passive corrosion rates. From the potentiostatic tests shown in table 3-1 performed with specimens that did not have creviced surfaces, it is apparent that the passive dissolution of Alloy 22 is low and similar to those reported for Fe-Cr alloys (Kirchheim et al., 1989). A strong temperature effect was also observed in dilute chloride solutions. The passive corrosion rates in 0.028 M chloride at 95 °C was 10 times that measured at 20 °C. At present, it is unclear if this apparent temperature effect in the 0.028 M chloride solution is a result of a higher passive dissolution rate at the elevated temperature or an artifact of the higher oxygen solubility at the lower temperature. The low passive corrosion rates measured here suggest that if localized corrosion is not initiated and the corrosion potential (E_{corr}) of the WP is less than 400 mV_{SCE}, the lifetime of the 20-mm thick Alloy 22 containers may be extended to over 20,000 yr. Improved modeling and mechanistic understanding of passive dissolution are necessary to evaluate the validity of these long-term predictions. At higher potentials where transpassive dissolutions were observed, failure may occur in a few thousand years. Transpassive dissolution at high potentials, rather than the initiation of localized corrosion, suggests that Alloy 22 is resistant to pitting corrosion in NaCl solutions.

Passive corrosion rate measurements were also performed on both heat treated and welded Alloy 22 because the formation of TCP phases in Ni-base materials may alter the resistance of the alloys to localized corrosion and increase the passive dissolution rate (Kasparova, 1998). Although the microstructure of the thermally aged specimens used in this study was not characterized, thermal aging at 870 °C for 4 h is expected to result in the formation of TCP phases such as μ - and P-phase (Raghavan et al., 1984; Cieslak et al., 1986a). Results obtained with the thermally aged specimens indicate the passive corrosion rate of Alloy 22 is not affected by the formation of TCP phases; however, the range of passivity is substantially reduced by thermal aging. The compositions of TCP phases are known to be Mo rich (Raghavan et al., 1984; Cieslak et al., 1986a). Although the role of Mo is not completely clear, consumption of Mo in the TCP phases, particularly at the grain boundaries, may reduce the amount of Mo that can stabilize the passive film. As a result, intergranular corrosion of the thermally aged specimens occurred at low potentials, whereas passivity was maintained on the mill annealed material.

In contrast to the results obtained for the thermally aged specimens, for the welded specimens both the passive corrosion rate and the potential range over which the passive film was stable were much closer to that of the mill annealed material. Because the formation of P, σ , and μ -phases in Alloy 22 weldments has been identified (Cieslak et al., 1986a), the welded regions can be expected to be less corrosion resistant than the base metal. Some preferential attack of the weld region occurred at potentials greater than 600 mV_{SCE}, but no deep intergranular penetration was observed. The relatively good performance of the weldments compared to the thermally aged specimens is consistent with the results reported by Heubner et al. (1989) using ASTM G28 Method A tests that consisted of boiling 42 g/L Fe₂(SO₄)₃ + 50 percent H₂SO₄ (American Society for Testing and Materials, 1999d). Heubner et al. (1989) indicated that the corrosion rate of the welded material was 1.61 mm/yr or slightly more than twice that of the mill annealed material (0.73 mm/yr). On the other hand, the corrosion rate for Alloy 22 thermally aged for 100 h at 800 °C was 7.38 mm/yr. The corrosion rates reported by Heubner et al. (1989) were based on weight loss measurements and do not accurately reflect the severity of localized attack at the grain boundaries. No intergranular penetration was observed for the mill annealed material after the ASTM G28 Method A test (American Society for Testing and Materials, 1999d). However, intergranular penetration of 1 to 2 μ m for the welds and penetrations of 100 to 250 μ m for the thermally aged material were reported by Heubner et al. (1989). It is apparent from the comparison of the mill annealed, thermally aged, and welded materials that the welds do not contain a sufficient amount of secondary phases to substantially increase the intergranular corrosion susceptibility in the absence of a crevice.

4.2 LOCALIZED CORROSION

Alloy 22 appears quite resistant to localized corrosion in chloride containing environments. Pitting corrosion of Alloy 22 was not observed and crevice corrosion was only observed in aggressive environments characterized by high chloride concentrations, elevated temperatures, and highly oxidizing conditions. The results of this investigation indicate that the transition from passive dissolution to localized corrosion is dependent on the alloy composition, potential, chloride concentration, and the presence of a crevice. In addition, previous results obtained with Alloy 825 specimens have shown that the initiation time for localized corrosion is also potential dependent (Sridhar et al., 1995). The complex nature of localized corrosion initiation has several implications. First, localized corrosion susceptibility studies, conducted by simply immersing a specimen in a test environment for a specified period without measuring the corrosion potential during exposure, are not useful for predicting the long-term performance of the material. Second, data obtained from standard test methods used to rank the relative performance of alloys, such as critical pitting

temperature tests, are difficult to apply to long-term performance calculations since the exposure conditions in the standard test and the actual application are usually dissimilar. Finally, the initiation time is potential dependent and the measurement of the pit initiation potential using short-term potentiodynamic polarization tests greatly overestimates the localized corrosion resistance.

In this investigation, the repassivation potential for crevice corrosion was measured as a function of alloy composition, chloride concentration, and temperature. The E_{rrev} for Alloy 22, which was dependent on chloride concentration and temperature, behaves in a manner similar to that of less corrosion resistant alloys (Sridhar et al., 1995). The effect of alloy composition was reflected in the repassivation potential measurements and was in agreement with the results of standard tests used to rank the relative corrosion resistance of alloys. The critical temperature for localized corrosion of Ni-base alloys has been shown to be dependent on the amount of Cr, and to an even greater extent the amount of Mo, in the alloy (Okayama et al., 1987; Kolts and Sridhar, 1985). For example, Alloy C-276 having 15 percent Cr and 16 percent Mo has been shown to be much more corrosion resistant than Alloy 625 which contains 21 percent Cr and 9 percent Mo. Alloy 22 was more resistant to localized corrosion than Alloy 625 especially in solutions containing 0.1 to 4 M chloride at 95 °C. The results shown in figure 3-7 indicate that as the Cr and Mo concentration are increased, the localized corrosion resistance, as measured by the repassivation potential, also increased. Alloy 22, which contains 21 percent Cr and 14 percent Mo, clearly can be expected to be much more corrosion resistant than Alloy 625. Likewise, the increased crevice corrosion susceptibility of Alloys 625 and 22 with increasing temperature (figures 3-6 and 3-9) is consistent with the concept of a compositionally dependent, critical temperature for localized corrosion.

The E_{rrev} for Alloy 22 at 95 °C shown in figure 3-11 (measured in the autoclave system) is substantially lower than the E_{rrev} value shown in figure 3-7 (measured in a glass cell). For example, in the autoclave system, an E_{rrev} of 40 mV_{SCE} was measured at 95 °C in 4 M chloride, whereas in the glass cells E_{rrev} values ranged from 350 to 580 mV_{SCE}. It is important to note that the specimens, machined from the same heat of material, were tested under identical conditions of solution concentration and temperature. In addition to the significant difference in the values of E_{rrev} , crevice corrosion was consistently more severe on the specimens tested in the autoclave system compared to those tested in the glass cells. Dunn et al. (1996a), using Alloy 825 specimens, have shown that for shallow penetrations, the value of E_{rrev} is strongly dependent on the localized corrosion penetration depth. A similar dependence of E_{rrev} on penetration depth may be valid for Alloy 22. While the deeper penetration may be the basis for the lower E_{rrev} values, it does not explain the apparent enhanced susceptibility of Alloy 22 to localized corrosion in the autoclave system. One possible explanation for the different results is the deposition of silica on specimens tested in glass cells that may act as a corrosion inhibitor. Silica deposition on specimens has been observed. Leaching of the glass test cell is the only source of silica because this is not intentionally added to the test solution. Another possibility is the leaching of F⁻ from the PTFE autoclave liner that may make the solution more aggressive. The effect of leachates from PTFE seems unlikely, however, since PTFE crevice washers are used on specimens tested in both systems. Finally, the composition of the passive films on specimens may be dependent on the test conditions. Beccaria et al. (1995) has shown that the Cr concentrations in passive films of types 304 and 316L SS exposed to sea water at 10 °C are dependent on water pressure. When exposed to ambient pressure seawater for 200 h, the passive film on type 316L SS was found to contain 24.5 atomic percent Cr and 3.0 atomic percent Mo. At 300 bar, the Cr concentration was 21.5 and the Mo concentration was 1.0 atomic percent. No significant compositional changes were observed at pressures of 1 bar. In this study, autoclave tests were conducted at pressures of 3 to 5 bar. Unfortunately, the test conditions used by Beccaria et al. (1995) are significantly different from those in this study and the effects of temperature, chloride concentration, and pressure on the passive film composition of Alloy 22 are not known. As a result,

some additional investigations are necessary to understand the increased localized corrosion susceptibility of Alloy 22 in the autoclave system.

Welding was observed to increase the localized corrosion susceptibility of Alloy 22. This was indicated by both lower values of E_{rev} for the welded specimens (figure 3-12) and preferential attack of the weldments. In addition, localized attack on the welded specimen had deep intergranular penetrations that were not observed in the as-received material. Cieslak et al., (1986b) has shown that the interdendritic regions of weldments are depleted in Ni and enriched in Mo and Ti. It is apparent that segregation of the alloying elements leads to an increased crevice corrosion susceptibility of the weldments. In this study, the welded specimens were machined from plate that was 12.7-mm thick; however, the Alloy 22 container proposed in the EDA II is 20-mm thick. The additional thickness will require more weld passes and, as a result, the container will be at an elevated temperature for a longer period during the closure weld. In addition, the TCP phase precipitation kinetics may be accelerated by cold work. Since the precipitation of TCP phases is dependent on both time and temperature, the results of this study indicate that the thermal mechanical history of the WP, including forming and cutting operations, welding, weld repairs, annealing cycles, and the temperature after emplacement are important considerations for the WP performance in the repository.

4.3 STRESS CORROSION CRACKING

The use of a fracture mechanics approach in SCC testing has several advantages over other traditional test methods using smooth test specimens because quantitative data such as the threshold stress intensity for the initiation of SCC and crack growth rate can be obtained as a function of environmental and electrochemical conditions. The fracture mechanics type specimen such as DCB or compact tension specimens provides a preexisting flaw to facilitate the initiation of SCC (Brown, 1968). Such methods may overcome the limitations of SCC initiation that occurs with smooth test specimens. In addition, for plain strain conditions, the stress intensity at the crack tip is well defined and can be calculated accurately (Brown, 1968). This permits obtaining crack velocity versus K_I curves. The SCC susceptibility and crack propagation testing performed in this work assures that the fracture mechanics technique would serve as a sound method for evaluating the SCC performance of candidate container materials.

Several authors have reported the effect of stress intensity on crack growth rate of austenitic SS under open-circuit conditions in chloride containing solutions. Speidel (1981) reported crack growth rate versus K_I curves for austenitic type 304L SS exposed to 42 percent MgCl_2 solution at 130 °C and to 22 percent NaCl solution at 105 °C. The crack growth rate at the plateau is almost one order of magnitude higher in MgCl_2 (5×10^{-8} m/s) than that in NaCl (5×10^{-9} m/s). In addition, the threshold stress intensity, K_{ISCC} , is significantly lower in the higher temperature MgCl_2 solution. Eremias and Marichev (1979) reported a K_{ISCC} value of 14 $\text{MPa}\cdot\text{m}^{1/2}$ for Fe-18Cr-10Ni-0.5Ti SS in a 44.5 percent MgCl_2 solution at 115 °C, whereas 10 $\text{MPa}\cdot\text{m}^{1/2}$ was measured by Lefakis and Rostoker (1977) for type 304 SS in boiling MgCl_2 . The K_{ISCC} (13.1 $\text{MPa}\cdot\text{m}^{1/2}$) and crack growth rate (1.0×10^{-8} m/s) obtained in this work for type 316L SS under open-circuit conditions in a 30 percent MgCl_2 solution at 110 °C are consistent with those reported in the literature. The crack growth rates as a function of initial stress intensity for type 304L SS reported by Speidel (1981), along with the data for type 316L SS from this work, are shown in figure 4-1. It is apparent that considering the differences in material and the variations in chloride concentration and temperature, the data obtained in this investigation are within the range defined by measurements of Speidel (1981).

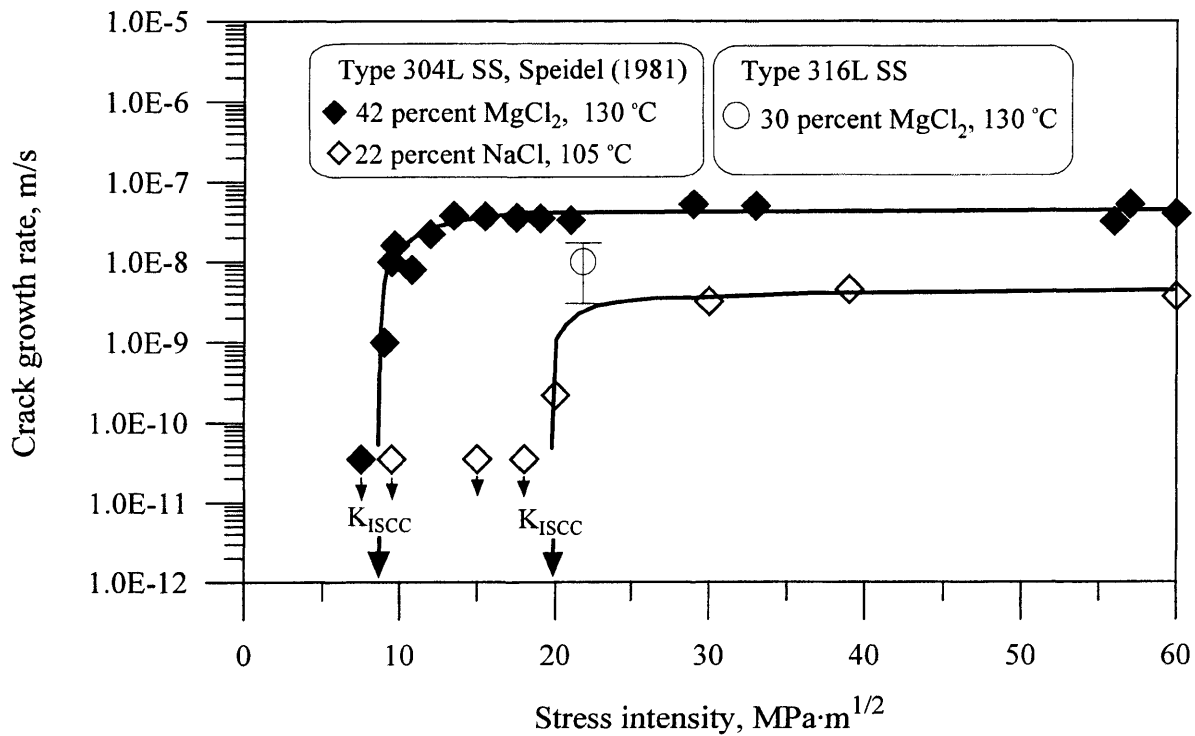


Figure 4-1. Effect of stress intensity on the crack growth rate of solution annealed type 304L stainless steel exposed to 42 percent MgCl₂ solution at 130 °C and to 22 percent NaCl solution at 105 °C (Speidel, 1981). Datapoint from this study using type 316L stainless steel in 30 percent MgCl₂ solution at 110 °C is included.

The effect of potential on the SCC propagation of type 316L SS has been previously studied in similar test environments. Russell and Tromans (1979) tested type 316L SS T-double notch (TN)-DCB specimens in MgCl₂ solutions at temperatures ranging from 116 to 154 °C and initial stress intensities ranging from 12 to 100 MPa·m^{1/2}. Specimens were cold worked 25 and 50 percent. At 116 °C, the SCC propagation rates were 6×10^{-8} m/s for specimens with K_I greater than 20 MPa·m^{1/2} at potentials more noble than -280 mV_{SCE}. This increased to 5×10^{-7} to 8×10^{-7} m/s at 154 °C. When the potential was reduced below -350 mV_{SCE}, no SCC was observed on the specimens with 30 MPa·m^{1/2} < K_I < 35 MPa·m^{1/2} tested in 44.7 percent MgCl₂ at 154 °C. Work performed by Silcock (1982) using type 316L SS specimens in boiling 42 percent MgCl₂ solutions at 154 °C also shows that the SCC propagation rate decreased as the potential was decreased. The repassivation potential for type 316L SS in 30 percent MgCl₂ at 95 °C is approximately -390 mV_{SCE} based on measurements conducted at the Center for Nuclear Waste Regulatory Analyses (CNWRA) (Cragolino et al., 1994). The SCC propagation rates plotted in figure 3-9 clearly indicate that at potentials greater than the repassivation potential, the crack growth rate increases as the potential increases. The results of Silcock (1982) and Russell and Tromans (1979) also suggest that at potentials below the repassivation potential SCC is not initiated.

SCC susceptibility of Alloy 22 has been evaluated by Roy et al. (1998) at LLNL in deaerated 5 percent NaCl solutions acidified to pH 2.7 HCl at 90 °C. Based on the reported results, the K_I of Alloy 22 was in a range of 35.3 to 42.2 MPa·m^{1/2} and the K_{ISCC} was measured between 30.4 and 35.3 MPa·m^{1/2}. In addition, the crack growth rate for Alloy 22 was 1.3×10^{-10} to 1.8×10^{-10} m/s. In contrast, no SCC initiation

and propagation was observed in this work on Alloy 22 tested in an identical environment with a K_I of $32.7 \text{ MPa}\cdot\text{m}^{1/2}$, which is close to the highest stress intensity that can be attained without deforming the arms of the DCB specimens. Furthermore, no SCC was found in Alloy 22 tested in a much more severe solution containing 40 percent MgCl_2 at 110°C .

Work by Speidel (1981), who tested a variety of austenitic Fe-Cr-Ni alloys in boiling 22 percent NaCl at 105°C using fracture mechanics type specimens, is perhaps the best comparison to the work performed by Roy et al. (1998). While similar approaches were used in these studies, there are several important differences that must be recognized. First, the work at LLNL used 5 percent NaCl acidified to pH 2.7 at 90°C and all solutions were deaerated with N_2 . Speidel (1981) used a more concentrated, and presumably more aggressive solution consisting of boiling 22 percent NaCl (105°C). The specimens used at LLNL were DCB specimens where the initial stress intensity was limited to values less than $48 \text{ MPa}\cdot\text{m}^{1/2}$, whereas stress intensities up to $67 \text{ MPa}\cdot\text{m}^{1/2}$ were used by Speidel (1981). The crack propagation rates reported by Speidel (1981) and Roy et al. (1998) are summarized in figure 4-2. Note that for alloys containing more than 30 percent Ni, Speidel (1981) found no SCC using fatigue precracked fracture mechanics type specimens (crack propagation rate less than $3 \times 10^{-11} \text{ m/s}$) after 3 mo (2,016 h) of testing. On the other hand, Roy et al. (1998) reported SCC propagation rates in the range of 7.6×10^{-11} to $3.5 \times 10^{-10} \text{ m/s}$ that are practically independent of alloy composition.

Figure 4-3 shows the relationship between K_{ISCC} and Ni content originally reported by Speidel (1981) in boiling 22 percent NaCl along with the data reported by Roy et al. (1998) in 5 percent NaCl at 90°C and pH 2.7. Speidel (1981) did not observe SCC with alloys containing more than 35 percent Ni tested with initial stress intensities up to $60 \text{ MPa}\cdot\text{m}^{1/2}$. On the other hand, Roy et al. (1998) reported SCC of alloys with up to

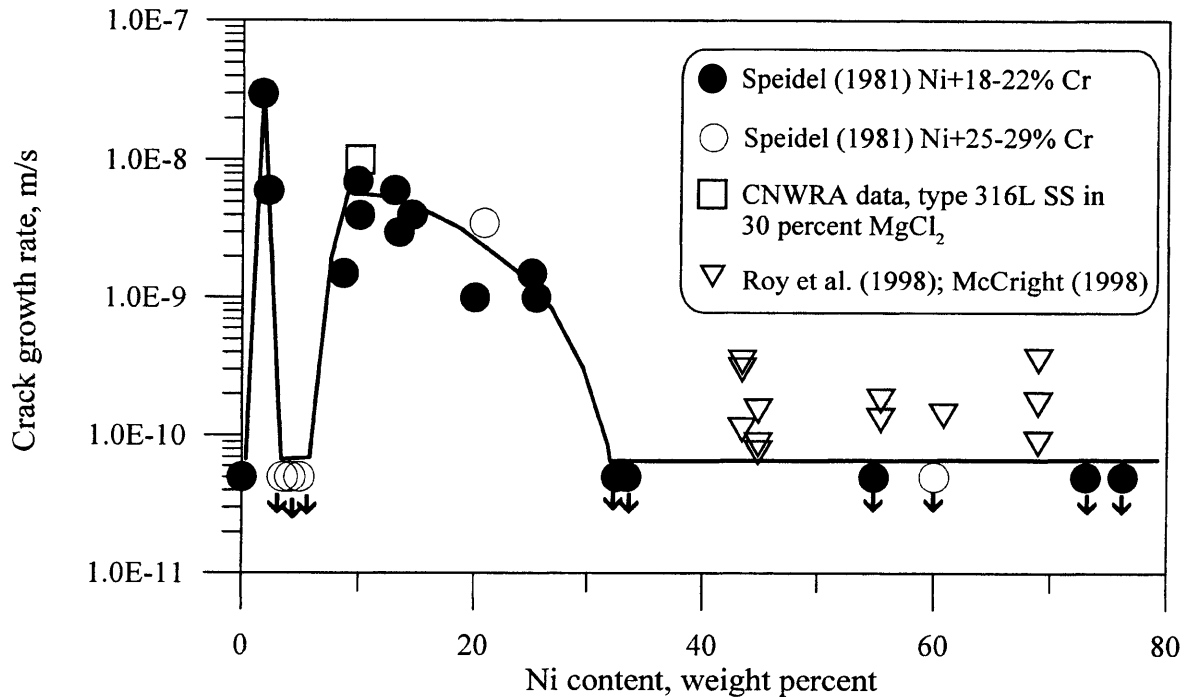


Figure 4-2. Effect of Ni content on the crack growth rate of various Ni-Cr-Mo-Fe alloys in 22 percent NaCl solution at 105°C (Speidel, 1981), 5 percent NaCl solution at 90°C (Roy et al., 1998; McCright, 1998), and type 316L stainless steel in 30 percent MgCl_2 solution at 110°C

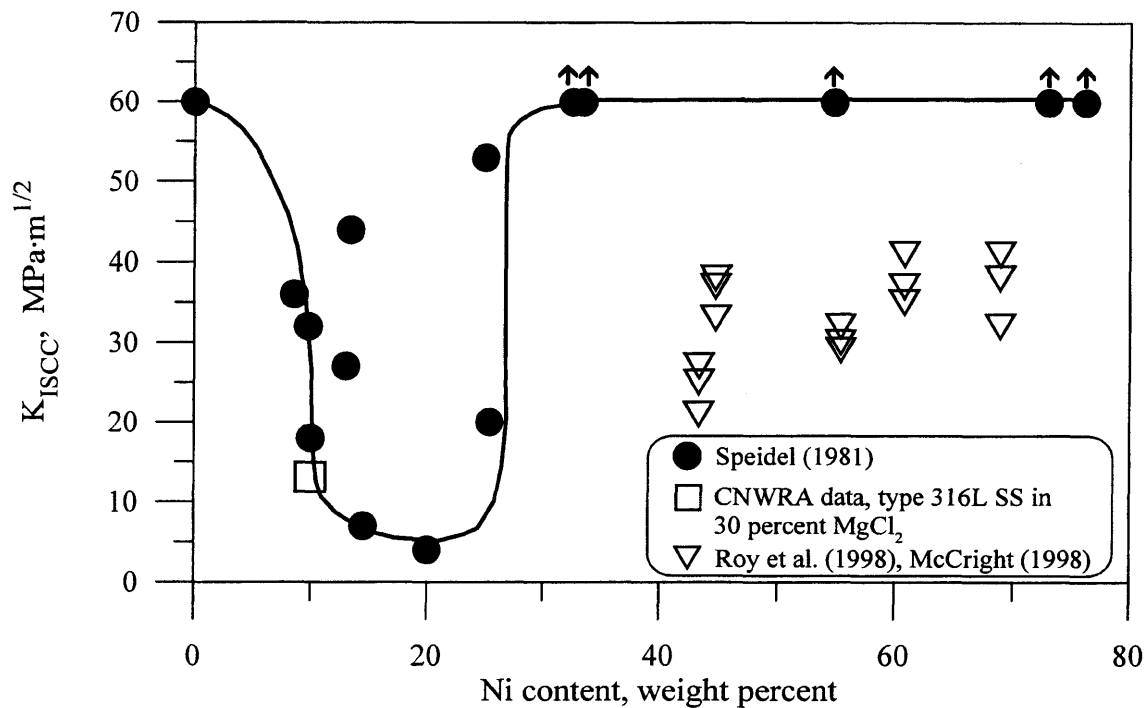


Figure 4-3. Effect of Ni content on the threshold stress intensity of various Ni-Cr-Mo-Fe alloys in 22 percent NaCl solution at 105 °C (Speidel, 1981), 5 percent NaCl solution at 90 °C (Roy et al., 1998; McCright, 1998), and type 316L stainless steel in 30 percent MgCl₂ solution at 110 °C

68 percent Ni tested using initial stress intensities in the range of 28 to 49 MPa·m^{1/2}. It is difficult to attribute the discrepancies in these reports as shown in figures 4-2 and 4-3 to differences in test techniques because much greater SCC resistance was observed by Speidel (1981) using more aggressive conditions including initial stress intensity, chloride concentration, and temperature, all of which have been demonstrated to promote SCC. Results obtained in this investigation with type 316L SS are also plotted on figures 4-2 and 4-3. The K_{ISCC} and crack growth rate data obtained in the present work compare favorably with the measurements by Speidel (1981).

The lack of SCC on the Alloy 22 specimens tested in 5 percent NaCl is clearly in contradiction to the results of SCC tests performed at LLNL (Roy et al., 1998). In addition, no SCC was observed on type 316 L SS in the same test environment. Because type 316 L SS is known to be more susceptible to SCC than Alloy 22 and the other Ni-Cr-Mo alloys tested at LLNL, the results reported by Roy et al. (1998) are questionable. Control tests performed in this study have shown that the fracture surface of a fatigue precracked and mechanically failed specimen contains artifacts, described as ductile tearing, that may be misinterpreted as transgranular SCC. Although this artifact was not observed on the type 316L SS control specimen, it is speculated that the other Ni-Cr-Mo alloys tested at LLNL may also contain this ductile tearing artifact arising from the final mechanical failure. Additional tests with specimens loaded to higher K_I values will provide a stronger basis to resolve the controversial findings of Roy et al. (1998).

Residual stresses from WP fabrication or stresses resulting from rockfall on the containers combined with the necessary electrochemical conditions may be sufficient for the SCC. Residual stress measurements

conducted after WP fabrication (TRW Environmental Safety Systems, Inc., 1998b) have shown that high residual stresses are present in the vicinity of the welds. Accurate stress measurements could not be obtained because the residual stress measurements were greater than 50 percent of the yield strength of the material (American Society for Testing and Materials, 1995). While the fabrication welds can be annealed, it may not be practical to adequately anneal the final closure weld without heating the SNF inside the WPs to temperatures above 350 °C. Short-term tests conducted in this study and those reported by Speidel (1981) suggest that high Ni alloys are not susceptible to SCC even in concentrated chloride solutions at temperatures up to the boiling point of water and high stress intensities. The long-term initiation and propagation of SCC for high Ni alloys in chloride solutions has not been adequately investigated. High residual stresses from fabrication and welding suggest that the mechanical component necessary for SCC will be present in every WP placed in the repository. This is supported by the results of Cragnolino et al. (1996) who observed severe SCC adjacent to spot welds on the otherwise unstressed legs of U-bend specimens exposed to chloride solutions. The results presented in this report suggest that SCC initiation and propagation may be predicted using an electrochemical method not critically dependent on stress intensity determinations; however, additional tests are necessary to confirm the validity of this approach.

4.4 MODELING OF CONTAINER CORROSION IN TOTAL PERFORMANCE ASSESSMENT VERSION 3.2 CODE

As noted, the EBSFAIL module in the TPA code Version 3.2 (Mohanty and McCartin, 1998) is used to calculate the failure times of the WPs from various corrosion processes. As presented in detail in the technical description of the EBSPAC Version 1.1 (Mohanty et al., 1997), the corrosion models calculate the WP failure times using appropriate rates of uniform corrosion and localized corrosion in the aqueous environment in contact with the WPs. The dominant corrosion process at any given time depends on the corrosion potential and the appropriate critical potential required to initiate a particular localized corrosion process.

The corrosion potential is explicitly calculated in EBSPAC Version 1.1 and in TPA code Version 3.2 by considering the combined electrochemical kinetics of oxygen reduction, water reduction, and metal oxidation. Metal oxidation for the Ni-Cr-Mo alloys in the expected repository environment occurs under passive dissolution conditions unless that localized corrosion can be initiated, a process that depends on alloy composition and the aggressiveness of the environment. Therefore, it was assumed on the bases of limited experimental data obtained at the CNWRA that for simplicity the passive current density used to calculate the corrosion potential can be considered independent of potential within the passive range and also independent of both chloride concentration and temperature (Mohanty et al., 1997). For Alloy 825, a constant value of 2.0×10^{-7} A/cm², equivalent to 2.0 μm/yr, was adopted in the deterministic calculations performed with EBSPAC Version 1.1 (Mohanty et al., 1997). Instead, in the TPA code Version 3.2 values ranging from 6.3×10^{-8} to 2.0×10^{-7} A/cm² (0.63 to 2 μm/yr) were used for the passive corrosion rate of Alloys 825, 625, and 22. It should be noted that these values of the passive corrosion rate, assumed to be independent of time under steady-state conditions, are also used in the code to calculate the uniform penetration of the container walls in the absence of localized corrosion.

As discussed in section 4.1, the experimental data obtained for Alloy 22 under a broad range of environmental conditions indicate that the passive corrosion rate, measured electrochemically, is practically independent of chloride concentration, pH, and potential within the passive range, exhibiting only a strong dependence on temperature, at least within a certain chloride concentration range. The range of experimental

values measured at 95 °C lies within the lower end of the range used in the TPA code Version 3.2. In addition, welded specimens did not exhibit significant increases in the passive corrosion rate. However, it should be noted that for wall thickness of about 20 mm, minor variations in the passive current density may lead to significant differences in container lifetimes which may change by several ten of thousands of years.

Both in EBSPAC and the TPA code, localized corrosion, mainly in the form of crevice corrosion, is conceived as the most detrimental corrosion failure mode for containers made of Ni-Cr-Mo alloys. Empirically derived equations are used in EBSPAC for the dependence of critical potentials on environmental parameters. Both crevice or pit initiation and repassivation potentials are assumed to depend only on the chloride concentration and temperature. The dependence of the critical potentials on chloride concentration and temperature is given by

$$E_{\text{crit}} = E_{\text{crit}}^0(T) + B(T) \text{Log}[Cl^-] \quad (4-1)$$

where $E_{\text{crit}}^0(T)$ and $B(T)$, which are dependent on the material, are considered to be linear functions of temperature. It should be noted that $E_{\text{crit}}^0(T)$ is the value of $E_{\text{crit}}(T)$ for a Cl^- concentration equal to 1 M. Eq. (4-1) is considered valid above a critical concentration value that is the minimum Cl^- concentration required to promote localized corrosion. Either the initiation potentials (E_p and E_{crev}) or the repassivation potentials (E_{rp} and E_{rcrev}) can be adopted as the critical potential for localized corrosion. As demonstrated experimentally in long-term tests conducted over more than 1,400 d (close to 4 yr) using Alloy 825 creviced specimens in chloride solutions at 95 °C, E_{rcrev} (or E_{rp}) is an appropriate parameter for predicting the occurrence of localized corrosion because E_{crev} (or E_p) tends to coincide with E_{rcrev} (or E_{rp}) at long times. In addition, E_{rp} becomes equal to E_{rcrev} for pits of sufficiently large size and, hence, both in EBSPAC Version 1.1 and TPA code Version 3.2, E_{rcrev} is conservatively adopted as the critical potential for the initiation of localized corrosion.

Expressions and values used for E_{rcrev} and the critical Cl^- concentration required for the localized corrosion of the Ni-Cr-Mo alloys in the TPA code Version 3.2 (Mohanty and McCartin, 1998) are as follows, for Alloy 825,

$$E_{\text{rcrev}}(\text{mV}_{\text{SHE}}) = (422.8 - 4.1T) + (-64.0 - 0.8T) \log[Cl^-] \quad (4-2)$$

with $[Cl^-]_{\text{crit}} = 2.0 \times 10^{-3}$ M;

for Alloy 625,

$$E_{\text{rcrev}}(\text{mV}_{\text{SHE}}) = 98.5 - 160.0 \log[Cl^-] \text{ at } 95^\circ\text{C} \quad (4-3)$$

with $[Cl^-]_{\text{crit}} = 3.0 \times 10^{-2}$; and

for Alloy 22,

$$E_{\text{rcrev}}(\text{mV}_{\text{SHE}}) = 1,140 \text{ at } 95^\circ\text{C} \quad (4-4)$$

with $[Cl^-]_{\text{crit}} = 1.0$ M

where the temperature is given in °C. Whereas Alloy 825 is susceptible to localized corrosion over a broad range of chloride concentrations and temperatures below the boiling point of water (60 to 95 °C), the temperature range is restricted in the case of Alloy 625. The data obtained for Alloy 22 (Gruss et al., 1998) indicated that localized corrosion may have occurred at high potentials and chloride concentrations. To account for variability in the experimental determination of the values of these parameters and uncertainty regarding the metallurgical conditions of the material, it is considered in the TPA code Version 3.2 that E_{rcrev}^0 exhibits a variation of ± 50 to 100 mV. As an input parameter, E_{rcrev}^0 varies with a uniform distribution from 372.8 to 472.8 mV_{SHE} for Alloy 825 and from 48.5 to 148.5 mV_{SHE} for Alloy 625. For Alloy 22 a range of ± 100 mV, around 1,140 mV_{SHE}, was adopted. After appropriate confirmation, the values of the parameters obtained in the present study for Alloy 22, as given by the coefficients in Eq. (3-3), can be used as input parameters in the code instead of the single value given by Eq. (4-4). Use of the coefficients in the expression for E_{rcrev} as input parameters in the TPA code Version 3.2 provides flexibility for evaluating different container materials. In addition, with some modifications in the code it would be possible to introduce the influence of materials variability and fabrication effects such as the effect of closure welds that exhibit a lower value of the repassivation potential with respect to that of the base metal.

The propagation of localized corrosion for Ni-Cr-Mo alloys is considered in a simplified manner in the TPA code Version 3.2, assuming a constant value for the localized corrosion rate, which is time-independent. Instead, the propagation of pits for the carbon steel overpack was considered by introducing an empirical equation developed by Marsh and Taylor (1988) for carbon steel in chloride containing bicarbonate/carbonate solutions using an extreme values statistics approach. In this equation, pit penetration is time-dependent and given by

$$P = At^n \quad (4-5)$$

where P is the pit penetration in mm, t is time in yr, A is an experimentally determined constant, and n = 0.5. The value of n = 0.5 implies a diffusively controlled pit growth rate. A constant rate of penetration for pit growth for the Ni-Cr-Mo alloys implies that n = 1 in Eq. (4-5).

Recent experimental results (Dunn et al., 1996b) have shown that this is quite conservative because a parabolic rate law (n = 0.5) was found to apply. The rates of localized penetration for type 316L SS and Alloy 625 under open circuit conditions are shown in figure 4-4. Data for type 316L SS were generated by measuring the localized corrosion penetration depth after exposure to air saturated 1 M chloride solutions at 95 °C (Dunn et al., 1996b). Pit penetration rates for Alloy 625 exposed to Salton Sea wellhead brine for periods of 15 to 45 d (Cramer et al., 1984) are also shown in figure 4-4. It can be observed that the penetration rate decreases substantially with increasing exposure time. It appears from the limited data shown in figure 4-4 that the penetration rate is diffusion controlled. In the same figure, it is also shown that the localized corrosion penetration rate used for the TPA code Version 3.2 calculations is supported by the localized corrosion penetration rates reported by Dunn et al. (1996b) and Cramer et al. (1984).

Calculations performed using TPA code Version 3.2 code illustrate the significant differences in corrosion modes and container lifetimes between the three Ni-Cr-Mo alloys evaluated. As shown in figure 4-5, a significant fraction of WPs made of either Alloys 825 or 625 failed at about 1,300 to 2,000 yr as a result of localized corrosion. Although the fraction of Alloy 825 WPs that failed due to localized corrosion is higher than that of Alloy 625, the difference is not significant (less than 15 percent), reflecting the fact that at chloride concentrations greater than 0.03 M there is practically no difference between the

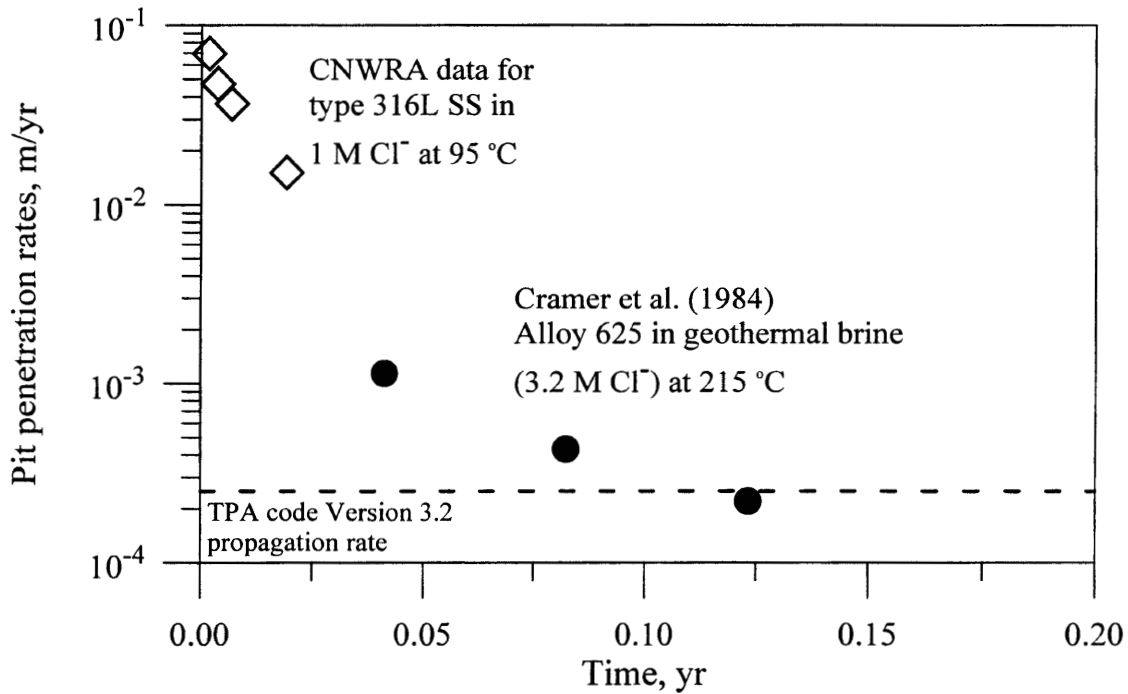


Figure 4-4. Localized corrosion penetration rate measured using type 316L stainless steel (SS) and Alloy 625. Data from Dunn et al. (1996b); Cramer et al. (1984); and TPA code Version 3.2.

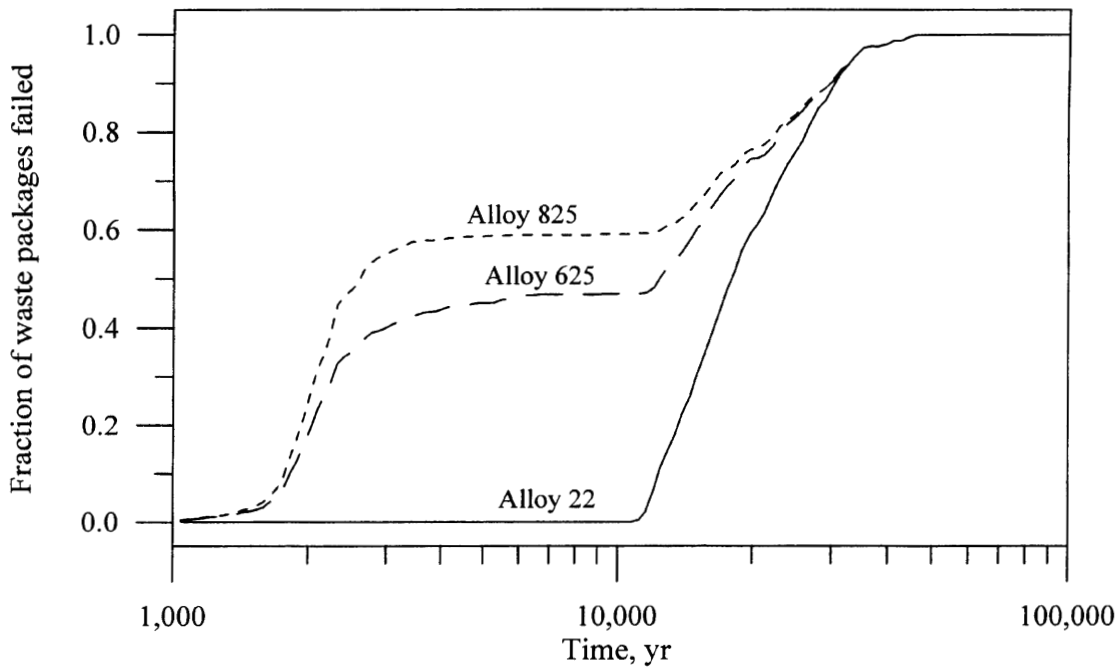


Figure 4-5. Waste package failure distribution for various container materials using TPA code Version 3.2 calculations

repassivation potentials of Alloys 825 and 625. An additional increase in the fraction of failed WPs made of Alloys 825 and 625 occurred at about 10,000 yr, but it is determined by uniform passive corrosion. The failure at about 10,000 yr for Alloy 22 as WP material is due only to uniform passive corrosion. The absence of WP failures for Alloy 22 containers at times shorter than 10,000 yr is an indication that no localized corrosion failure occurred as a result of the high repassivation potential. Nevertheless, localized corrosion failures may occur as a result of incorrect thermal or welding processes. Results of experimental work measuring the effect of these factors on the repassivation potential would allow their inclusion in the PA of the EBS.

The TPA code Version 3.2 does not include the consideration of SCC as a failure mode for the container materials. If the current experimental program reveals the potential for SCC of Alloy 22 to occur, an appropriate model should be incorporated into the code, presumably including empirical parameters such as the repassivation potential and the threshold stress intensity.

5 SUMMARY AND FUTURE WORK

Potentiostatic tests in chloride solutions have shown that passive dissolution of Alloy 22 occurs at potentials at or below $400 \text{ mV}_{\text{SCE}}$. At $600 \text{ mV}_{\text{SCE}}$ and above, transpassive dissolution occurs. The passive corrosion rate was shown to be independent of chloride concentration, potential, and pH but strongly dependent on temperature. Although the passive corrosion rate increased at elevated temperatures, the corrosion rate at $95 \text{ }^\circ\text{C}$ is less than $1 \text{ } \mu\text{m}/\text{yr}$, which translates to container lifetimes of more than 20,000 yr. Welding had only a minor effect on the passive dissolution rate.

The initiation and repassivation of localized corrosion was dependent on the composition and thermal history of the material, chloride concentration, and temperature. Alloy 22, which contained the greatest concentration of Cr and Mo, was much more resistant to localized corrosion than Alloys 625, 825, and type 316L SS. No pitting corrosion was observed on Alloy 22, and crevice corrosion was only observed in solutions containing at least 0.5 M chloride. A regression equation for the crevice corrosion repassivation potential was obtained for Alloy 22, which is similar to that used to predict the onset of localized corrosion for the previous candidate container materials. The expression is valid for temperatures at or above $95 \text{ }^\circ\text{C}$ and chloride concentrations in excess of 0.5 M. Additional tests must be conducted to determine if Alloy 22 is susceptible to localized corrosion under less aggressive conditions.

Significantly different results for the localized corrosion susceptibility of Alloy 22 were obtained in the autoclave tests compared to those obtained in the glass test cells. A satisfactory resolution of these differences has not been found. One possible explanation, the inhibition of localized corrosion by dissolved glass, has important implications for the proposed HLW repository at YM. It is well known that the YM site has an abundance of silica. If the presence of dissolved silica in the groundwater can be shown to inhibit localized corrosion, the results of this study, obtained in glass test cells, suggest that the conditions necessary to initiate localized corrosion of Alloy 22 are unlikely in the repository environment.

SCC tests were performed with type 316L SS and Alloy 22 fracture mechanics type specimens that were fatigue precracked and wedge loaded. In contrast to the previous reports by LLNL, no SCC was observed on either type 316L SS or Alloy 22 in deaerated acidified 5 percent NaCl solutions at $95 \text{ }^\circ\text{C}$. The propagation rate of SCC on type 316L SS specimens tested in hot concentrated MgCl_2 solutions was strongly dependent on potential. A substantial decrease in the SCC propagation rate was observed when the potential of the specimen was reduced and approached the repassivation potential for crevice corrosion. The K_{ISCC} and crack growth rate of type 316L SS tested in 30 percent MgCl_2 solution at $110 \text{ }^\circ\text{C}$ were measured to be $13.1 \text{ MPa}\cdot\text{m}^{1/2}$ and $1.0 \times 10^{-8} \text{ m/s}$, respectively. In contrast, Alloy 22 was found to be resistant to SCC when tested in concentrated MgCl_2 solutions. Minor secondary cracking was observed; however, continued exposure to the concentrated chloride did not result in additional crack propagation. Ductile tearing, with SCC-like appearance, was observed on the fracture surface of an Alloy 22 control specimen that was fatigue precracked, heat-tinted, and mechanically overloaded to failure. The lack of SCC on either Alloy 22 or type 316L SS specimens tested in acidified 5 percent NaCl, along with the analysis of the Alloy 22 control specimen fracture surface conducted in this study, strongly suggests that the reported SCC of the Ni-Cr-Mo alloy specimens in tests at LLNL are incorrect and based on artifacts in the fracture surfaces induced during mechanical fracture after the completion of the SCC tests.

Future work will focus on the measurement of passive dissolution rates of both mill annealed and welded material as a function of temperature chloride concentration and pH. If possible, the results of these tests will

be summarized in a lookup table or a regression equation that can be used in the TPA code to calculate the passive corrosion rate of the WP in the absence of localized corrosion. Similarly, the localized corrosion susceptibility of Alloy 22 in terms of chloride concentration, temperature, and thermal history will be examined to provide a mechanistic understanding of localized corrosion and the necessary input to the TPA code. At present, it appears that welding has a significant effect on the repassivation potential for crevice corrosion. Additional tests will be performed to compare the performance of the mill annealed to the welded material. SCC tests will focus on determining the effect of potential on the initiation and crack propagation. Additional tests using compact tension test specimens will be performed using stress intensities up to 55 MPa·m^{1/2}. As with the passive dissolution and localized corrosion tests, the ultimate goal of these tests is to arrive at a relationship that can be used in future versions of the TPA code to predict the onset and propagation of SCC.

6 REFERENCES

- American Society for Testing and Materials. Standard test method for determining residual stresses by the hole-drilling strain-gage method: E837-94a. *Annual Book of ASTM Standards. Volume 03.01: Metallography. Metals—Mechanical Testing: Elevated and Low-Temperature Tests*. Philadelphia, PA: American Society for Testing and Materials: 661-667. 1995.
- American Society for Testing and Materials. Standard test method for plain-strain fracture toughness of metallic materials: E399-90. *Annual Book of ASTM Standards. Volume 03.01: Metallography. Metals—Mechanical Testing: Elevated and Low-Temperature Tests*. West Conshohocken, PA: American Society for Testing and Materials: 422-452. 1999a.
- American Society for Testing and Materials. Standard test method for conducting cyclic potentiodynamic polarization measurements for localized corrosion susceptibility of iron-, nickel- or cobalt-based alloys: G61-86. *Annual Book of ASTM Standards. Volume 03.02: Wear and Erosion—Metal Corrosion*. West Conshohocken, PA: American Society for Testing and Materials: 237-241. 1999b.
- American Society for Testing and Materials. Standard practice for calculation of corrosion rates and related information from electrochemical measurements: G102-89. *Annual Book of ASTM Standards. Volume 03.02: Wear and Erosion—Metal Corrosion*. West Conshohocken, PA: American Society for Testing and Materials: 416-422. 1999c.
- American Society for Testing and Materials. Standard tests methods of detecting susceptibility to intergranular attack in wrought, nickel-rich, chromium-bearing alloys: G28. *Annual Book of ASTM Standards. Volume 03.02: Wear and Erosion—Metal Corrosion*. West Conshohocken, PA: American Society for Testing and Materials: 84-88. 1999d.
- Atkins, J.E., and J.H. Lee. *User's Guide to Waste Package Degradation (WAPDEG) Simulation Code. Version 1.0. Preliminary Draft*. Las Vegas, NV: INTERA, Inc. 1996.
- Beccaria, A.M., G. Poggi, and G. Castello. Influence of passive film composition and sea water pressure on resistance to localized corrosion of some stainless steels in sea water. *British Corrosion* 30(4): 283-287. 1995.
- Blink, J. Enhanced design alternative II. *DOE/NRC CLST Appendix 7 Meeting on Container Life and Source Term, Lawrence, California, July 7-8, 1999*. Lawrence, CA: Lawrence Livermore National Laboratory. 1999.
- Brown, B.F. The application of fracture mechanics to stress-corrosion cracking. *Metallurgical Reviews* 13: 171-183. 1968.
- Cieslak, M.J., T.J. Headley, and A.D. Romig, Jr. The welding metallurgy of Hastelloy alloys C-4, C-22, and C-276. *Metallurgical Transactions* 17A: 2,035-2,047. 1986a.

- Cieslak, M.J., G.A. Knorovsky, T.J. Headley, and A.D. Romig, Jr. The use of PHACOMP in understanding the solidification microstructure of nickel base alloy weld metal. *Metallurgical Transactions* 17A: 2,107–2,116. 1986b.
- Cragolino, G.A., and N. Sridhar. *A Review of Localized Corrosion of High-Level Nuclear Waste Container Materials–I*. CNWRA 91-004. San Antonio, TX: Center for Nuclear Waste Regulatory Analyses. 1991.
- Cragolino, G.A., and N. Sridhar. *A Review of Stress Corrosion Cracking of High-Level Nuclear Waste Container Materials–I*. CNWRA 92-021. San Antonio, TX: Center for Nuclear Waste Regulatory Analyses. 1992.
- Cragolino, G.A., D.S. Dunn, and N. Sridhar. *Environmental Effects on Stress Corrosion Cracking of Type 316L Stainless Steel and Alloy 825 as High-Level Nuclear Waste Container Materials*. CNWRA 94-028. San Antonio, TX: Center for Nuclear Waste Regulatory Analyses. 1994.
- Cragolino, G.A., D.S. Dunn, and N. Sridhar. Environmental factors in the stress corrosion cracking of type 316L stainless steel and Alloy 825 in chloride solutions. *Corrosion* 52(3): 194–203. 1996.
- Cragolino, G.A., D.S. Dunn, C.S. Brossia, V. Jain, and K.S. Chan. *Assessment of Performance Issues Related to Alternate Engineered Barrier System Materials and Design Options*. CNWRA 99-003. San Antonio, TX: Center for Nuclear Waste Regulatory Analyses. 1999.
- Cramer, S.D., J.P. Carter, and R.K. Conrad. Corrosion and scaling of nickel alloys in Salton Sea geothermal environments. *Proceedings of the International Symposium on Solving Corrosion and Scaling Problems in Geothermal Systems*. Houston, TX: NACE International: 215–235. 1984.
- Crandall, S.H., N.C. Dahl, and T.J. Lardner. *An Introduction to the Mechanics of Solids*. 3rd Edition. New York: McGraw-Hill, Inc. 1978.
- Dunn, D.S., N. Sridhar, and G.A. Cragolino. Long-term prediction of localized corrosion of Alloy 825 in high-level nuclear waste repository environments. *Corrosion* 52(2): 115–124. 1996a.
- Dunn, D.S., G.A. Cragolino, and N. Sridhar. Localized corrosion initiation, propagation, and repassivation of corrosion resistant high-level nuclear waste container materials. *Proceedings of the CORROSION '96 Conference*. Paper No. 97. Houston, TX: NACE International. 1996b.
- Dunn, D.S., G.A. Cragolino, and N. Sridhar. Methodologies for predicting the performance on Ni-Cr-Mo alloys proposed for high level nuclear waste containers. *Scientific Basis for Nuclear Waste Management*. Pittsburgh, PA: Materials Research Society. In press. 1999.
- Eremias, B., and M.A. Marichev. Environmental aspects of stress corrosion crack growth in austenitic stainless steel. *Corrosion Science* 28: 1,003–1,018. 1979.
- Gruss, K., G.A. Cragolino, D.S. Dunn, and N. Sridhar. Repassivation potential for localized corrosion of alloys 625 and C-22 in simulated repository environments. *Proceedings of the CORROSION '98 Conference*. Paper No. 149. Houston, TX: NACE International. 1998.

- Harrington, P. License application design selection (LADS) overview and process. *111th Meeting Advisory Committee on Nuclear Waste, Washington, DC, July 20, 1999*. Washington, DC: Nuclear Regulatory Commission. 1999.
- Heady, R.B. Evaluation of sulfide corrosion cracking resistance in low alloy steels. *Corrosion* 3(7): 98–107. 1977.
- Heubner, U.L., E. Altpeter, M.B. Rockel, and E. Wallis. Electrochemical behavior and its relation to composition and sensitization of NiCrMo alloys in ASTM G-28 solution. *Corrosion* 45(3): 249–259. 1989.
- Howard, R. Reference design for site recommendation. *Presentation at the DOE/NRC Technical Exchange on Total System Performance Assessment*. May 25–26, 1999. San Antonio, Texas. 1999.
- Kasparova, O.V. The break-down of the passive state of grain boundaries and intergranular corrosion of stainless steels. *Protection of Metals* 34(6): 520–526. 1998.
- Kessler, J., and R. McGuire. *Yucca Mountain Total System Performance Assessment: Phase 3*. EPRI TR-107191, 3055-02. Palo Alto, CA: Electric Power Research Institute. 1996.
- Kirchheim, R., B. Heine, H. Fischmeister, S. Hofmann, H. Knotte, and U. Stoltz. The passivity of iron-chromium alloys. *Corrosion Science* 30(7): 899–917. 1989.
- Kolts, J., and N. Sridhar. Temperature effects in localized corrosion. *Proceedings of the Corrosion of Nickel-Base Alloys*. R.C. Scarberry, ed. Metals Park, OH: American Society for Metals: 191–198. 1985.
- Lee J.B. Elevated temperature potential-pH diagrams for the Cr-H₂O, Ti-H₂O, Mo-H₂O, and Pt-H₂O systems. *Corrosion* 37(8): 467–481. 1981.
- Lefakis, H., and W. Rostoker. Stress corrosion crack growth rates of brass and austenitic stainless steels at low stress intensity factors. *Corrosion* 33(5): 178–181. 1977.
- Marsh, G.P., and K.J. Taylor. An assessment of carbon steel containers for radioactive waste disposal. *Corrosion Science* 28: 289–320. 1988.
- McCright, R.D. *Engineered Materials Characterization Report. Volume 3, Revision 1.1: Corrosion Data and Modeling—Update for the Viability Assessment*. UCRL-ID-119564. Livermore, CA: Lawrence Livermore National Laboratory. 1998.
- Mohanty, S., and T.J. McCartin. *Total-system Performance Assessment (TPA) Version 3.2 Code: Module Descriptions and User's Guide*. San Antonio, TX: Center for Nuclear Waste Regulatory Analyses. 1998.

- Mohanty, S., G.A. Cragnolino, T. Ahn, D.S. Dunn, P.C. Lichtner, R.D. Manteufel, and N. Sridhar. *Engineered Barrier System Performance Assessment Code (EBSPAC) Version 1.1 Technical Description and User's Manual*. CNWRA 97-006. San Antonio TX: Center for Nuclear Waste Regulatory Analyses. 1997.
- NACE International. *Testing of Metals for Resistance to Sulfide Stress Cracking at Ambient Temperatures*. NACE Standard TM0177-90. Houston, TX: NACE International. 1990.
- Nuclear Regulatory Commission. *NRC Iterative Performance Assessment Phase 2: Development of Capabilities for Review of a Performance Assessment for a High-Level Waste Repository*. R.G. Westcott, M.P. Lee, T.J. McCartin, N.A. Eisenberg, and R.G. Baca, eds. NUREG-1464. Washington, DC: Nuclear Regulatory Commission. October 1995.
- Okayama, S., Y. Uesugi, and S. Tsujikawa. The effect of alloying elements on the repassivation potential for crevice corrosion on stainless steels in 3% NaCl solution. *Corrosion Engineering* 36(3): 157-168. 1987.
- Pasupathi, P. *License Application Design Selection Feature Report: Waste Package Corrosion Resistant Materials (Metal and Ceramic)*. B00000000-01717-2200-00216. Revision 00A. Las Vegas, NV: Office of Civilian Radioactive Waste Management System, Management and Operating Contractor. 1998.
- Raghavan, M., R.R. Mueller, G. A. Vaughn, and S. Floreen. Determination of isothermal sections of nickel rich portion of Ni-Cr-Mo system by analytical electron microscopy. *Metallurgical Transactions* 15A: 783-792. 1984.
- Roy, A.K., D.L. Fleming, and B.Y. Lum. Stress corrosion cracking of Fe-Ni-Cr-Mo and Ni-Cr-Mo and Ti alloys in 90 °C acidic brine. *Proceedings of the CORROSION '98 Conference*. Paper No. 157. Houston, TX: NACE International. 1998.
- Russell, A.J., and D. Tromans. A fracture mechanics study of stress corrosion cracking of type-316L austenitic steel. *Metallurgical Transactions* 10A: 1,229-1,238. 1979.
- Silcock, J.M. Nucleation and growth of stress corrosion cracks in austenitic steels with varying Ni and Mo contents. *Corrosion* 38(3): 144-156. 1982.
- Speidel, M.O. Stress corrosion cracking on stainless steels in NaCl solutions. *Metallurgical Transactions* 12A: 779-789. 1981.
- Sridhar, N., G.A. Cragnolino, and D.S. Dunn. *Experimental Investigations of Failure Processes of High-Level Nuclear Waste Container Materials*. CNWRA 95-010. San Antonio, TX: Center for Nuclear Waste Regulatory Analyses. 1995.
- Szklarska-Smialowska, Z. *Pitting Corrosion of Metals*. Houston, TX: NACE International. 1986.

- TRW Environmental Safety Systems, Inc. *Total System Performance Assessment—1995: An Evaluation of the Potential Yucca Mountain Repository*. B00000000-01717-2200-00136. Revision 01. Las Vegas, NV: TRW Environmental Safety Systems, Inc. 1995.
- TRW Environmental Safety Systems, Inc. *Total System Performance Assessment (TSPA-VA) Analyses Technical Basis Document. Waste Package Degradation Modeling and Abstraction*. B00000000-01717-4301-00005. Revision 00. Las Vegas, NV: TRW Environmental Safety Systems, Inc. 1998a.
- TRW Environmental Safety Systems, Inc. *Waste Package Phase II Closure Methods Report*. BBA000000-01717-5705-00016. Revision 00. Las Vegas, NV: TRW Environmental Safety Systems, Inc. 1998b.
- U.S. Department of Energy. *Repository Safety Strategy: U.S. Department of Energy's Strategy to Protect Public Health and Safety after Closure of a Yucca Mountain Repository*. YMP/96-01. Revision 2. Las Vegas, NV: U.S. Department of Energy, Office of Civilian Radioactive Waste Management. 1998a.
- U.S. Department of Energy. *Viability Assessment of a Repository at Yucca Mountain. Volume 3: Total System Performance Assessment*. DOE/RW-0508/3. Las Vegas, NV: U.S. Department of Energy, Office of Civilian Radioactive Waste Management. 1998b.
- U.S. Department of Energy. *Viability Assessment of a Repository at Yucca Mountain. Volume 2: Preliminary Design Concept for the Repository and Waste Package*. DOE/RW-0508/2. Las Vegas, NV: U.S. Department of Energy, Office of Civilian Radioactive Waste Management. 1998c.
- Wilson, M.L., J.H. Gauthier, R.W. Barnard, G.E. Barr, H.A. Dockery, E. Dunn, R.R. Eaton, D.C. Guerin, N. Lu, M.J. Martinez, R. Nilson, C.A. Rautman, T.H. Robey, B. Ross, E.E. Ryder, A.R. Schenker, S.A. Shannon, L.H. Skinner, W.G. Halsey, J.D. Gansemer, L.C. Lewis, A.D. Lamont, I.R. Triay, A. Meijer, and D.E. Morris. *Total-System Performance Assessment for Yucca Mountain—SNL Second Iteration (TSPA-1993)*. SAND93-2675. Albuquerque, NM: Sandia National Laboratories. 1994.